A MODIFIED DISTRIBUTED ACTIVATION ENERGY MODEL FOR THE PYROLYSIS OF SOUTH AFRICAN SOLID FUELS

Qasim Fakir

A dissertation submitted to the Faculty of Engineering and the built Environment at the University of the Witwatersrand, in accordance with the requirements for a Master of Science (Engineering)

Johannesburg, 2012

Declaration

I declare that this dissertation is my own, unaided effort. It is being submitted for the degree of Master of Science in Engineering at the University of the Witwatersrand, Johannesburg.
It has not been submitted before for any degree or examination in any form, at any other University.

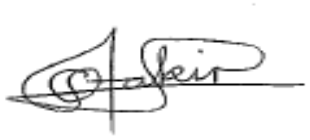

_____
(Signature of Candidate)

20th day of August 2012

Abstract

A mathematical model is used to describe the pyrolysis of South African coal, biomass and coal-biomass blends. The model makes use of a modified form of the Distributed Activation Energy Model (DAEM) to predict and characterize the underlying distribution of reactions occurring during the pyrolysis process. The DAEM was successfully applied to determine the Activation Energy, *E*, and Pre-exponential Factor, *A*, for each reaction during the pyrolysis of coal as well as biomass. The results obtained showed for a Medium Rank 'C' coal, 23 underlying reactions occurring within the given temperature range, with activation energies in the ranges of 29 - 198 kJ/mol and pre-exponential factors in the ranges of $1x10^{5}$ – $1.2x10^{13}$ s^{-1}. Results for biomass showed the three distinctive reactions underlying the pyrolysis process, with activation energies of 17.3, 86.8 and 209 kJ/mol obtained for the decomposition of lignin, hemi-cellulose and cellulose, respectively. The returned pre-exponential factors corresponding to the activation energies were 0.0154, $5.28x10^{5}$ and $1.13x10^{15}$ s^{-1}, respectively.

The model was also used to show the clear distinction between coal and biomass blends undergoing pyrolysis, and the non-dependence of the two fuels on each other. The synergistic effect of their pyrolysis products on pyrolysis is noted and this was found to be the observation of other researchers within the literature. The results obtained compare favorably with similar results for biomass given in the literature.

The model was also successfully applied to obtain high resolution images of the pyrolysis profile by simulating low heating rates, or high heating rates. The images obtained utilizing the DAEM model for coal tested at the heating rate of 20 K/min returned a relative error of 0.587 when compared to actual TGA data, whereas at 5 K/min, this error was minimized to 0.786. This lack of confidence in the DAEM model at heating rates above 5K/min for coal is a direct result of the effect of secondary reactions between the primary pyrolysis products, and the use of the selected heating rate for purposes of prediction used in the model. The results for biomass obtained at the heating rate of 10 K/min returned a relative error of 0.991 whilst at the high heating rate of 100 K/min, this decreased slightly, to 0.923. This is attributed to the simple chemical nature of the fuel and lack of interactions between pyrolysis products.

The model was also used to show how the area under the curve of the representative peak lies on a straight line of calculable gradient, for increasing biomass concentration. Biomass-blended samples of increasing biomass concentration by mass, were tested at various heating rates, and the results obtained showed that at heating rates of 25, 10 and $1x10^{-22}$ K/min, the sum of squared errors for the line obtained, improved from 0.976 to 0.989 to 0.991, respectively. For complex structured fuels, such as coal, the model gives a fair representation of the pyrolysis profile, whilst for more simply structured fuels such as sawdust, the model gives a better and accurate fit.

Acknowledgements

I would like to take this opportunity to acknowledge all the people who helped make the completion of this dissertation possible, and who stood by me as pillars of strength and support when things seemed bleak and goals looked far away:

To my Professor, supervisor and study leader, Nicola Wagner, for her understanding, firmness, and leadership in helping me to become a better writer, and also cracking the whip when needed.

To my co-supervisor, Dr. Shehzaad Kauchali for his superior skills at writing Matlab® code and endless hours spent debugging code.

To my friends, colleagues and new-found academic family of the Coal & Carbon Research Group for all their input, help and constructive criticism.

To my parents and Habibi for all their prayers and sacrifices,

And lastly to my Creator for allowing me the opportunity to make a small contribution to the advancement of knowledge.

Table of Contents

Chapter 3: Literature Review

Chapter 4: Historical Development of Pyrolysis Models

Chapter 5: Experimental

Chapter 6: Results & Discussion

Chapter 7: Conclusions

List of Figures

Figure ***Page***

List of Tables

Table ***Page***

Nomenclature

A	Pre-exponential factor, s^{-1}
A_i	Pre-exponential factor, $s^{-1,}$ for reaction *i*
B	Rate of heating (dT/dt), $K.s^{-1}$
B_1, B_2	Rate of heating (dT/dt), $K.s^{-1}$ in experiments 1 and 2
dT/dt	Rate of Temperature change with respect to time, dimensionless
E_i	Activation energy for reaction I, $kJ.mol^{-1}$
E	Activation energy, $kJ.mol^{-1}$
E*	Activation energy at which Ψ(E) = 0.58, $kJ.mol^{-1}$
f	Mass fraction of material, dimensionless
f_i	Mass fraction of material associated with reaction *i*, dimensionless
$f_{i,0}$	Initial value of fi, dimensionless
$\underline{f}$	A vector containing the values of fi,0 for all reactions, dimensionless
F(E)	$=\int_0^E g(E)dE$, Cumulative fraction of material with activation energy less than E, dimensionless

g(E)	Fractional density function such that g(E)dE= fraction of material with activation energy between E and E+dE, mol.kJ^{-1}
i	Reaction number, dimensionless
m(E)	Mass density function such that m(E)dE= mass of material with activation energy between E and E+dE, kg.mol.kJ^{-1}
m_0(E)	Initial value of m(E), kg.mol.kJ^{-1}
M	Mass of fuel sample, kg
M_0	Initial mass of fuel sample, kg
$\underline{M}$	A vector which contains the mass of fuel remaining at different points in time, kg
M_v	Mass of volatiles, kg
M_{v0}	Initial mass of volatile matter, kg
R	Ideal gas constant, kJmol^{-1}K^{-1}
t	Time, *s*
t_0, t_1, t_2, t_3,….	Times at which the mass of fuel is measured, *s*
T	Temperature, °C or K
T_0	Initial temperature, °C or K
T_1, T_2	Temperatures at which a specified conversion is reached, °C or K
u	Dummy variable for integration, kJ.mol^{-1}
w	Mass fraction of sample which is inert, dimensionless
V	Yield of volatiles, kg
α	Degree of conversion, dimensionless
Ψ	$=\exp\left[-A(E)\int_0^t \exp\left(\frac{-E}{RT(t)}\right)dt\right]$, dimensionless
$\underline{\underline{\Psi}}$	A matrix whose elements *i*, *j* are given by Ψi(t_j), dimensionless
Ψi	The value of Ψi(*t*) for reaction *i*,$= \exp\left[A_i\int_0^t \exp\left(\frac{-E_i}{RT(t)}\right)dt\right]$

Chapter 1: Introduction

1.1 Introduction & Background

Coal has been used since ancient times to provide heat, cook food, and even in early metallurgical applications for the production, smelting and fashioning of various semi- and precious metals.

The importance of coal to the technological advancement of mankind is witnessed by the fact that it was one of the major driving forces for the Industrial Revolution. Numerous authors confirm this, such as Church (1986), Braudel (1981) and Deane (1965) to name but a few. They also identify the impact of coal as a precursor to many modern amenities such as: transportation through the development of steam-driven locomotive trains which lead to the development of the internal combustion engine; power generation for electricity supply; and even the development of many high-end chemical products and drugs that could now be manufactured on a large scale due to machination and automation.

With the rise of the transportation sector brought on by the development of the internal combustion engine, as well as the discovery of vast oil and natural gas reserves in areas such as the Middle-East, the use of coal to drive industrial and technological innovation was back-tracked. Oil and natural gas provided an easier, cheaper and apparently 'cleaner' way to provide these energy demands. However, the wide-spread use of these oil and gas reserves has led to a quickly-diminishing supply, and coal has once again become the focus of much research into its sustainable and efficient use in providing energy, as well as fuels.

Numerous authors have attested to the general widespread availability of coal deposits, such as Snyman and Botha (1993), Ward (1984) and Williamson (1967). These authors also mention that coal reserves are more evenly distributed than gas or oil reserves, which are largely limited to politically unstable areas such as the Middle-East, or in remote, inaccessible areas like off-shore, deep-sea rigs.

An additional problem for South Africa is its continuing development of its economy and production of energy for export to other African regions. It is expected that energy demand will continue to rise, possibly reaching critical levels in the next 20 years if appropriate measures are not taken (Maniatis et al., 2002). Figure 1.1 shows the continual rise of South Africa's energy demands.

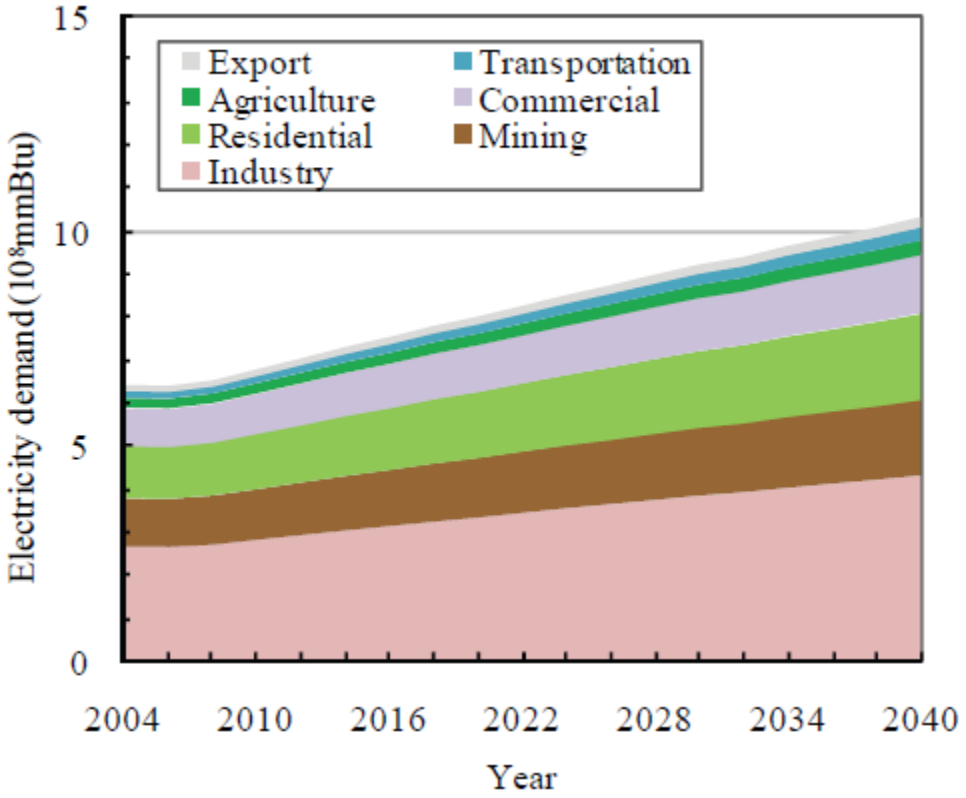

Figure 1.1: Electricity Demand in South Africa by Various Sectors (Matsumoto & Nakata, 2007)

It is obvious that a robust energy policy has to be implemented in order to address this unsatisfactory situation and envisage reversing this trend. Any such a policy has to carefully examine the role of renewable energy sources and the role they will play in supplementing the National Energy Grid.

The current tendency is oriented to support research and demonstration activities, in connection with other regulatory and economy-based measures, so as to efficiently increase the share of renewable energies.

Because of the vast differences in the content of South African coal according to region, and sometimes within the same coal seam (Snyman and Barclay, 1989) crucial information regarding the physical and chemical properties of the coal is required. This information allows for the use of such coals to be maximised whilst minimizing the cost to the environment.

The general availability of coal reserves effectively means that for developing nations or areas where oil and gas are not in abundance, such as South Africa, coal remains the primary source of fuel and energy production.

The rise of the environmental movement, as well as increasing pressure from various governmental bodies and environmental activist groups, has exerted immense pressure on coal-dependant economies to look at ways of utilizing coal in as clean and efficient a way as possible. This will allow these economies to limit green-house gas emissions and thus mitigate the global warming phenomenon. The aim of such pressure being to minimize the long-term environmental impacts of continued coal use.

A good example of the gap between coal dependant economies shifting towards more renewable sources of energy can best be seen with South Africa. According to the International Energy Agency, current electricity demand in South Africa as at 2008, was estimated at approximately 232.23 TWh of energy per year, and is produced by 92% of fossil fuels, all of which is coal. The contribution of renewable energies remains relatively low, at less than 1% in 2004 (Matsumoto & Nakata, 2007). Increasing knowledge about the use of biomass as a feedstock to combustion and gasification will help narrow the gap, and thus the dependence of an economy like South Africa, solely on coal.

An extensive amount of research has gone into the development of new technologies to better utilize coal and thus gain maximum efficiency while providing the least amount of emissions.

Biomass has been identified as one of the fuels of the future, owing to its relatively high energy content, renewability and carbon-neutral lifespan (Biagini et al., 2002). Biomass consists of various crops (mainly non-food providing crops) which are grown and then harvested to provide fuel in power generation or industry. Present

technological limitations during combustion cannot yet cope with a feed supply of pure biomass, and new technologies to overcome this are in the process of being developed (Biagini et al., 2002).

Biomass has historically supplied human needs for food, fibre, energy, and structural material. The potential for biomass to supply much larger amounts of useful energy with reduced environmental impacts, as compared to fossil fuels, has stimulated substantial research and development into systems for handling, processing, and converting biomass into heat, electricity, solid, liquid and gaseous fuels, and other chemicals and products (Diaz, 2006). Greater use of biomass has also been motivated by improvements experienced in local and global environmental quality. Pyrolysis and other thermochemical conversion processes offer an important opportunity for the utilization of biomass and waste (Scott et al., 2006[b]).

Pyrolysis is a step in the preparation of organic, carbonaceous material for use in either combustion or gasification. During pyrolysis, the organic matter is heated in an inert or oxygen-deficient atmosphere, in order to produce a concentrated carbon char. Pyrolysis occurs whenever any material is heated, and forms one of the basic processes that occur according to ignition theory (Gavalas, 1982).

Pyrolysis is used extensively in the preparation of organic matter for further use in chemical reactions such as gasification, or combustion. In order to facilitate the thermal decomposition and thus provide an indication of the amount of volatile organic matter and moisture present in the fuel, a typical pyrolysis experiment can be carried out. The result of the pyrolysis process is the solid carbon (also called the char) and mineral matter (or ash). The products from the thermal decomposition process include gases, chemical water and tars which may or may not be useful in further downstream processes.

In the gasification industry, large scale reactors are used to convert solid organic, carbon-rich fuels into synthesis gas, which can then be used to generate electricity, or produce high-end chemical and petroleum products. In such a reactor, fuel undergoes three key processes as recorded by Smoot and Smith (1985) which ultimately results in the production of synthesis gas being formed. These three steps include:

i. ***Pyrolysis:*** Also known as devolatilization. In this process the fuel particle begins to heat up, driving off moisture and volatiles, resulting in the formation of the char. Tar is also released. This process depends largely on the properties of the fuel being pyrolised, and determines the behaviour of the char particles in further processes.

ii. ***Combustion:*** As the volatiles are driven off, the char can ignite and combine with oxygen to form oxides of carbon, which results in heat generation for further processes.

iii. ***Fuel Conversion:*** At this stage the char reacts with oxygen and water present in the reactor to form the synthesis gas. The synthesis gas is then utilized downstream for further processing.

It is important to note here, that the process described above, is typical for a top-fed Siemens gasifiers.

The increasing dependence on imported oil as well as the urgency to reduce greenhouse gas emissions abounds in justifying an energy policy that carefully considers the role of renewable sources as energy carriers. Although numerous projects have been promoted, pyrolysis commercialization is progressing at a slow pace not only in South Africa but also globally (Diaz, 2006). In this sense, a better knowledge of the kinetics concerning the thermal decomposition of lignocellulosic material is required. The abundant research literature on the field of biomass pyrolysis kinetics still leaves many key issues unsolved. The exploitation of the information provided by thermogravimetry, a relatively low priced, simple technique suitable for studying several reactions of interest in biomass conversion and combustion, requires the establishing of appropriate models and evaluation strategies for the various biomass materials. The kinetic description of experiments measured at different conditions by exactly the same reaction kinetics is criticized due to some small, but inevitable systematic errors that depend on the experimental conditions (Diaz, 2006). Practical models that predict the evolution of specific products of interest are still expected in the literature.

To overcome this hurdle, research globally continues to investigate the use of a blend of coal and biomass to substitute the total amount of coal used in energy production. Research in this field has been very promising. Researchers such as Vuthaluru (2003)

and Pokothoane (2008) have shown that coal and biomass blends not only lead to increases in thermal efficiencies within industrial boilers, but also reduced carbon dioxide emissions. As a result of such promising research, many new and innovative technologies may well be developed.

Ultimately, the use of biomass alone seems far off, especially in a country like South Africa where agricultural land would now compete with food-crop production, for the population or for the production of biomass crops. South Africa is also a water-scarce country, and the additional use of water to grow biomass crops is at this stage not feasible. It would thus seem logical to investigate the effects of utilizing blends of coal and biomass-derived wastes such as sawdust, sugar cane bagasse or straw, to name but a few, in order to pave the way for incoming renewable energy sources and technologies.

Modelling provides crucial information about how and when a reaction occurs. More importantly, kinetic data can be obtained which allows for the prediction of a particular material's behaviour at conditions which favour investigation. Numerous models exist for the pyrolysis process, each with their advantages and disadvantages. They range in complexity from simple first-order models to more mathematically complex models incorporating various factors which influence the kinetics of pyrolysis. These models will be analysed and compared, and the most suitable model for the pyrolysis of the particular sample will be utilized for the purposes of this study.

The experimental work carried during this research was conducted on: *a typical medium rank C, high ash content South African Coal*, as well as *biomass in the form of sawdust*, and *blends of both coal and biomass in increasing increments of biomass concentration, by mass*.

1.2 Problem Statement

In this work a study of the modelling of the pyrolysis process using a modified form of the Distributed Activation Energy Model (DAEM) will be carried out on coal, biomass and coal-biomass blends. The model will be used to determine the behaviour of coal, biomass and blends of coal and biomass undergoing pyrolysis at various constant heating rates, under atmospheric conditions. This has numerous benefits, as a major concern regarding the modelling of the pyrolysis process currently makes use of simple kinetic models, which are adequate for predicting pyrolysis behaviour at low heating rates and temperatures, and cannot be extrapolated with certainty to high heating rates and temperatures, and conversely to very low, nearly-isothermal heating rates. Fuel conversion reactors operate at conditions which cannot be easily simulated in a laboratory, but with the development of an effective kinetic model, the pyrolysis behaviour can easily be inferred. Various works such as that by Miura (1995), Navarro et al. (2008) and Please et al. (2003), to name but a few, have already been carried out to develop better models that can accurately predict the kinetics of the pyrolysis process, but the most successful model developed to date is that of the DAEM as mentioned by Braun and Burnham (1987). This model however, is computationally intensive, and it is the intent of this researcher to adapt and modify this model so that data obtained for pyrolysis at low heating rates can easily be extrapolated to predict pyrolysis at high heating rates.

A modified form of the DAEM has already been proposed by Scott et al. (2006[a], 2006[b]) and was shown to give effective, accurate kinetic data for both Northern Hemisphere coals and biomass, and it is thus of interest to this research to test the applicability of the model in effectively determining these parameters for a South African coal, since these coals behave differently. Work of this nature has not been carried out on South African fuels, and successful development of such a model will be of great benefit to numerous industries which make use of fuel conversion processes, as kinetic data for the pyrolysis process can now be easily determined. A modified form of the DAEM was used as this model was ear-marked as the most advanced, and best suited model by authors such as Burnham et al. (1987), Miura (1995) and Navarro et al. (2008), to name but a few, to provide a model-free approach to determining the inherent kinetic

parameters, such as the activation energy and pre-exponential factor, of the fuel undergoing pyrolysis.

Much research has gone into the understanding of the pyrolysis process, and numerous models have been developed to try and predict the kinetic parameters of the process. Owing to the complexity of the fuel used, these models differ accordingly. Most of these models have been developed by researchers working on Northern Hemisphere coals. By contrast, South African coals are very different to these coals; they are much younger in age and have much higher ash content (Snyman and Botha, 1993). It is thus relevant that research be carried out to understand the pyrolysis process of South African fuels, and develop a model that will accurately predict the kinetic parameters of not only South African fuels, but any solid fuel, including fuels utilising a blend of coal and biomass.

The model will thus be able to predict the pyrolysis behaviour of coal, biomass and coal-biomass blends undergoing pyrolysis at various, but constant heating rates.

1.3 Aims and Objectives

The aim of this research is to apply the modified form of the DAEM to the kinetic modelling of coal, biomass and coal-biomass blends.

The intention of this research is to demonstrate the importance of matching the correct coal, biomass, or coal-biomass kinetics to the correct operating conditions at which pyrolysis occurs, in order to maximise the use of the fuel.

Owing to the numerous advantages of the research, the specific objectives are to:

- Investigate the pyrolysis of coal, biomass and blends thereof, using a TGA at various heating rates
- Investigate previous and current kinetic models used to model the pyrolysis process, and understand their applicability, limitations and short-comings

- Use the results of the TGA analyses and the modified DAEM to enable accurate predictions on the pyrolysis behaviour at very high and very low heating rates
- Show how the modified DAEM can then accurately be used to predict kinetic parameters for any given fuel, with any given number of components in the fuel, at any given heating rate
- Confirm the efficacy of the kinetic model by rigorous scenario testing and hypothetical testing

1.4 Project Scope

This dissertation provides information on the pyrolysis process, as well as outlines various models used in predicting pyrolysis behaviour, and will ultimately lay the foundation for further work into both gasification and combustion testing using the modified DAEM.

The focus of this research will be to understand the process of pyrolysis in order to better predict the conditions under which it occurs, and ultimately to develop a model which can accurately predict the pyrolysis process for any given solid fuel.

To address this focus, this dissertation is divided into the following sections:

- *Theory*: In this section the mechanism of pyrolysis is explained, as well as the key differences between South African coals, and coals from the Northern Hemisphere
- *Literature Review*: In this section the various factors that influence the pyrolysis process are investigated. The use of biomass and the rise of biomass in fuel-conversion technologies are investigated. The historical development of kinetic models is also outlined, as well as the advantages and disadvantages of each.
- *Experimental*: In this section details about the experimental procedure and apparatus used to gather data are given.

- *Results and Discussion*: This section presents the data obtained from the modelling process, and compares it to data obtained from the experimental process. It also analyses the data at extreme conditions which are typically experienced in industry.
- *Conclusion and Recommendations*: In this section, key conclusions from the modelling exercise are drawn, and recommendations are made for future and further investigations.
- *References*: This section provides a detailed list of all sources used in the compilation of this dissertation, as well as key research inputs which validate or contradict the results obtained.
- *Appendices*: This section contains the source code of the model used to do the calculations, as well as the data obtained from the experimental section, together with data about the veritability and repeatability of the data, in order to ensure the integrity of the data.

1.5 Summary

This chapter highlighted the importance of coal as a source of energy within a South African context. It also earmarks the use of biomass as a substitute for complete coal dependence, and as a means of meeting environmental impact mitigation goals from CO_2 emissions. The importance of pyrolysis as a pre-treatment step within industry is outlined, as well as the necessity for accurate kinetic data of the pyrolysis process, and what this information implies for further downstream processing parameters. The aims and objectives of the research are detailed, and the modified form of the DAEM is introduced as the preferred model for predicting kinetic parameters of pyrolysis on a South African solid fuel. Lastly, the scope of the dissertation is presented in order to better direct the reader.

Chapter 2: Theory

2.1 Introduction

In this chapter, the concept of pyrolysis is scientifically defined. The mechanism of how this chemical process occurs is detailed, and the use of Thermogravimetric Analyses (TGA) as the preferred tool for kinetic studies is outlined. The various types of TGA machines are explained, and the key differences between South African coals and coals from the Northern Hemisphere are outlined.

2.2 Understanding Pyrolysis

The word 'pyrolysis' is derived from the combination of two ancient Greek words: 'pyros' meaning fire, and 'lysis' meaning to untie. According to Morgan (1991), a concise scientific definition of pyrolysis would thus be the thermal decomposition of a fuel in an inert or oxygen-deficient atmosphere, due to exposure to high temperatures. The basic effect of heating fuel under non-reactive conditions is to convert the fuel into two distinct fractions. A concentrated carbon, solid fraction called the char, and a volatile fraction, rich in hydrogen-compounds consisting of liquids, light gases and tars.

When a solid fuel is exposed to high temperatures in an inert gaseous environment or oxygen-deficient environment, pyrolysis is said to occur. Pyrolysis occurs whenever any solid fuel is burnt, and occurs during combustion, gasification or liquefaction. During pyrolysis, the volatile gaseous matters within the fuel as well as the liquid matter are driven off. The pyrolysis process is thus also known as devolatilization (Gavalas, 1982). The former is then the driving force for the combustion reaction, while the latter forms a mixture of water and tar. The result of the pyrolysis process produces the char, which is a mass of porous, concentrated carbon, which can then be used to produce energy, as in power plant furnaces, or manufacture chemicals as in industrial gasifiers.

Various physical changes occur when the fuel begins to heat. The fuel becomes more porous, as the hydrogen molecules, liquids, moisture and tars are released to the atmosphere and changes to the swelling and softening properties can also occur (Smoot & Smith, 1985). In order to better develop models to predict the pyrolysis process, it is first necessary to understand the mechanism of how pyrolysis occurs.

2.3 The Mechanism of Pyrolysis

Numerous chemical changes to the coal occur during pyrolysis, and as the coal decomposes, the chemical bonds within the various components of the coal are broken down. Work on the pyrolysis of coal carried out by Morgan (1991) has confirmed earlier work carried out by Jüntgen (1984), in which the bond energies of various hydrocarbon compounds found between the aromatic building blocks has been determined. The most common of these hydrocarbon compounds consist of the oxygen, sulphur and methylene bridges. Bond energy values for these hydrocarbons found in coal are given in Table 2.1 below.

Table 2.1: Bond Energies of Various Hydrocarbon Compound (Jüntgen, 1984)

Compound	Bond Energy kJ/mol
Ar-Ar-CH_2—CH_2-Ar-Ar	*210*
Ar-CH_2—CH_2-Ar	*235*
H_3C—CH_3	*349*
Ar-CH_2—Ar	*350*
Ar-CH_2—CH_3	*364*
Ar—CH_3	*382*
C_2H_5—H	*406-410*
H_3C—H	*423-436*
Ar—Ar	*480*
Ar—H	*544*

Wiser (1975) has shown that at temperatures above the onset of pyrolysis (>400°C), breakage of the weaker bonds occurs, resulting in a chain of free radical reactions.

According to Cheong (1977), these primary free radical reactions occurring during pyrolysis can be classified into six categories:

i. **Bond Scission**

These radicals are a highly reactive species. In this reaction, the bonds of larger compounds are broken to produce smaller compounds which participate in further reactions, most notably reactions occurring during the hydrogen abstraction phase. An example of such a reaction is shown below:

$$Ar - CH_2CH_3 \rightarrow Ar - CH_2 \bullet + CH_3 \bullet$$

ii. **Hydrogen Abstraction**

These are alkyl radicals, which rapidly participate in a series of hydrogen abstractions from a neighbouring hydrogen-rich environment. Some new radical species are thus generated through these hydrogen exchanges. Examples of such alkyl radicals are shown below:

$$CH_3 \bullet \text{ and } Ar - CH_2CH_2 \bullet$$

iii. **β-Scission of Longer Chain and Bridge Radicals**

This is similar to bond scission, where longer, more complex radicals are broken up. An example of such is given below:

$$Ar - CH_2CH_2\dot{C}H - Ar \rightarrow ArCH_2 \bullet + Ar - CH = CH_2$$

iv. **Hydrogen Elimination**

During this phase, radicals are capable of eliminating a hydrogen atom to form a double bond, as shown below:

$$Ar - CH_2CH_2 \bullet \rightarrow Ar - CH = CH_2 + H \bullet$$

v. Addition

As double bonds are formed by β-scission or hydrogen elimination, they are vulnerable to attack by surrounding radicals, as can be seen in the example below:

$$CH_3 \bullet + Ar - CH = CH_2 \rightarrow Ar - \dot{C}HCH_2CH_3$$

vi. Recombination

This occurs when two α-radicals combine to form an ethylene bridge.

According to Wiser et al. (1967), the stabilisation of a radical by hydrogen addition will lead to a molecule which, depending on its vapour pressure, will evolve as volatile matter.

The polymerization and condensation reactions occurring via the recombination of both volatile and non-volatile components leads to the formation of a solid char particle. Hydrogen, as well as carbon monoxide (at very high temperatures), are evolved as a result of these condensation reactions. The volatile products formed after stabilisation of the radical components may also undergo secondary gas phase reactions such as cracking or condensation if further exposed to high temperatures. This will result in an increase in the amount of char produced and gases evolved. The pyrolysis process can best be summarised according to Tromp (1987) in Figure 2.1 below.

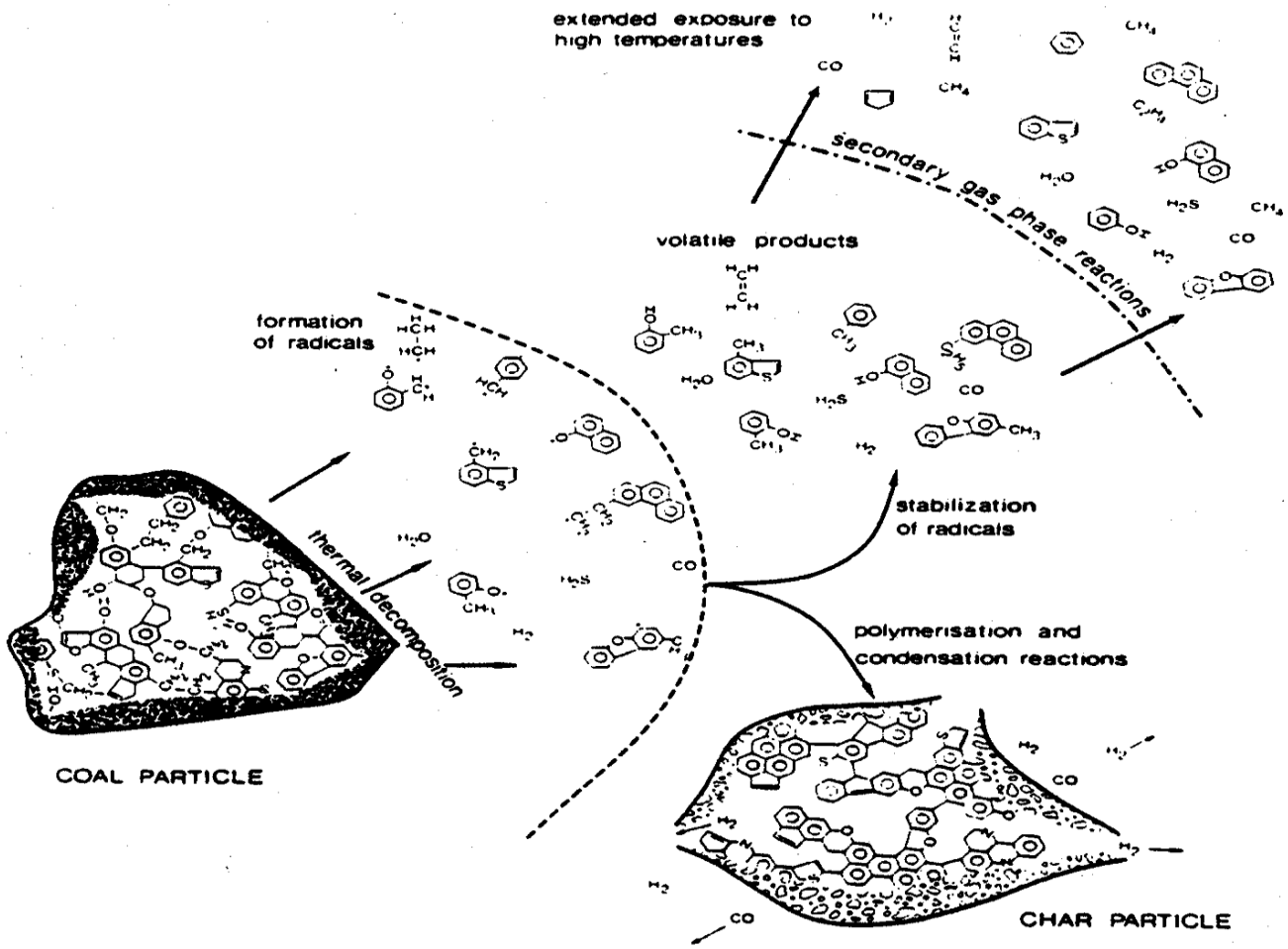

Figure 2.1: Reactions and Processes Which Occur During Coal Pyrolysis (Tromp, 1987)

2.4 The Use of Thermo-Gravimetric Analyses

Thermo-gravimetric analysis is a technique used to determine changes in weight of a known quantity of sample in relation to a change in temperature (Vuthaluru, 2003). The machine used to carry out these analyses is known as a thermo-gravimetric analyser (TGA), which heats a sample up at a constant heating rate and records the weight loss as a function of the temperature. The data obtained from the TGA gives valuable information about the rate at which pyrolysis occurs. Using these results, various thermodynamic data can be obtained or calculated, which can then be used to model the pyrolysis process.

The TGA has become the standard tool for performing basic proximate analyses on coal and biomass samples as well as determining many thermodynamic properties of samples of coal and biomass. There exists numerous prescribed standards for carrying out proximate analyses for coals using TGA from both the American Society for Testing and Materials and the International Organization for Standardization (ASTM D5142 – 09, ASTM D7582 – 10, ISO 17246:2010), respectively. These standards provide a proven method of determining the components present in a sample, and ensure that results can be easily reproduced.

Typically three types of TGA exist (Information extracted from Perkin-Elmer®, Thermal Analysis Software):

I. *Top Loading*
II. *Horizontal Beam*
III. *Bottom Loading*

In a top-loading TGA design, the balance is located below the sample, where it is completely protected from accidental damage and contamination. During an analysis, residues from decomposed products are carried away from the balance and other electronic components.

In a horizontal TGA design, a beam or beams is suspended from the balance mechanism into a furnace assembly. The horizontal design of the system allows for the addition of a DTA/DSC signal. Simultaneous measurements of the DTA/TGA-DSC signals determine whether an endo- or exo- thermic reaction is associated with the weight loss of the sample. The design of the horizontal TG/DTA ensures that the sample is exposed to the identical thermal treatment and environment when comparing the two signals. This gives an accurate and reliable means for performing material characterization.

In a bottom-loading TGA design, the balance is located above the sample. A wire with the sample pan hangs down from the balance into the furnace area. This vertical design provides the best method of ensuring reproducibility of results for highly accurate measurements. The most important feature of this design is the thermal

isolation of the microbalance from the sample and furnace, thus minimizing temperature effects on weight readings.

Numerous authors have published work on the validity of the use of the TGA as an instrument in determining kinetic parameters. These authors such as Feng and Bhatia, (2002), Gomez-Barea and Arjona (2005) and Ollero et al. (2002) to name but a few, have criticised the use of the TGA as an instrument in determining kinetic parameters. They offer numerous reasons why results obtained from thermogravimetric experiments are either inaccurate or do not completely describe the true nature of the reactions occurring within the sample particle. These reasons are attributed to effects such as diffusion, particle size, crucible shape and geometry, and purge gas flow rates amongst others. During the course of this research, every caution was taken to ensure that these effects are either minimised so as to be negligible, or accounted for in the kinetic model of the pyrolysis. Assumptions that need to be considered in the development of the DAEM take into account the limitations experienced by the TGA machine, such as diffusion effects, particle size and heating rate.

2.5 The Unique Nature of South African Coals

Extensive research has gone into understanding the fundamental differences between coals found in the Southern Hemisphere and coals from the Northern Hemisphere. Studies carried out by many authors including Plumstead (1957) and Falcon & Ham (1988), to name but a few have shown the major differences in coals from the two regions as summarized in Table 2.2 below.

In order to understand the specific mechanism by which a South African coal undergoes pyrolysis, it is thus imperative to determine the inherent characteristics that make South African coals unique as compared to coals obtained in the Northern Hemisphere, especially Europe and North America.

Falcon (1986) has done much research into the formation and prevailing geological conditions under which South African coals were formed. The major differences between South African coals and Northern Hemisphere coals as detailed by Falcon (1986) are summarised in Table 2.2.

Table 2.2: Main Features Distinguishing Coals of the Northern and Southern Hemispheres (Falcon, (1986))

Feature	**Northern Hemisphere**	**Southern Hemisphere**
Climate	Hot, Humid, Equatorial	Cold-cool-warm temperate; wet and dry
Plant Growth	Rapid, long continuous growing seasons	Moderate, short growing seasons
Rates of Plant Degradation	Relatively rapid	Slow to moderately rapid
Geological Setting of Coal-bearing basins	Uncompacted deep, rapidly subsiding geosynclines	Relatively stable continental (cratonic and intercratonic) regions
Depositional Condition	Wide coastal lowlands	Fluviatile, lacustrine, deltaic, coastal back-swamps
Geochemical Condition	Predominantly marine	Fresh water, brackish to marine
Plants	Lycopod flora	Glossopterid flora
Factors Inducing Rank	Geothermal heat from deep burial and pressure (regional)	Geothermal heat from crustal fractures and local igneous intrusions (regional and local)

In general, it can be said that South African coals are higher in ash, have a lower amount of volatiles, and are more inertinite-rich than coals from the Northern

Hemisphere (Snyman and Botha, 1993). It is this nature that makes the pyrolysis behaviour of these coals valuable to investigate. And it is these characteristics that influence the utilization of South African coals in the coal-conversion industries. These differences also serve to highlight the importance of not generalising results obtained by American and European researchers to Southern African coals. The coal sample to be used during this research was obtained from the Witbank coalfields, and is typical of coal from that area. The coal used is a low rank bituminous coal, with a moderate to high ash content and moderate to high inertinite content.

2.6 Summary

This chapter outlined the concept of pyrolysis, where it occurs, and what it is useful for. It detailed the chemical mechanism of how pyrolysis occurs, as well as how the TGA is the technique of choice in analysing thermodynamic data for kinetic studies. The types of TGA machines were discussed, with a brief comparison of the different types of configurations.

Also provided, was a brief criticism of the use of TGA for these data by established authors, and the measures that will be taken to ensure that these issues do not affect the experimental results.

The nature of South African coals was also discussed, and the prevailing geological differences that led to its formation were outlined. In order to better utilize South African coals, it is imperative that a thorough understanding of their physical and chemical properties be undertaken so as to better predict the behaviour of these coals.

Chapter 3: Literature Review

3.1 Introduction

There has been an ample amount of research into the effects of the conditions under which the pyrolysis process occurs. Howard (1981), Jones et al. (1964) and Badzioch (1967), to name but a few, provide excellent reviews into the effects of various conditions on the coal behaviour during pyrolysis.

This literature review will summarize the most important results obtained from public domain literature to provide a general view of how varying certain conditions can affect the pyrolysis process.

3.2 Effects of Pyrolysis Conditions on Coal Devolatilization Behaviour

The total amount of the volatiles, as well as the distribution of these volatiles released from coal during pyrolysis are both dependant on the specific conditions utilised during heating. Most notably among these conditions are the effects of:

I. *Temperature*

II. *Heating Rate*

III. *Pressure*

IV. *Particle Size*, and

V. *Pyrolysis Atmosphere*

Each of these conditions will be investigated, and their effect on the pyrolysis process will be analysed.

3.2.1 The Effect of Temperature

Since pyrolysis is initiated by thermal decomposition, it would thus be no surprise that the most important factor influencing the total yield and the distribution of volatile products between gas, liquid and solid phases would be temperature. According to Morgan (1991), in the absence of secondary reactions, the yield of a given component increases with temperature. If secondary reactions occur in the gas phase, the yield may go through a maximum as the consumption reactions dominate over the generation reactions. Howard et al. (1981) and Berkowitz (1985) defined various regimes to describe the progress of pyrolysis with temperature. The exact temperature ranges of these three regimes depend very much on coal type and heating rate. These regimes are detailed as follows:

I) Preliminary Regime

This region occurs between temperatures in the range of ambient conditions up to 350°C. In this region, little or no product evolution occurs other than the devolatilization of inherent moisture present within the coal structure.

II) Primary Phase

This region ranges from temperatures of 350°C up to 600°C. Here evolution of light volatiles and tars occurs with minimal complications of secondary reactions, except for systems wherein primary products remain in contact with a heated environment, as in the case of large particles in a fixed bed.

The bulk of the coal's volatile matter in the form of tars and light oils is generated through the progressive dehydrogenation of hydro-aromatic units, scission of $–CH_2–$ bridges and rupture of acyclic rings. The aromatic character of the solid also increases due to the loss of non-aromatic side chains.

III) Secondary Phase

This region occurs at temperatures between 700°C and 1000°C. In this region secondary reactions inside the particle become largely significant. By this stage, the coal has been converted to a char and is almost completely aromatised. The gases emitted in this regime include H_2 and CO and small amounts of CH_4 and CO_2.

Jüntgen and Van Heek (1977) have made an in-depth study into the rate of gas evolution from coal as a function of temperature at constant heating rates. Typical data obtained using a helium-swept fixed bed at one atmosphere is shown in Figure 3.1 below.

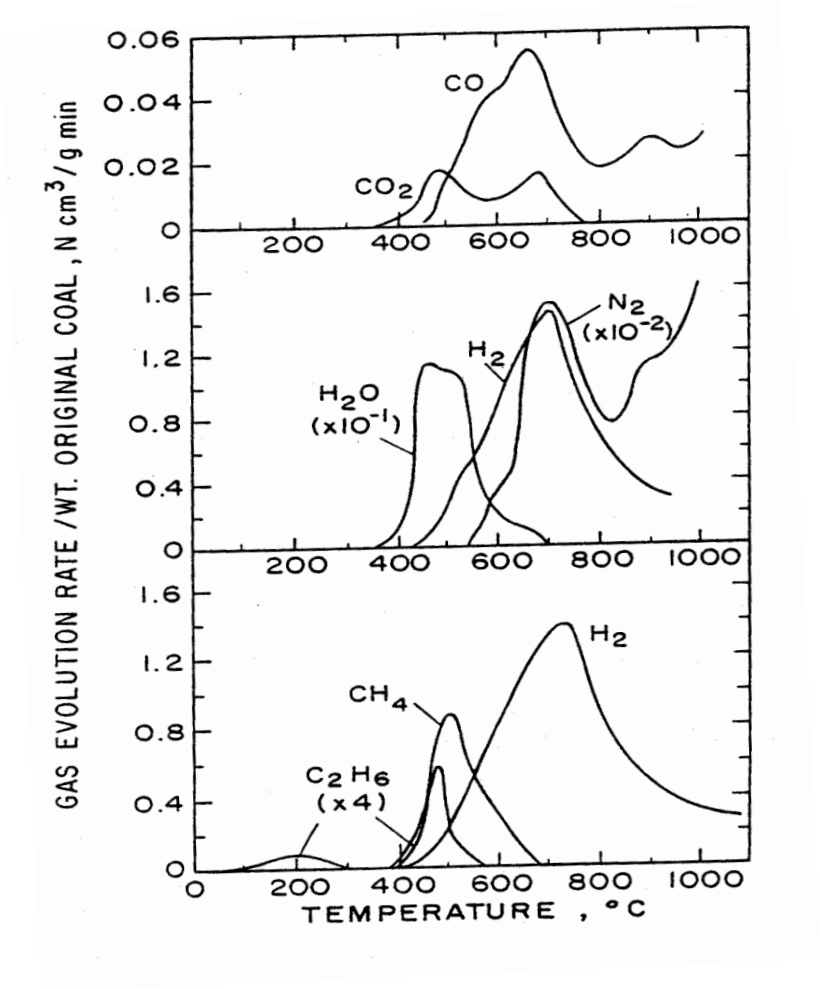

Figure 3.1: Variation of Gaseous Species Evolution vs. Temperature during Pyrolysis at Constant Heating Rate (Jüntgen and Van Heek, 1977)

Suurberg (1977) also focused on the effect that temperature has on the distribution of pyrolysis product distributions. The experiment conducted consisted of the heating of a thin layer of coal on a screen at high heating rates. The conclusions drawn from the experiment were as follows:

The pyrolysis of lignite occurs in five principle stages:

i. Ambient up to 100°C – Low temperature removal of inherent moisture
ii. 450°C up to 600°C – Low temperature CO_2 and hydrocarbon evolution
iii. 600°C up to 700°C – Evolution of pyrolytically formed water
iv. 700°C up to 900°C – Evolution of hydrocarbons, hydrogen and carbon oxides
v. >1000°C – Evolution of carbon oxides

Bituminous coal was found to be different to lignite in that the products evolved are dominated by tars and other hydrocarbons. The pyrolysis of bituminous coal occurs in four general stages:

i. Ambient up to 100°C – Removal of surface moisture
ii. 300°C up to 400°C – Evolution of pyrolytically formed water
iii. 400°C up to 900°C – A broad phase in which the coal softens and tar and hydrocarbons are evolved
iv. > 900°C – Evolution of CO and H_2

This research will utilise a low-rank bituminous coal heated to a maximum temperature of 950°C. The expected behaviour is in keeping with that predicted for bituminous coal.

3.2.2 The Effect of Heating Rate

In contrast to the experiments at low heating rates (rates of up to 10°C/min) conducted during the 1960's, the majority of pyrolysis studies carried out today are done utilizing extremely high rates (in excess of 1000°C/s) not uncommon to fluidized bed reactors. By using low heating rates it was typically found that volatile yields were less than those obtained using the ASTM proximate analysis method (Gavalas, 1982). In this test using the ASTM method, the fuel is heated at 15°C/min to 905°C and held at this temperature for 7 minutes. Higher heating rates thus increased the yield. Loisson and Cauvin (1964) used a heating rate of 1500°C/min to confirm this, and also found that the ratio of tar to gas obtained was higher than that obtained at lower heating rates.

One of the reasons for the higher yield of volatiles at higher heating rates is due to the fact that as heating rate is increased, more pyrolysis of the sample occurs at a higher temperature. The coal structure is thus more disordered at a given temperature and this leads to a more extensive pyrolysis reaction occurring (Gray et al. 1974). Another theory concerns the pressure build-up within the particle. According to Peters and Bertling (1965), at low heating rates the rate of generation of volatiles is lower and so is the internal pressure of the particle. The residence time of volatiles within the particle is therefore longer, allowing more secondary reactions to occur, which results in more char and less tar being formed.

Analysis of the effects of heating rate described in literature indicates that the effects observed could be related to the conditions used to achieve high heating rates, i.e. small, well-dispersed particles which avoid much of the secondary reactions of the volatiles occurring in fixed beds (Howard et al., 1981). This is supported by Anthony et al. (1974), who varied only heating rate between 650°C/min and 10 000°C/min whilst holding all other variables constant. They looked at both softening and non-softening coals and found that the yield of volatiles does not change significantly. This seems to indicate that heating rate alone is not important with regard to volatile yield under the experimental conditions used (small particles in a thin bed).

It thus appears that over a wide range of heating rates, the total yield of products from pyrolysis is independent of heating rate. If volatile yield increases are attributed to an increase in heating rate, it is probably the result of the experimental conditions used in order to achieve faster heating rates.

Anthony et al. (1974) investigated the effect of heating rate on the product distribution from a carbonisation retort. It was found that yields of tar increased at the expense of char and light gas as the heating rate was increased. It was thus concluded that competition occurs between the tar distillation and tar decomposition reactions.

For this research, the heating rate will also be varied, but the range of heating rates used will be in the order of 1°C/min to 100°C/min. These heating rates are sufficiently low that the effects of secondary reactions will not be a factor influencing the pyrolysis behaviour of the fuel.

3.2.3 The Effect of Pressure

Anthony et al. (1974) has confirmed that the total volatile yield in a bituminous coal decreases with an increase in pressure. This is due to an increase in residence time of the volatiles within the particle which results in cracking and carbon deposition. The effects of varying pressure and temperature on the weight loss of a Northern Hemisphere bituminous coal can be seen in Figure 3.2 below.

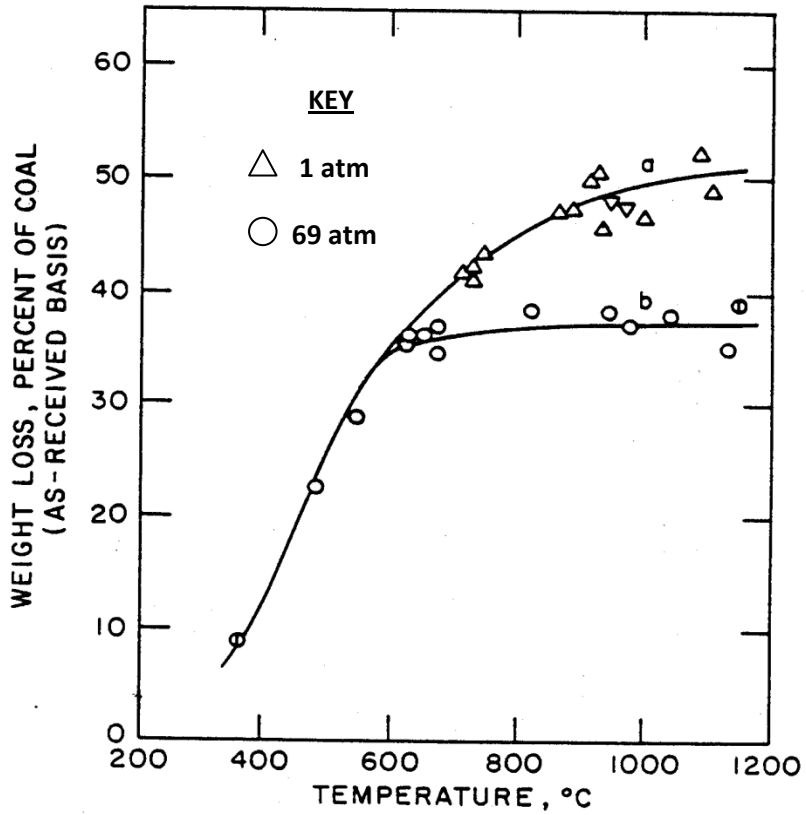

Figure 3.2: The Effect of Temperature on Weight Loss for a Bituminous Coal Heated in Inert Atmosphere at Different Pressures (Anthony et al., 1974)

The figure clearly shows how weight loss percent decreases as the pressure increases.

Suurberg (1977) has studied the effect of composition changes associated with an increase in pressure of up to 60 atmospheres for Northern Hemisphere bituminous coals. The work revealed that pyrolysis under pressure conditions produces more char, less tar, more methane and more carbon oxides. This results from an increase in the residence time of the volatiles within the coal particle and thus an increase in the cracking of tar molecules.

It can thus be seen that higher pressures promote secondary reactions such as, condensation, polymerization, cracking of primary products, and reactions between

some gases in the primary volatile products such as hydrogen and char. This occurs due to a longer residence time within the particle and higher concentrations of volatiles at higher pressures leading to a high rate of secondary reactions. This produces more char and light gases and less tar.

For the nature of this research, pressure will be strictly limited to atmospheric conditions, as the equipment being used cannot operate at higher pressures. It is also beyond the scope of this project, and lays the foundation for the investigation of pyrolysis of South African coals under pressurised conditions.

3.2.4 The Effect of Particle Size

The effects of particle size can be directly related to heat and mass transfer effects. If pyrolysis was chemically controlled, the rate would be independent of particle size or physical structure. Under a given set of conditions, heat and/or mass transfer will become limiting at some critical particle diameter.

Anthony et al. (1974), and Anthony and Howard (1976) conducted experiments with varying particle size over a range from 53µm to 1000µm using a wire mesh heater. The effect of increasing particle size of a bituminous coal resulted in a decrease in weight loss of approximately 3% by weight of the original coal. This result is shown in Figure 3.3 below.

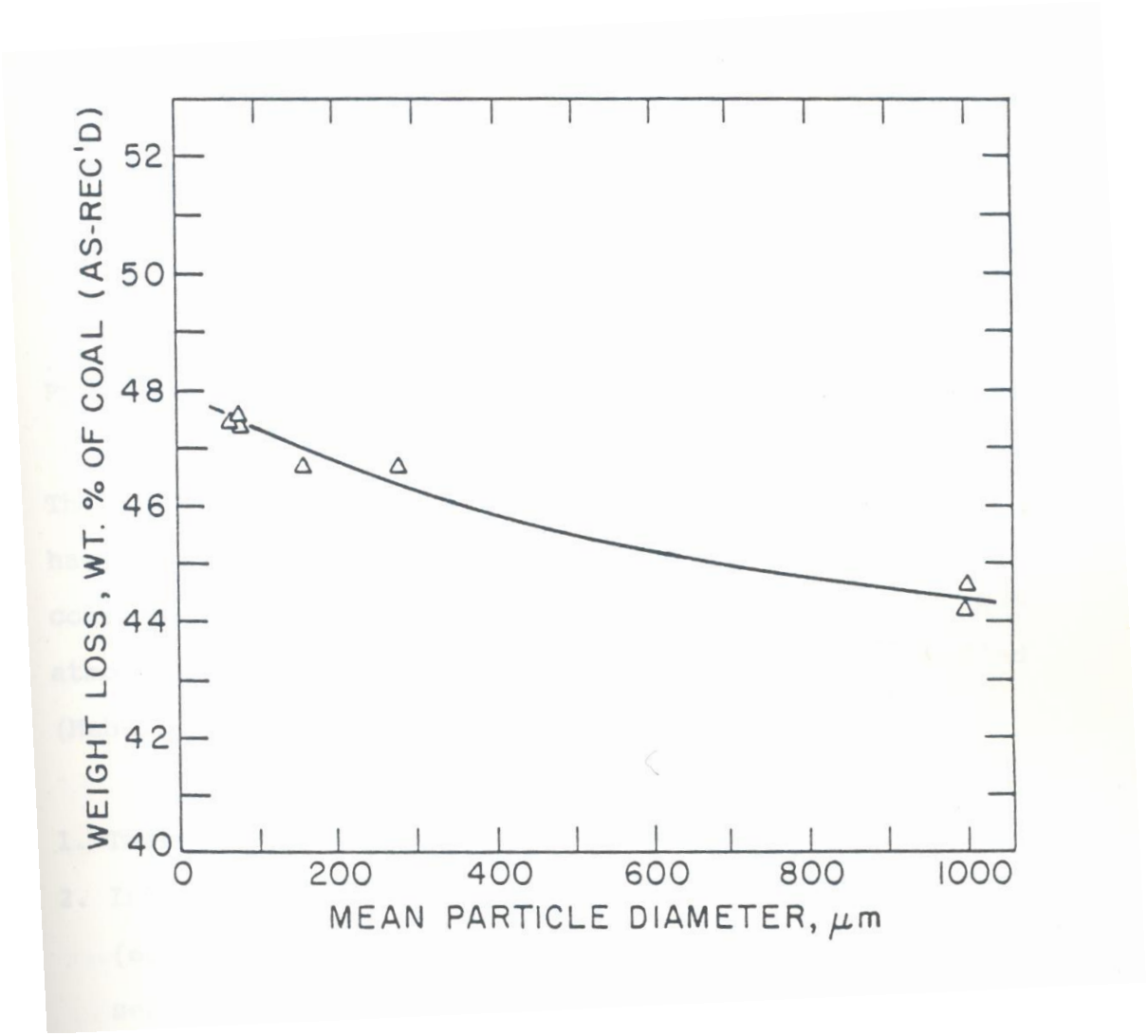

Figure 3.3: Effect of Particle Size on Weight Loss for Bituminous Coal (Anthony et al., 1974)

This was explained by the fact that large particles provide more resistance to volatiles escape, thereby increasing the amount of secondary reactions and resulting in carbon deposition.

The same experiments conducted on lignite, by contrast, showed no significant effect of temperature in the stated range (Smoot and Smith, 1985).

Particle size has been found to have a significant effect on the plastic behaviour of coal in packed beds. Gavrikov et al. (1967) found that the temperature for the onset of plasticity falls and the plastic temperature range increases as the particle size increases. This can have a significant impact on the caking properties of coal.

For the purposes of this study, coal and biomass particles were crushed and sieved to the same size of 0.1mm. It is thus expected that this size fraction will not affect the pyrolysis of the fuel, as secondary reactions will be severely limited.

3.2.5 The Effect of Pyrolysis Atmosphere

The effect of the composition of the pyrolysis atmosphere is important because of the variety of gases that are evolved from the particle. The majority of experimental work has been carried out in inert atmospheres without the complication of reactive gases. According to Mahalingam (1985), in any reactive atmosphere, three distinct processes can be identified:

i. Thermal decomposition (pyrolysis)
ii. Interaction of reactive gas with the pyrolysis products, either in the primary formation stage or through secondary reactions
iii. Combustion or gasification of the fuel by the reactive gas

Walker (1979) suggested that pyrolysis in a reactive environment can be divided into three fundamental steps when the fuel is subject to temperature increases:

a. Release of volatiles
b. A concurrent rapid reaction between reactant gases and the carbon active sites of the char
c. A slow reaction between the reactive gases and the carbon active sites of the char

The volatiles released in (a) can either: decompose, polymerise, react with the gaseous environment, or be effectively quenched.

Walker (1979) postulated that the active sites arise from the removal of functional groups from the periphery of the aromatic and hydro-aromatic structures within

the coal. As decomposition of these groups occur, gases like CO, CO_2, H_2, CH_4 etc. are produced and new active carbon sites on the surface are exposed. These have a high probability of reacting further if a reactive atmosphere is present.

Howard et al. (1981) summarised the effects of pyrolysis in reactive atmospheres by saying, “There is little evidence to suggest that any reactive gas affects the rate of the primary thermal decomposition of coal.” However, all such gases have an effect on the yield and product distribution of the products. This is a result of the reactive gases participating in, or influencing the secondary reactions of the evolved volatiles.

For the nature of this research, the pyrolysis atmosphere will be limited to nitrogen, as this is a highly inert gas and will thus exclude the possibility of secondary reactions occurring via interaction with the volatile matter released.

3.2.6 The Effect of Coal Type

Coal is highly heterogeneous with large differences in chemical and physical structure between different coal types, and often between coals of the same seam. Since coal is a collection of a variety of macerals in varying concentrations, differences may even be found within the same coal type.

Both the physical structure and the chemical structure of coal can affect the pyrolysis process. The physical structure, like for instance the pore structure, affects the accessibility of coal to reactants as well as the transport of volatiles away from the coal. The chemical structure has a direct influence on the yields and nature of the pyrolysis products as well as on the physical structure.

Solomon (1979) performed vacuum devolatilization experiments on 13 American coals using an electrically heated grid apparatus. The gaseous products were analysed by gas chromatography and the liquid tar and solid char products with Fourier Transform Infrared (FT-IR), Nuclear Magnetic Resonance (NMR) and elemental analyses. The major conclusions from this study were:

1. While the mix of gaseous devolatilization products varied from coal to coal, the temperature dependence of the evolution of a particular product was similar for all coals.
2. The tar was similar in organic structure and elemental composition to the parent coal and could be considered as the 'monomer' released from the decomposing coal 'polymer'.

Suurberg et al. (1979) studied the differences in volatile products between lignite and a bituminous coal. The lignite was found to have predominantly oxygenated species whereas the volatiles evolved from the bituminous coal were dominated by hydrocarbons, especially tar. These differences reflect on the differences in the structure of the original coal. What is a significant finding was that the tar yield from the bituminous coal was found to be 23% by weight as compared to 5% for the lignite. This explains the relatively small effect of varying pyrolysis conditions on the devolatilization of a non-softening coal. The larger tar molecules would take longer to diffuse out of the particle and are therefore more susceptible to secondary reactions within the particle, thus affecting the yield and product distribution of volatile products.

Again, for the purposes of this study, the coal used will be a typical South African medium rank C coal. It is thus expected that the pyrolysis behaviour will resemble that of a bituminous coal.

3.3 Biomass: General Characteristics

Biomass can generally be defined as any hydrocarbon material. Some biomass types also carry significant proportions of inorganic species. Sources include various naturally-derived materials, such as woody and herbaceous species, woody wastes (e.g. from forest thinning and harvesting, timber production and carpentry residues), agricultural and industrial residues, waste paper, municipal solid waste, sawdust, grass, waste from food processing, animal wastes, aquatic plants and industrial and energy crops grown for biomass. For political purposes, some other materials (such as tyres, manufactured from either synthetic or natural rubbers) may be included under the general definition of biomass even though the material is not strictly biogenic (Klass (1998) and Hall and Overend (1987)).

Agricultural and forest residues are produced as secondary products of the primary commodity production system. Special attention is given to the production of energy crops. It refers to dedicated crops produced at relatively high photosynthetic efficiency, or high carbohydrate content and other hydrocarbon materials, so as to be used as energy source. A number of most commonly considered agricultural and woody residues, as well as energy crops are listed in Table 3.1 below. The end use for biomasses can influence the management and cultural inputs and practices employed to optimize the production system. Herbaceous species, for example, generally contain more ash than wood, and the ash is higher in alkali metals and silica. The latter combine at high temperature in combustion systems to form slags and deposits that increase maintenance costs.

Table 3.1: Selected Biomass Materials (Diaz, 2006)

Woody Species- Biomass/Fiber/Pulp
Alder (*Alnus spp.)* Beech (*Fagus sylvatica*) Birch (*Onopordum nervosum*) Eucalyptus (*Eucalyptus spp.)* Eastern cottonwood (*Populus deltoids)* Fir (*Douglas fir, White fir*) Maple (*Silver maple*) Oak (*Quercus coccifera, Quercus ilex*) Pine (*Pinus pinea, Pinus halepensis, Pinus brutia, Pinus pinaster*) Poplar (*Populus spp.)* Spruce (*Picea glauca*) Willow (*Salix spp.)*
Herbaceous Species- Biomass/Fiber/ Energy grain
Jose Tall wheatgrass (*Agropyrum elongata*) Miscanthus (*Miscanthus spp.)* Napier grass/Banagrass (*Pennisetum purpureum*) Spanish thistle or Cardoon (*Cynara cardunculus*) Spring barley (*Hordeum vulgare*) Switchgrass (*Panicum virgatum L.)* Triticale (*Triticosecale*) Winter wheat (*Triticum aestivum*)
Herbaceous Species- Sugar/Starch/Biomass
Buffalo gourd (*Curcurbita foetidissima*) Cassava (*Manihot esculenta*) Jerusalem artichoke (*Helianthus tuberosus*) Sugar/Energy cane (*Saccharum spp.)* Sugar/Fodder beet (*Beta vulgaris*) Sweet sorghum (*Sorghum bicolor*)
Other Agricultural Residues
Almond shells Corn stalk Grape residues Nutshells Olive husks and stones Rice husks

3.3.1 Structure, Composition and Properties of Biomass

Understanding of the chemical structure and major organic components in biomass is extremely important in the development of processes for producing derived fuels and chemicals. Biomass has a complex chemical composition, and both organic and inorganic constituents are important to the handling and conversion processes.

The dominant structural compounds making up plant biomasses are cellulose (C6 polymers), hemicellulose (predominantly C5 polymers but including C6 species) and lignins. Organic compounds in biomass also include extractives, non-structural compounds mostly soluble in water and/or various organic solvents (fatty acids, lipids, terpenoids, phenolic compounds, glycosides, proteins, triglycerides, terpenes, waxes, cutin, suberin, flavonoids, betalains, alkaloids). Plants accumulate inorganic materials sometimes in concentrations exceeding those of hemicellulose or lignin. The concentration of the ash arising from these inorganics changes from less than 1% in softwoods to 15% in herbaceous biomass and agricultural residues (Yaman, 2004). Cellulose is a linear crystalline polysaccharide, with general formula $(C_6H_{10}O_5)_n$. It serves as the framework substance, making up 40-50% of wood. The polymer is formed from repeating units of cellobiose, a disaccharide of β-linked glucose moieties as can be seen in Figure 3.4 below.

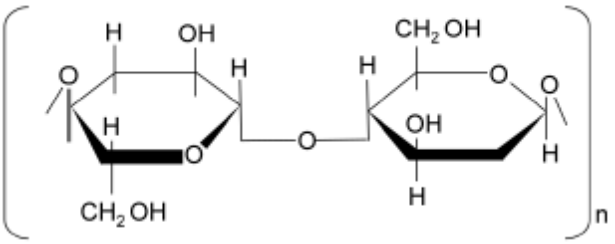

Figure 3.4: Cellobiose, the repeating unit of Cellulose (Salisbury & Ross, 1992)

Hemicelluloses are matrix substances between cellulose microfibrils. They are polysaccharides of variable composition containing both five (including xylose and arabinose) and six carbon monosaccharide units (including galactose, glucose, and mannose). Hemicelluloses constitute 20 to 30% of wood and other biomasses, generally with higher concentrations in hardwoods than softwoods. Partial structures

for the primary forms of hemicellulose in hardwood and softwood are shown in Figure 3.5 below.

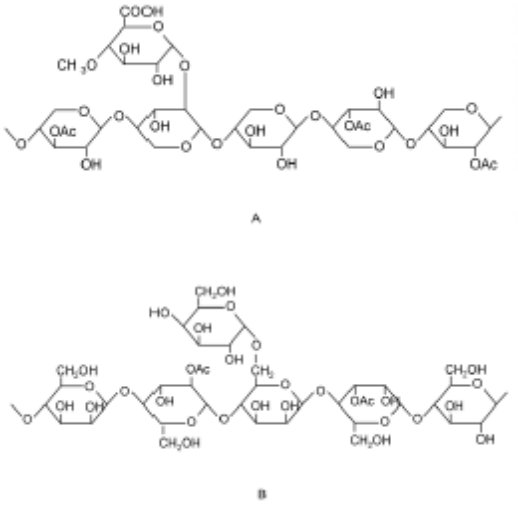

Figure 3.5: Partial Structures of the Principle Hemicelluloses in Wood (Salisbury & Ross, 1992)

O-acetyl-4-O-methylglucuronoxylan from hardwood (A) and O-acetyl-galactoglucomannan from softwood (B). Ac=acetyl group.

The most abundant monomeric unit of hemicellulose is xylan.

The lignins are highly branched, substituted, mononuclear polymers of phenylpropane units, derived from coniferyl, sinapyl, and p-coumaryl alcohols. They are often bounding to adjacent cellulose fibers to form a lignocellulosic complex. The structure varies among different plants. Softwood lignin is composed principally of guaiacyl units stemming from the precursor trans-coniferyl alcohol. Hardwood lignin is composed mostly of guaiacyl and syringyl units derived from trans-coniferyl and trans-sinapyl alcohols. Grass lignin contains p-hydroxyphenyl units deriving from trans-p-coumaryl alcohol. Almost all plants contain all three guaiacyl, syringyl, and p-hydroxyphenyl units in lignin. A partial structure of softwood lignin is shown in Figure 3.6 below.

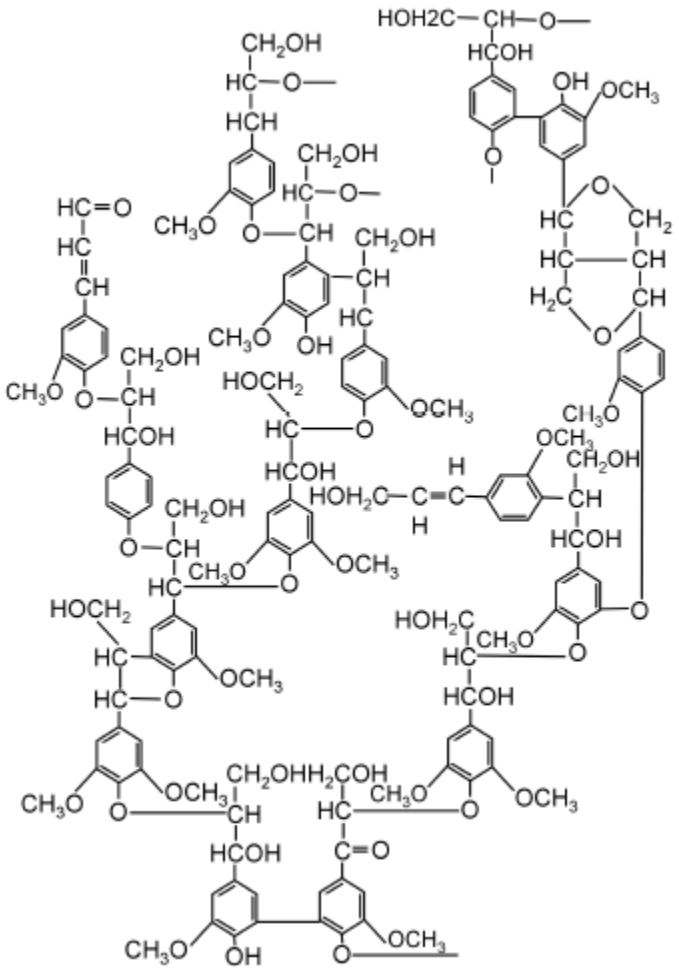

Figure 3.6: Partial Lignin Structure of Softwood (Salisbury & Ross, 1992)

The lignin contents on a dry basis generally range from 10% to 40% by weight in various herbaceous species (Yaman, 2004).

3.3.2 Biomass Thermochemical Conversion

Figure 3.7 below illustrates a few of the numerous possible pathways for generating energy and products from biomass resources.

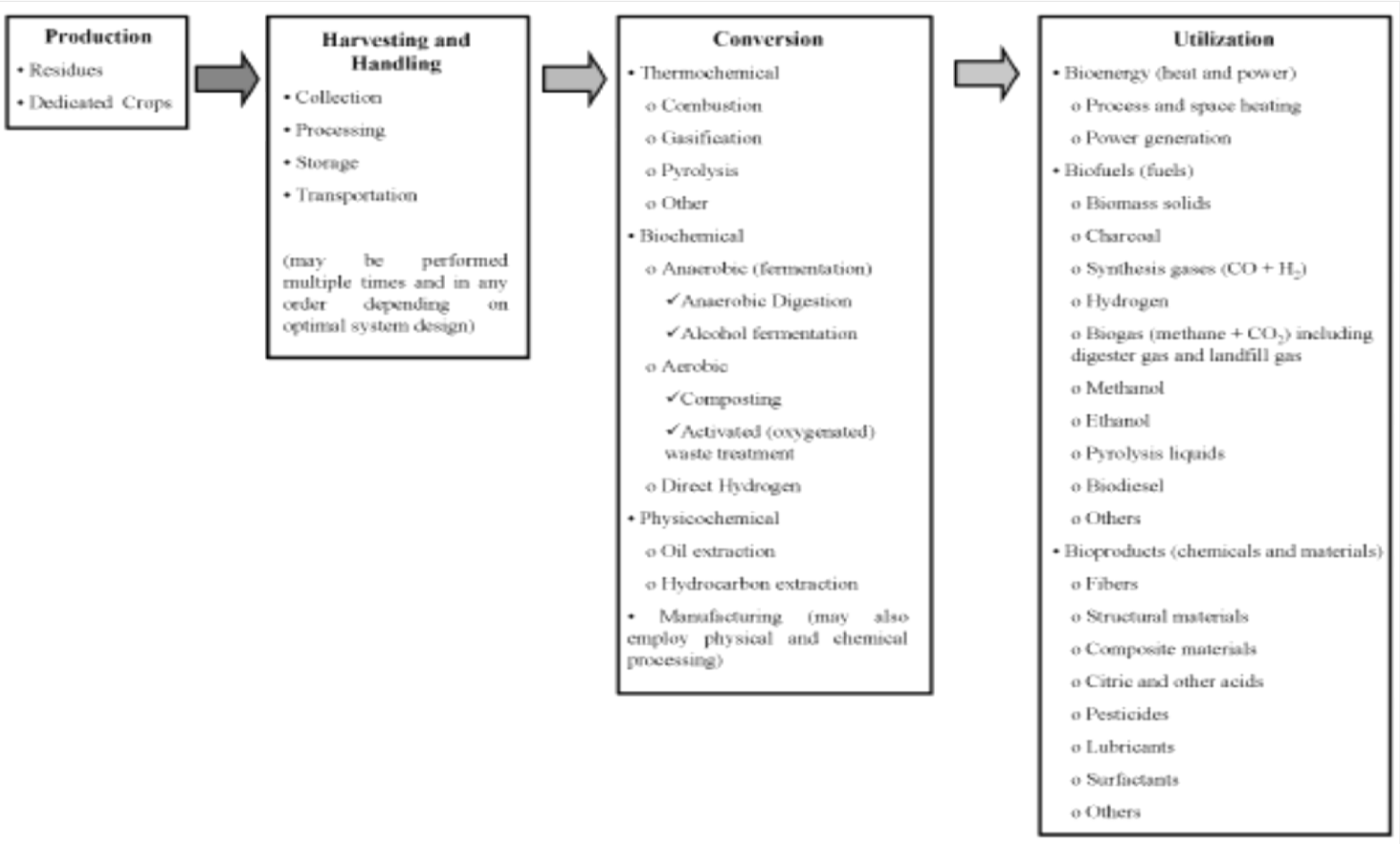

Figure 3.7: Biomass Processing Options (Adapted from Klaas (1998) and Hall & Overend (1987))

Three principal routes exist for converting biomass:

1) Thermochemical
2) Biochemical and
3) Physicochemical

In practice, combinations of two or more of these routes may be used.

Thermochemical conversion includes combustion, thermal gasification, and pyrolysis along with a number of variants involving microwave, plasma arc, supercritical fluid, and other processing techniques. Products include heat, fuel gases, liquids, and solids. Biochemical and physicochemical processes are in general more intended to upgrade biomass components and produce higher value products. Thermochemical routes can also be used in this case, as in the indirect production of methanol via gasification. The conversion strategies are integrally coupled to the properties of the biomass. In many cases, the properties of the biomass necessary for engineering design have not been properly characterized prior to commercial implementation of a technology.

According to the International Energy Agency, current electricity demand in South Africa as at 2008, was estimated at approximately 232.23 TWh of energy per year, and is produced by 92% of fossil fuels, all of which is coal. The contribution of renewable energies remains relatively low, at less than 1% in 2004 (Matsumoto & Nakata, 2007). This is shown in Figure 3.8 below.

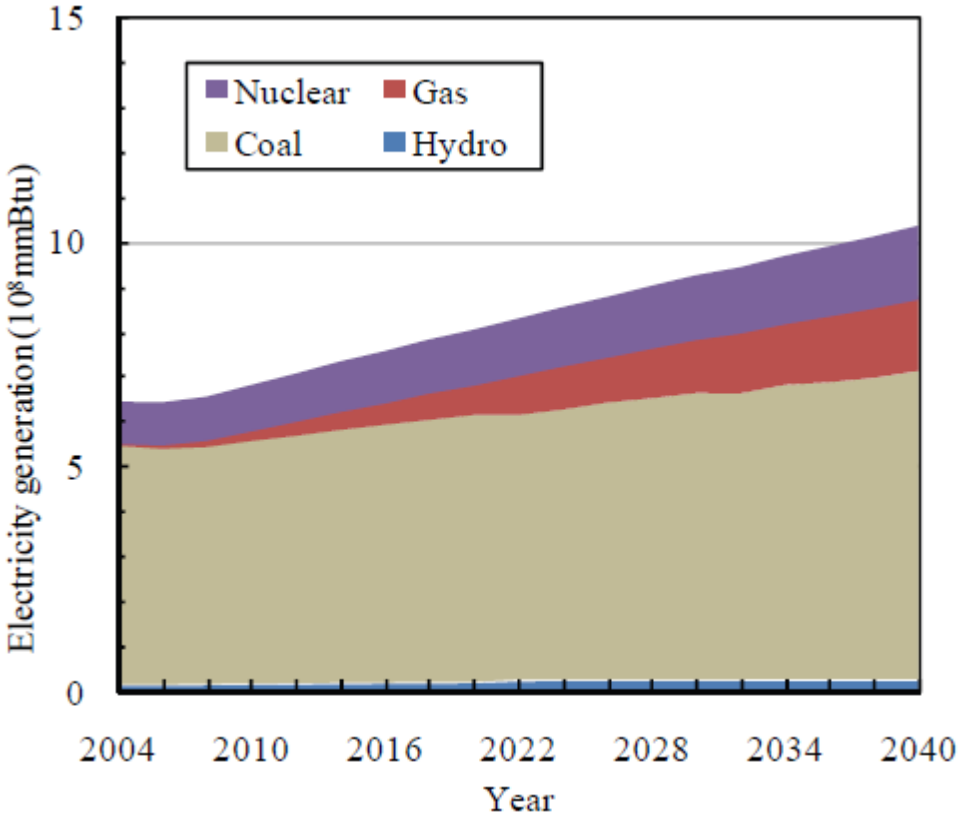

Figure 3.8: Electricity Generation by Resource in South Africa (Matsumoto & Nakata, 2007)

Burning fossil fuels causes greenhouse gas emissions. CO_2 emissions could, if prevailing trends persist, actually exceed 2004 levels by more than 50% by 2040 as can be seen if Figure 3.9 below

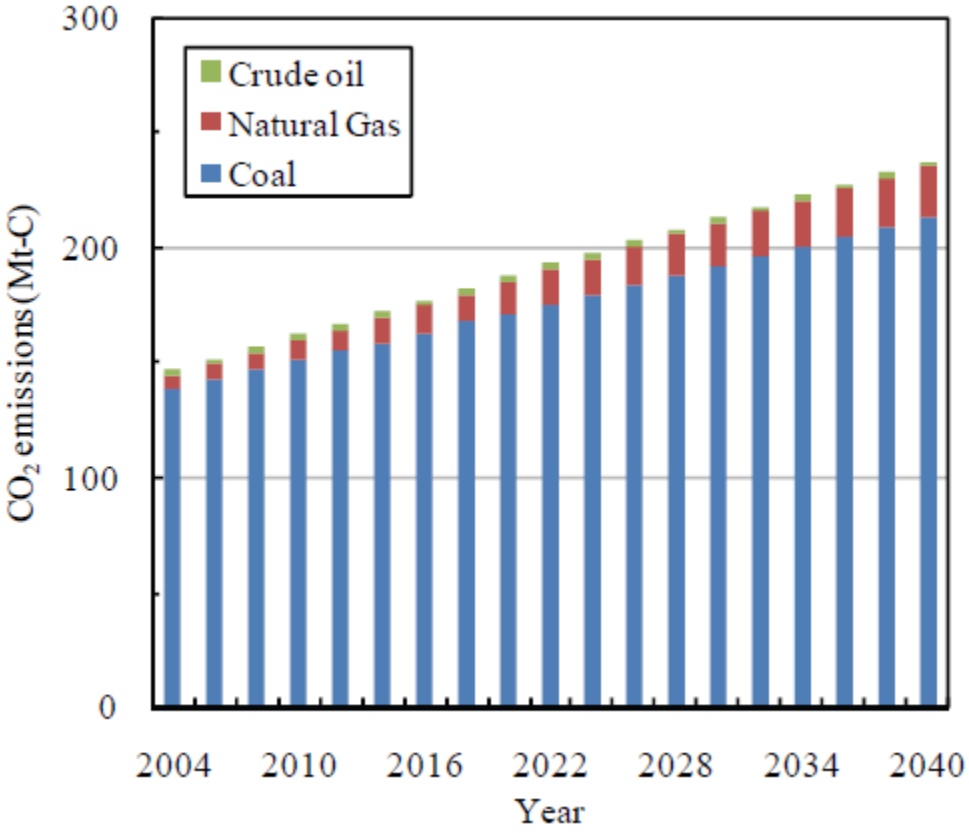

Figure 3.9: CO_2 Emissions Projection for South Africa (Matsumoto & Nakata, 2007)

These emissions, if unchecked, could result in major economic impacts to South Africa's energy economy, resulting in increased carbon trading and more expenditure on expensive, end-of-stack technologies in order to mitigate the added burden of flue gas cleanup strategies.

3.3.3 Energy Potential of Biomass

It is manifested that 'bio-energy' (energy from biomass and waste) has the highest contribution amongst all renewable materials towards reducing a country's carbon footprint and also fossil fuel dependence. Bio-energy is globally recognized as the renewable resource that will make the most significant contribution for sustainable energy in the near to medium term (Maniatis et al., 2002) due to its carbon-neutral lifespan. This is the only renewable resource that can directly replace fossil fuel based energy (Diaz, 2006). The use of biomass as fuel in substitution of fossil

resources results in low sulphur dioxide emissions and almost no net atmospheric carbon emissions, and hence serves to mitigate greenhouse gas and global climate change impacts (Kaltschmitt & Dinkelbach, 1997). Besides, upgrading of biomass represents an attractive way of use of agricultural and forestry residues that could renovate rural economies. Biomass crops can also be used for the restoration of degraded or deforested lands (Berndesa et al., 2003). Biomass production also serves to store solar energy, thus allowing continuous power generation.

However, the current use of renewable sources for energy production is limited to an extent, which is considerably lower than their potential (Diaz, 2006). In nearly all of the EU-countries less than 50% of the available biomass resources are currently used (Maniatis et al., 2002). In most countries, like South Africa, the share is even lower. This is mainly due to relatively high costs of the technologies of upgrading. The investment costs can be twice as high as compared to fossil-fired plants (the low energy density requires larger plant sizes, the wide variety of fuel characteristics and the objective to achieve a clean combustion require higher efforts in conversion and cleanup technology). Furthermore, a reliable market for biofuels has not yet been established that ensures availability of biofuels for customers (Maniatis et al., 2002). There is a public demand for use of biomass on a large scale above the current level. This can only be carried out, if biomass is processed in a way that makes this energy carrier fit into the South African energy system much better on the one hand and achieve a higher value and hence higher prices on the other hand. Modernized bio-energy systems are suggested to be important contributors to future sustainable energy systems and to sustainable development in industrialized countries as well as in developing countries like South Africa (Berndesa et al., 2003).

3.3.4 Challenges of Thermochemical Technologies

i. Combustion

Historically, and still so today, the most widely applied conversion method for biomass is combustion. The chemical energy of the fuel is converted via combustion into heat energy which may be transformed by heat engines into mechanical and

electrical energy. Direct combustion of biomass is not favoured by too high content of moisture, and lower density than that of coal, leading to important economic limitations (Diaz, 2006). The energy efficiency associated to the process is mostly lower than that obtained from a combined cycle gasification plant.

ii. Gasification

Gasification is a partial thermal oxidization, which results in a high proportion of gaseous products (carbon dioxide, water, carbon monoxide, hydrogen, gaseous hydrocarbons), small quantities of char (solid product), ash and condensable compounds (tars and oils) (Diaz, 2006). Steam, in addition to air or oxygen, is supplied to the reaction as oxidizing agents. Reaction conditions can be varied to maximize the production of fuel gases, fuel liquids, or charcoal. The term gasification is applied to processes that are optimized for fuel gas production (principally CO, H2, and light hydrocarbons). There is renewed attention to gasification due to the possibility to produce synthesis gas and subsequently liquid biofuels or hydrogen. The eventual markets for such bio-products are enormous on a global scale (Maniatis et al., 2002).There are, however, still two main problems that hinder the reliable and trouble-free operation of this technology:

a) A thorough systems approach to a gasification facility that will address all individual sub-systems as well as their interaction as a whole, and

b) The gas cleaning with the main problem the efficient and economically viable tar elimination

Gasification is characterized by a continuous and constant operation of all subsystems from the material feeding to the generation of power and/or heat, and unless all subsystems operate efficiently the gasification plant is rendered inoperable.

Indeed areas such as constant feeding, fouling of heat exchange surfaces, tar elimination, wastewater treatment, disposal of effluents and emissions of NO_x continue to present barriers to trouble-free optimum operation.

iii. Pyrolysis

Pyrolysis of biomass can be described as the direct thermal decomposition of the material in the absence of oxygen to obtain an array of solid, liquid and gas products. Conventional pyrolysis consists of the slow, irreversible, thermal decomposition of the organic components in biomass. Slow pyrolysis has traditionally been used for the production of charcoal. Short residence time pyrolysis (fast-, flash-, rapid- or ultra-pyrolysis) of biomass at moderate temperatures has generally been used to obtain high yield of liquid products. Fast pyrolysis is characterized by high heating rates and rapid quenching of the liquid products to terminate the secondary conversion of the products (Yaman, 2004).

The solid products from pyrolysis contain char, ash and unchanged biomass material. The pyrolysis conditions determine the chemical composition of those products. As a renewable fuel, charcoal has many attractive features: it contains virtually no sulphur or mercury and is low in nitrogen and ash; it is highly reactive yet easy to store and handle. Carbonized charcoal can be a good adsorbent with a large surface area and a semimetal with an electrical resistivity comparable to that of graphite. Recent advances in knowledge about the production and properties of charcoal presage its expanded use as a renewable fuel, reductant, adsorbent, and soil amendment (Yaman,(2004); Antal & Grønli, (2003)). Heating values of the chars obtained from pyrolysis are comparable with those of lignite and coke, and the heating values of liquids are comparable with those of oxygenated fuels, such as CH_3OH and C_2H_5OH, which are 40 - 50% of that for hydrocarbon fuels. The heating value of gases is comparable with those of producer gas or coal gas and is much lower than that of natural gas. The heating values of the products are functions of the initial composition of the biomass (Yaman, 2004). The use of biomass for materials can be expanded to new applications. For example, biomass can be used further as a carbon neutral alternative for coal and coke in the iron and steel industry. Biomass can also be used as a renewable carbon feedstock in the production of synthetic organic materials such as basic chemicals, plastics, paint and solvents (Hoogwijk et al., 2003).

3.4 Summary of the Effects of Pyrolysis Conditions

As discussed throughout this chapter, the pyrolysis of coal and biomass provides two valuable products, the char and the volatile products. It was also shown that various factors can influence the pyrolysis behaviour of a coal. These effects on the yield of volatiles and the reactivity of the char are best summarised in Table 3.2 below.

Table 3.2: Summary of Effects of Pyrolysis Conditions

Condition	***Yield***	***Reactivity***
Increase in Temperature	Increase in total yield	Decrease in reactivity at high temperatures due to annealing
Increase in Heating Rate	Increase in yield at very high rates. Less of an effect on non-softening coals	High heating rates produce a more porous char with more active sites The char is thus more reactive Non-softening coals do not swell resulting in less change in their porosity
Increase in Pressure	Increases in pressure increase the residence time of volatiles within the particle Secondary reactions increase the amount of char and light gases and reduce the amount of tar produced Less of an effect on non-softening coals	Due to secondary reactions and carbon deposition in the pores, reactivity is decreased at high pressures Non-softening coals have less tar so the effect is less pronounced
Increase in Particle Size	Closely associated with heat and mass transfer within the particle If either of these are limiting, yields will be lower at a particular temperature Larger particles also mean longer residence times and more opportunity for secondary reactions	Besides heat and mass transfer problems in large particles, carbon deposition in the pores as a result of secondary reactions, can reduce the reactivity of the char

The effects observed in Table 3.2 seem to be more prevalent in bituminous coals which soften on heating and release large amounts of tar, than other types of coals. The softening of the coal and the mode of volatile release by means of bubbles of volatiles

in the molten coal causes large changes in the physical structure on heating. These coals are thus more susceptible to changes in pyrolysis conditions. The high tar concentrations increase the occurrence of secondary reactions within the coal particle as a result of longer residence times within the particle.

Non-softening coals, on the other hand, contain a high percentage of the maceral inertinite which describes the stability of this type of coal during pyrolysis. The pore structure of these coals remains relatively unchanged during pyrolysis. Changes in pressure and heating rate thus have little effect on the internal structure and reactivity of the char. Variations in temperature are important since pyrolysis is a thermally initiated process. Reactivity of the char may also be affected by high temperatures as a result of thermal annealing. Non-softening coals have less volatile matter and the effects of secondary reactions are therefore much less resulting in total yields and product distributions being less sensitive to pyrolysis conditions. This is supported by Llewellen (1973) who found that the total product yields from non-softening coals did not vary over a wide range of pressures and heating rates.

3.5 Summary

This chapter outlined the various conditions that affect the pyrolysis process, as well as the extent to which these effects affect the pyrolysis behaviour of coal and biomass. The types of biomass were also explained, as well as the expected role that biomass will play in minimizing South Africa's coal dependence and offsetting it's CO_2 emissions. The development of biomass conversion technologies using pyrolysis conditions was also examined and the details were provided.

Chapter 4: Development of Pyrolysis Models

4.1 Introduction

In this chapter, the current state of kinetic modelling for coal and biomass, using thermogravimetry, is discussed. The historical development of kinetic models, and the advances made by contributing researchers to better and more comprehensively describe the pyrolysis process is outlined. These models range in complexity, from the simplest, elementary descriptions, to the more complex and computationally intensive. Examples of these models can be found in the literature, and are commonly named after the researcher who first proposed them, such as the Coats-Redfern (1964) model, Ozawa (1965) model or the Friedman (1964) model.

4.2 Experimental Studies of Coal Pyrolysis Models

Smoot and Smith (1985) reviewed papers by Anthony and Howard (1976) , Howard (1981), and to a less general extent, Horton (1979), Wendt (1980), and Solomon (1980). These researchers provided reviews of coal pyrolysis over the period from 1960 to 1980. Anthony and Howard (1976) also note several reviews of pyrolysis research over the period from 1963 to 1972.Most of these works have emphasized finely pulverized coal particles at high temperatures. According to Anthony and Howard (1976), significant pyrolysis does not start until temperatures of 625 K-675 K are reached. The heating causes thermal rupture of bonds, and volatile fragments escape from the coal. Table C1 in Appendix C, obtained principally from Anthony and Howard (1976), provides a detailed summary of much of the experimental methods and test conditions of previous studies of pyrolysis.

4.3 Pyrolysis Models

Currently many models exist to predict the kinetic parameters of the pyrolysis process. They range in complexity, and find different applications for different conditions. These models are usually variations of the underlying mathematics that describe them. This will be discussed in subsequent sub-sections.

The use of thermo-gravimetric data to evaluate kinetic parameters of solid-state reactions involving weight loss (or gain) has been investigated by a number of authors and has led to the development of numerous models as will be discussed below. Smoot and Smith (1985) and Gavalas (1982) provide a detailed review of these researchers and their respective models.

Some of the earliest work regarding coal devolatilization kinetic studies was carried out by Freeman and Carroll (1958). These researchers have stated some of the advantages of this method of utilizing finely pulverized coal particles over conventional isothermal studies. To these reasons may be added the advantage of using one single sample for investigation. However, the importance of procedural details, such as crucible geometry, heating rate, pre-history of sample, and particle size, on the parameters has yet to be fully investigated. It is also necessary to ensure accurate temperature measurement, both for precision and also to detect any departure from a linear heating rate due to endo- or exo- thermal reactions.

Descriptions of the most popular models used to model the pyrolysis process are discussed in the following section. These descriptions depend largely on the underlying mathematics that describes weight loss as a function of temperature and rate. The various models suggested by various researchers in the literature are all variations or more complex mathematical representations of the pyrolysis reaction.

4.3.1 Single First Order Reaction Model

The first model developed to predict the results of TGA analyses was provided by Coats and Redfern (1964). This simplistic model, named the Coats-Redfern model, makes use of the Arrhenius expression to correlate the rate of mass loss with temperature. Subsequent work by other authors has shown that this model predicts the kinetic parameters fairly well for a single, first order reaction, but is inadequate to describe more complex fuels according to Braun and Burnham (1987). This simplistic model assumes that the devolatilization process can be represented by the reaction as shown by Arenillas et al. (2001):

$$\text{fuel} \xrightarrow{k_1} X\ \textit{(volatiles)} + (1\text{-}X)\ \textit{(char)}$$

This can be written mathematically as:

$$\frac{dv}{dt} = k_1(v_\infty - v) \tag{1}$$

where X is the volatile fraction (or alternatively, dv/dt represents the rate of volatile release) and k_1 is the rate constant given by the Arrhenius equation:

$$k_1 = A_1 \times e^{\left[\frac{-E_1}{RT}\right]} \tag{2}$$

This treatment of the rate of reaction required a method for relating the amount of 'total' volatile matter, v_∞ to that obtained from proximate analyses. The correlation used was:

$$v_\infty = Q(1 - v_c)v_p \tag{3}$$

The parameters *Q* and v_c were empirically determined, although a value of 0.15 for v_c was suitable for all of the non-swelling coals tested by Coats and Redfern (1964). This description of the mass loss of volatiles is a satisfactory single-step reaction to describe pyrolysis.

The Coats and Redfern (1964) model lacks the flexibility required to describe much of the experimental data available, and, according to Smoot and Smith (1985), may be inadequate to describe non-isothermal pyrolysis. The fact that the parameters v_p, *Q*, v_c, *A*, and *E* may depend upon the specific type of coal used also tends to limit the generality of this model.

Arenillas et al. (2001) then applied the assumption that the devolatilization occurs as a single step, which thus allows the reaction rate to be modelled using:

$$\frac{dX}{dt} = k_1(X^* - X)^n \tag{4}$$

Where *X** represents the volatiles released at complete decomposition, and n is the reaction order.

Upon integration of equation (4) for a single order reaction (n=1), Deng et al. (2007) have shown that, for non-isothermal heating at a constant heating rate, the resultant integral becomes:

$$ln\left[\frac{-\ln(1-\alpha)}{T^2}\right] = ln\left[\frac{AR}{\varphi E}\left(1 - \frac{2RT}{E}\right)\right] - \frac{E}{RT} \tag{5}$$

Where φ is the constant heating rate in °C/min, and α is the degree of conversion, defined in each decomposition stage as $\frac{m_s - m}{m_s - m_f}$, in which m_s, m_f and m represent the initial, final and instantaneous mass of sample, respectively.

By assuming that the right hand side of equation (5) has a constant heating rate, Deng et al. (2007) have shown that plotting $ln\left[\frac{-\ln(1-\alpha)}{T^2}\right]$ versus $\frac{1}{T}$, yields a straight line with a gradient of $\frac{-E}{R}$.

Thus by substituting in experimental data obtained from the TGA into equation (5), it allows for the solution of *E* and *A* by performing a least-squares fit on the data that minimises the error between α obtained using equation (5) and actual experimental data for α.

Braun and Burnham (1987) have offered some short-comings of the Coats-Redfern model, stating that generally a single first-order reaction does not accurately fit a reaction with a non-zero sum of squared errors. They proposed that an n^{th} order reaction works quite well, but the effective kinetic parameters then become a function of the relative error, and either temperature (if non-isothermal) or heating rate.

Gavalas (1982) stated that the use of the Single First Order Reaction model is only best when used for crude estimates and comparisons, as the values obtained for A and E vary largely and often span several orders of magnitude. Gavalas (1982) concluded that this large variability arises from the forcing of the results of experimental data into an arbitrary kinetic mould. The work done by researchers like Coats and Redfern (1964) helped lay the foundation for a more in-depth mathematical description of the pyrolysis reaction kinetics, and would lead to the development of more complex and comprehensive models.

4.3.2 Parallel First Order Irreversible Reactions Model

This model built on the earlier work done by Coats and Redfern (1964), to provide a more realistic description of the pyrolysis process.

Kobayashi et al. (1977) suggested that pyrolysis could be modelled with the following pair of parallel, first-order, irreversible reactions:

$$\text{fuel} \xrightarrow{k1} Y_1V_1 \textit{ (volatiles)} + (1\text{-}X_1)S_1 \textit{ (char)}$$

$$\text{fuel} \xrightarrow{k2} Y_2V_2 \textit{ (volatiles)} + (1\text{-}X_2)S_2 \textit{ (char)} \quad (6)$$

With the rate equations $dc/dt = -(k_1+k_2)c$ (7)

And $$\frac{dv}{dt} = \frac{dv1+dv2}{dt} = (Y_1k_1 + Y_2k_2)c \quad (8)$$

Here, as in the single reaction model, both k_1 and k_2 are Arrhenius-type coefficients.

An important feature of this Parallel First Order Irreversible Reactions model is that $E_1<E_2$. This approach satisfactorily correlates the data of Badzioch et al. (1970), Kimber and Gray (1976) and Kobayashi et al. (1977) obtained under conditions of transient temperature as illustrated in Figure 4.1 below.

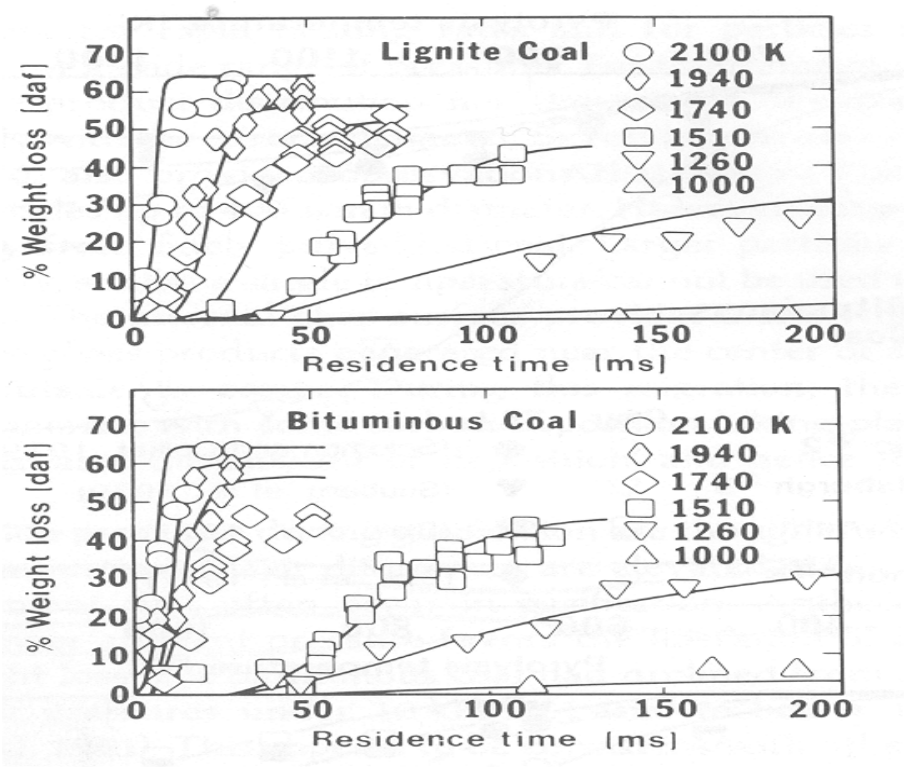

Figure 4.1: Comparison of Calculated Weight Losses with Experiments for Pyrolysis of Lignite and Bituminous Coals (Kobayashi et al., 1977)

From the figure 4.1, it can be seen that by using equations (2) and (8), values of Y_1=0.3, E_1=104.6 MJ/kmol, A_1= 2x10^5 s^{-1}, Y_2=1.0, E_2=167.4 MJ/kmol and A_2=1.3x10^7 s^{-1} are obtained.

This model is conceptually sound in that the variation in volatiles yield with temperature is explained by a second reaction rather than by a correlating parameter like that of equation (3). As in section 4.2.1, the general use of this model may be limited because the parameters Y_1, Y_2, A_1, A_2, E_1 and E_2 will depend on the specific coal used. The defining difference in these researchers' works is the assumption that the coal used is a single entity, undergoing pyrolysis at a single rate. This view was challenged by contemporary researchers like Pitt (1962).

4.3.3 Several First Order Reactions Models

A conceptual improvement in the modelling of weight loss was made by Pitt (1962) who treated coal as a collection of an infinite number of species decomposing by parallel and independent first order reactions. The rate constants were assumed to have a common *A*-factor but different activation energies, varying in range from E_{min} to E_{max} according to a probability density function *f(E)*. Thus *f*(E) *d*E is the weight fraction of volatile precursor species with rate constants having activation energies in [E, E+*d*E].

Under isothermal conditions the total weight loss is given by:

$$W_v(t) = W_v^* \int_{Emin}^{Emax} f(E)\{1 - \exp\left[-tAe^{\left(-\frac{E}{RT}\right)}\right]\}dE \qquad (9)$$

According to equation (9), $W_v \rightarrow W^*_v$ as $t \rightarrow \infty$, independently of temperature.

However, since the pyrolysis is time-limited in practice, the calculated ultimate weight loss will be temperature dependant in agreement with the experimentally observed behaviour.

Equation (9) can be viewed as an integral equation relating the unknown function f(E) to the experimentally measured function $W_v(t)$. Pitt (1962) was able to solve this equation using an approximate technique that utilized weight loss data from the pyrolysis of a high volatile bituminous coal at temperatures from 300°C to 650°C and times of 10 seconds up to 100 minutes. In these calculations, A was given the value of 10^{15} s^{-1}. Figure 4.2 shows the results of Pitt's (1962) experiments.

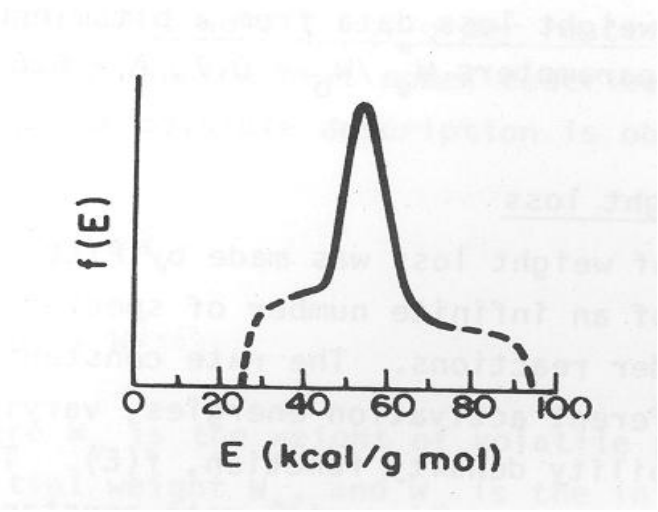

Figure 4.2: Distribution of Activation Energies from Pitt's Model (Pitt, 1962)

The weight loss calculated with the curve *f(E)* of figure 4.2 was in good agreement with the experimental weight loss.

A chemical interpretation of Pitt's (1962) model would attribute the sharp peak in Figure 4.2 at about 50 to 55 kcal to a corresponding tar species. According to Gavalas (1982), tar constitutes 75% or more of weight loss for high volatile bituminous coals. This behaviour is consistent with the hypothesis that the main tar forming reaction involves dissociation of the ethylene bridge whose activation energy would be in the range of 48-57 kcal depending on the size and substituents of the aromatic nucleus. A similar interpretation suggests that the part of the curve at low *E* corresponds to the formation of H_2O and CO_2 while the part at high *E* corresponds to the formation of hydrocarbon gases, CO and H_2.

In another treatment, Anthony et al. (1974) postulated that pyrolysis occurs through an infinite series of parallel reactions. A continuous Gaussian Distribution of Activation Energies is assumed, along with a common value for the frequency factor so that

$$\frac{v_\infty - v}{v_\infty} = [\sigma(\sqrt{2\pi})^{-1}\left\{\left[\int_0^\infty \exp\, -\left(\int_0^t k\, dt\right) f(E) dE\right]\right\} \quad (10)$$

With $$f(E) = \left[\sigma(\sqrt{2\pi})\right]^{-1} exp\left(\frac{-(E-E_0)^2}{2\sigma^2}\right) \quad (11)$$

This approach also provided very good correlation of the data from Anthony et al. (1974) as well as the experimental results of Suurberg et al. (1977). The model is attractive because it requires only four correlating constants. However, the use of the Several First Order Reactions model may be restricted by the need to determine the parameters v_∞, k, E_0 and σ for the specific coal used.

Sprouse and Schuman (1981) compared the lignite data of Figure 4.1 in section 4.3.2 with predictions from equations (10) and (11) as shown in Figure 4.3a below.

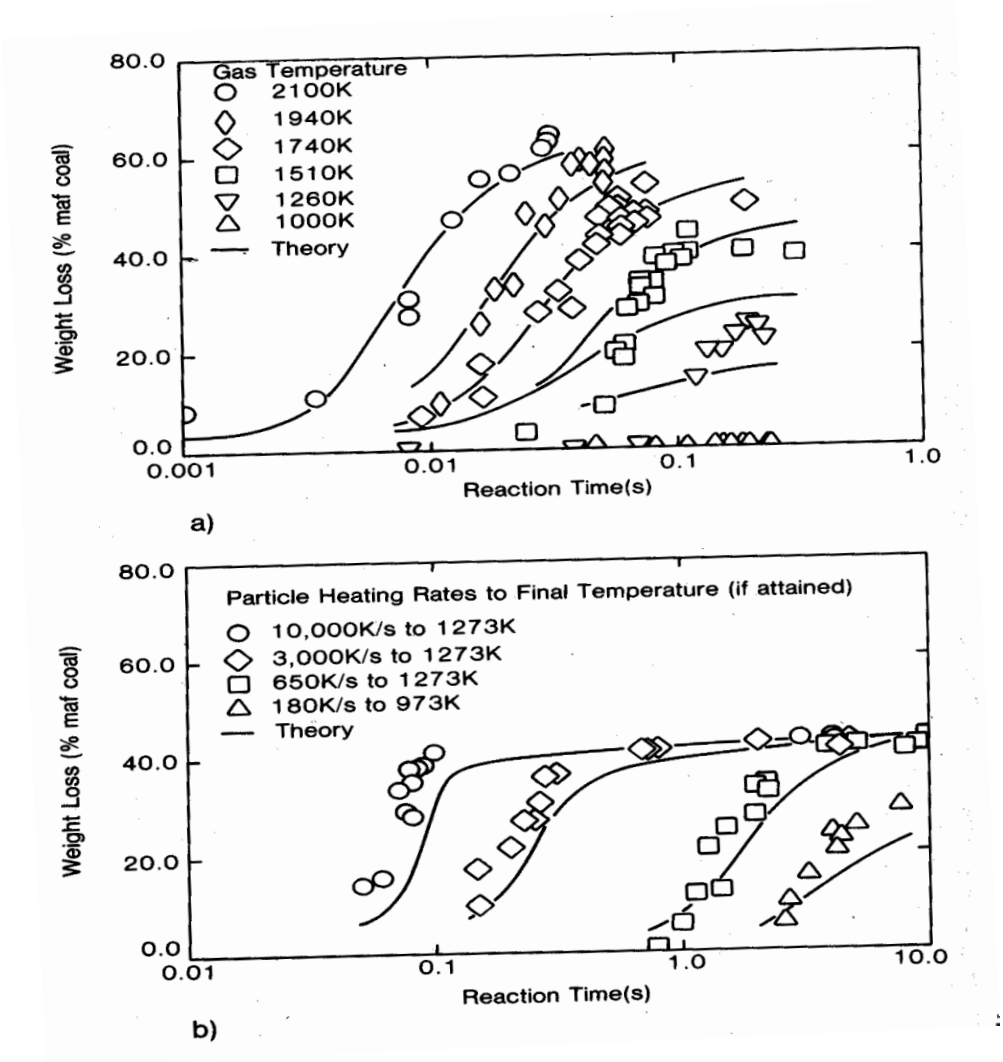

Figure 4.3: Comparison of Measured Lignite-Weight-Loss Data (0.1 MPa) and Predictions from Equations (10) and (11) (Sprouse and Schuman, 1981)

(a): Effects of Temperature, Laminar Flow Reactor

(b) Effects of Temperature and Heating Rate from Electric Screen

(Data from Anthony et al., 1974)

Parameters shown in Figure 4.3 provided near optimum agreement with the data. From this figure, the values for the parameters are σ=1x10^5 J/mol, v_∞=63.5 wt%, E_0=3.15x10^5 J/mol and k=1.67x10^{13} s^{-1}. Parameters were not quite optimum but were common in both Figures 4.3 (a) and (b). Sprouse and Schuman (1981) note the excellent agreement with four parameters as compared to five parameters for Figure 4.1. A further comparison for lignite data generated by Anthony et al. (1974) for lower temperatures but variable heating rates is shown in Figure 4.3b. Again, agreement is very good with the same parameters. It is also interesting to note the absence of significant effect of heating rate on the maximum extent of pyrolysis.

Both methods (i.e. Equation (8) and Equations (10) and (11)) give very good results. Differences in the number of coefficients is considered secondary, since it is likely that a priori information may be available for coefficients for Equation (8).

More complex reaction mechanisms were reviewed by Anthony and Howard (1976), and often involved several coal reaction steps. The two-step model of equation (6) produces information about the composition of the volatile gaseous products and the residual char, whilst the infinite series of parallel reactions of equations (10) and (11) can not provide a description of the resulting products. It is this description of the pyrolysis process as an infinite series of reactions that led to the development of the Distributed Activation Energy Model.

4.3.4 Distributed Activation Energy Model (DAEM)

As the understanding of the pyrolysis process became more advanced, the models developed to describe the process became similarly more advanced, taking into account more complex descriptions of the chemical and physical processes. Pitt (1962) first treated the coal as a mixture of a large number of species decomposing by parallel first order reactions with different activation energies. The pyrolysis behaviour of coal is described as a complex of first-order reactions, each with its own rate constants. Further work carried out by Anthony and Howard (1976) and Braun

and Burnham (1987) modified the model developed by Pitt (1962) and extended its use to coal, biomass and even blends of the two.

The DAE-model makes use of the description that the pyrolysis of a complex fuel is carried out as the first-order decomposition of many different chemical groups, where each group is characterized uniquely by its activation energy for the decomposition. The complexity of the fuel is such that a continuous distribution of activation energies is assumed where the mass of volatile material with activation energies between the initial activation energy and the activation energy at some point in time can be related as a function of activation energy and time. Mathematically this can be expressed as shown by Scott et al. (2006 [a]):

$$M_v(t) = \int_0^\infty m(E,t)dE \tag{12}$$

Where $M_v(t)$ is the total mass of volatile matter, E is the activation energy and t is the time.

Scott et al. (2006 [a]) have shown that by assuming that the material in the interval E+*d*E decomposes via a first-order reaction, with a pre-exponential factor of A(E), equation (12) above then reduces to:

$$m(E,t) = m_0(E)e\left(-A(E)\int_0^t e^{\left(\frac{-E}{RT}\right)}dt\right) \tag{13}$$

Where $m_0(E)$ is the initial mass of volatile material decomposing with an activation energy in the interval E to E+*d*E.

In practice, the quantity m(E,t) cannot be measured; only the total amounts $M_v(t)$, or the total rates of decomposition are measured. Thus by integrating over all energies, Scott et al. (2006 [a]) have shown that equation (13) becomes:

$$\frac{M_{v(t)}}{M_{vo}} = \frac{M_{vo}-V(t)}{M_{vo}} = \int_0^\infty g(E) \times \underbrace{e^{\left[-A(E)\int_0^t e^{\left(\frac{-E}{RT}\right)}dt\right]}}_{\Psi(E,t)} dE \tag{14}$$

where M_{vo} is the initial value of Mv(t), Ψ(E,t) is the double exponential term in equation (14), V(t) is the yield of volatiles and g(E) is the underlying distribution of

activation energies, which characterises the material. The function g(E) is normally given by equation (15) as shown by Scott et al. (2006 [a]) below:

$$g(E) = \frac{m_{0(E)}}{\int_0^{\infty} m_0 dE} \quad (15)$$

If g(E) and A(E) are known, the yield of volatile material can be calculated from equation (14).

Scott et al. (2006[b]) have pointed out the shortcomings of the DAEM model for the prediction of kinetic parameters. The authors have shown that the DAEM model suffers limitations when used as a sub-model in combustion codes with variations in temperature from point to point. Also, the integration over all activation energies adds an extra dimension to the problem. Scott et al. (2006 [a]) thus proposed a modified form of the DAEM model in order to mitigate the computationally intensive DAEM model and thus overcome its shortcomings.

4.3.5 Modified DAEM

Numerous approximations have been suggested to give a closed form of the double integral term in the DAEM (Equation 14, Section 4.3.4) in order to prevent the need for numerical integration. Rostami et al. (2004) showed how it is possible to obtain an approximate closed form of the model which allows the rate of mass loss to be calculated without numerical integration, by assuming that as conversion proceeds, the functional groups with the lowest activation energies are pyrolised first. Please et al. (2003) authored a paper that deals entirely with the discussion of the various approximations.

Braun and Burnham (1987) were the first to discretize the distribution of activation energies, replacing a continuous distribution of reactions with a finite set of discrete first-order reactions. Further work conducted by Scott et al. (2006[b]) on this model, has led to the development of a modified version of the DAEM.

For a material decomposing via several first-order reactions, the weight loss as a function of time can be expressed as was shown by Scott et al. (2006[a]):

$$\frac{M(t)}{M0} = w + \sum_{All\ reactions\ i} fi, 0\ e\left[-Ai\int_0^t e \times \left(\frac{-Ei}{RT(t)}\right) dt\right] \quad (16)$$

Where M(t) is a mass of sample that contains a fraction w of inert material, M_0 is the initial value of M, $f_{i,0}$ is the fraction of M_0 which decomposes with an activation energy E_i and pre-exponential factor A_i.

Using experimentally measured M(t), the problem is to find the other terms in equation (16). The DAEM can be generated by increasing the number of reactions to infinity and imposing the constraint that the reactions are characterised uniquely by their activation energies. However this is not true of the modified DAEM, since there might be more than one reaction with the same activation energy, but a different pre-exponential factor. This is the major advantage of the modified DAEM over the DAEM: whilst the DAEM cannot easily determine the kinetic parameters for these cases, the modified DAEM can. This modified DAEM model is the model that will form the basis for this work.

If the reactions were known, together with each value of E and A, then equation (16) would be linear: the mass of solid fuel remaining at a given time would be the sum of the masses of each of the components remaining. This implies that equation (16) may be written as a matrix equation as shown by Scott et al. (2006 [a]), where, for any set of times t_1, t_2, t_3, etc., the mass of fuel remaining, $M(t)$, is given by

$$\underbrace{\frac{1}{M_o}\begin{bmatrix} M(t_0) \\ M(t_1) \\ M(t_2) \\ \vdots \end{bmatrix}}_{\underline{M}} =$$

$$\underbrace{\begin{bmatrix} \psi_1(t_0) & \psi_2(t_0) & \dots & \psi_n(t_0) & 1 \\ \psi_1(t_1) & \psi_2(t_1) & \dots & \psi_n(t_1) & 1 \\ \psi_1(t_2) & \psi_2(t_2) & \dots & \psi_n(t_2) & 1 \\ \psi_1(t_3) & \psi_2(t_3) & \dots & \psi_n(t_3) & 1 \\ \vdots & \vdots & \ddots & \ddots & 1 \end{bmatrix}}_{\underline{\underline{\Psi}}} \times \underbrace{\begin{bmatrix} f_{1,0} \\ f_{2,0} \\ f_{3,0} \\ \vdots \\ w \end{bmatrix}}_{\underline{f}} , \quad (17)$$

i.e. $\underline{M} = \underline{\underline{\Psi}} \times \underline{f}$

With, as an example, an experiment with a constant dT/dt = B has been shown by Scott et al. (2006 [a]) to reduce to:

$$\Psi_i(t) = \Psi_i(T) = e^{\left[\frac{-A_i}{B}\int_{T_0}^{T} e^{\left(\frac{-E_i}{RT(t)}\right)}dT\right]} \quad (18)$$

Here, T_0 is the initial temperature of the fuel. It should also be noted that Ψ_i in equation (11) is the same as Ψ in equation (14).

Calculating the initial mass fractions, $f_{i,0}$, decomposing in each reaction i is then a matter of solving equation (10), which is linear. Since there are usually more experimental results than reactions, the system is over-specified. However, it is possible to solve equation (17) using linear least squares; each mass fraction, $f_{i,0}$, becomes a parameter, which is altered to minimize the difference between the values of $\underline{M}$and $\underline{\underline{\Psi}} \times \underline{f}$, subject to the constraint that only positive values of $f_{i,0}$ are allowed.

Equation (10) was then inverted by Scott et al. (2006 [a]) using the *lsqnonneg* algorithm in Matlab (Matlab® R14, The Mathworks Inc.). A similar method was used by Burnham and Braun (1999).

To use equation (17), a set of reactions must first be generated, each with a known value of A and E. Once the reactions have been specified, the matrix $\underline{\underline{\Psi}}$ can then be calculated. It is first assumed that, at a given conversion, there will be a single reaction dominating. For the i^{th} component, assuming a first-order reaction, the fraction of the initial mass remaining, when the fuel is subjected to a constant rate of heating, is given by equation (15) by Scott et al. (2006 [a])as:

$$f_i(T) = f_{i,0}e^{\left[-A_i\int_0^t e^{\left(\frac{-E_i}{RT}\right)}dt\right]} = f_{i,0}\Psi_{\mathrm{i}}(\mathrm{T}) \quad (19)$$

using the definition of Ψ in equation (14). If the conversion in two separate experiments at different heating rates, B_1 and B_2, is considered and the i^{th} reaction is the only reaction taking place at this conversion, then f_i (B_1, T_1)=f_i (B_2, T_2) at two particular temperatures, T_1 and T_2.

Thus, from equation (19), and noting that $\Psi_i(T)$ is also a function of the rate of heating, B=dT/dt, it can be shown that:

$$\Psi_i(B_1, T_1) = \Psi_i(B_2, T_2) \tag{20}$$

Substituting for $\Psi_i(B_1,T_1)$ and $\Psi_i(B_2,T_2)$ from equation (14) and taking logarithms on each side as done by Scott et al. (2006 [a]) yields:

$$\frac{1}{B_1}\left[T_0 e^{\left(\frac{-E_i}{RT_0}\right)} - \frac{E_i}{R}\int_{\frac{E}{RT_0}}^{\infty}\frac{e^{-u}}{u}du - T_1 e^{\left(\frac{-E_i}{RT_1}\right)} + \frac{E_i}{R}\int_{\frac{E}{RT_1}}^{\infty}du\right] =$$

$$\frac{1}{B_2}\left[T_0 e^{\left(\frac{-E_i}{RT_0}\right)} - \frac{E_i}{R}\int_{\frac{E}{RT_0}}^{\infty}\frac{e^{-u}}{u}du - T_2 e^{\left(\frac{-E_i}{RT_2}\right)} + \frac{E_i}{R}\int_{\frac{E}{RT_2}}^{\infty}\frac{e^{-u}}{u}du\right] \tag{21}$$

This is a non-linear equation, which can be solved for the unknown E_i.

If a solid is made up of several components, the value of the activation energy calculated from equation (21) will be exact, provided that only one reaction is dominating the overall loss of mass at the conversion of interest. Errors in the value of the activation energy will occur when several reactions are occurring simultaneously at the chosen conversion.

To determine the pre-exponential factor, A_i, once E_i has been calculated from equation (21), it is assumed that the dominating reaction is at some conversion, here Scott et al. (2006 [a]) have shown that the following value can be used:

$$X = 1 - \frac{1}{e} \Rightarrow \Psi_{\mathrm{i}} = \frac{1}{e} \approx 0.368 \tag{22}$$

This is, of course, the conversion of the individual component *i*, *not* the overall conversion of the mass of fuel to volatile material. A value of $\Psi_i = e^{-1}$ corresponds to the

conversion at which a single first-order reaction would reach a maximum in the rate of decomposition, if the material were heated at a constant rate, i.e. as shown by Scott et al. (2006 [a]), when

$$\frac{d}{dt}\left(\frac{df_i}{dt}\right) = \frac{d}{dt}\left(\left\{f_{i,0}A_i e^{\left(\frac{-E_i}{RT}\right)}\right\} \times e^{\left[-A_i \int_0^t e^{\left(\frac{-E_i}{RT}\right)} dt\right]}\right) = 0 \qquad (23)$$

with dT/dt=B. Since E_i is already known from equation (21), this allows A_i to be calculated from the following equation as shown by Scott et al. (2006 [a]):

$$\ln(\Psi_i) = -1$$

$$= \frac{A_i}{B_1}\left[T_0 e^{\left(\frac{-E_i}{RT_0}\right)} - \frac{E_i}{R}\int_{E/RT_0}^{\infty}\frac{e^{-u}}{u}du - T_2 e^{\left(\frac{-E_i}{RT_2}\right)} + \frac{E_i}{R}\int_{E/RT_2}^{\infty}\frac{e^{-u}}{u}du\right] \qquad (24)$$

The approximations used to derive equation (10) do, however, lead to some error in the calculated value of A_i. This is because it has been assumed that the dominant reaction is at a conversion of 63.2%, when the pre-exponential factor is evaluated. This error is discussed more fully, below, where the algorithm is used to recover the kinetic parameters from a simulated first-order reaction.

The method of obtaining the values of A and E at various conversions, using equations (7) and (10) above, is central to the method of Miura and Maki (1998) for inverting the DAEM. They used the approximate form of Ln($\Psi_i(E^*)$) given by equation (14) to derive the equivalents of equations (21) and (10). However, Miura and Maki (1998) made the assumption that each reaction is uniquely characterized by an Activation Energy and used Equation (14), which relies on the 'step function' approximation, to estimate the amount of each reaction occurring. Thus, the algorithm developed by Scott et al. (2006, a), neither requires that each reaction is uniquely characterized by its Activation Energy, nor the use of the step function approximation.

4.4 Summary

This chapter detailed the various models used to predict the kinetic parameters of the pyrolysis process. They range from models used prior to the use of advanced computer-aided modelling software, developed under basic or first-principle conditions, to the more complex models that arose as the understanding of the pyrolysis process increased, and the rise of automated mathematical modelling allowed for more complex descriptions of the pyrolysis process to be taken into account. These complex models are thus more accurate at predicting pyrolysis behaviour, and give a 'real-world' understanding of how pyrolysis occurs, and can allow for pyrolysis processes to be easily optimized and predicted for situations not unlike experienced in industry.

The success of the modified form of the DAEM at providing an easier, faster way for calculating the Activation Energy and Pre-exponential Factor as compared to the traditional DAEM was shown. The earlier DAEM utilized a complex numerical integration technique requiring considerable amount of time and processing power. The modified DAEM was also shown to work effectively to model the pyrolysis behaviour of coal, biomass and blends of coal and biomass as the model requires only data from TGA experiments, and calculates the kinetics independent of sample composition. This provides an advantage of the DAEM as a means of providing a model-free approach to determining the Activation Energy (A) for any sample undergoing pyrolysis.

Chapter 5: Experimental

In this section, details of the experimental apparatus and procedure are given. The results of the laboratory experiments are used in the algorithm to compute data for the relevant fuel at both high, and low heating rates. The data is also used to indicate the effectiveness of the algorithm at determining the kinetics of the pyrolysis of coal and biomass, as well as coal-biomass blends.

5.1 Apparatus

In order to conduct the experimental work, various apparatus were required. These apparatus include: a mill to prepare the sample, a thermo-gravimetric analyser, a computer with controlling software, and another computer in order to analyse the data and prepare the results for modelling purposes.

5.1.1 Perkin-Elmer Thermo-gravimetric Analyser

For this study, a Perkin Elmer, Top-Loading Series STA-6000 was used. This machine is housed in the Coal and Carbon Research Group Laboratory, at the University of the Witwatersrand.

The data obtained from the TGA gives valuable information about the rate at which pyrolysis occurs. Using these results, various thermodynamic data can be obtained or calculated, which can then be used to model the pyrolysis process. A schematic representation of this machine is given in Figure 5.1.

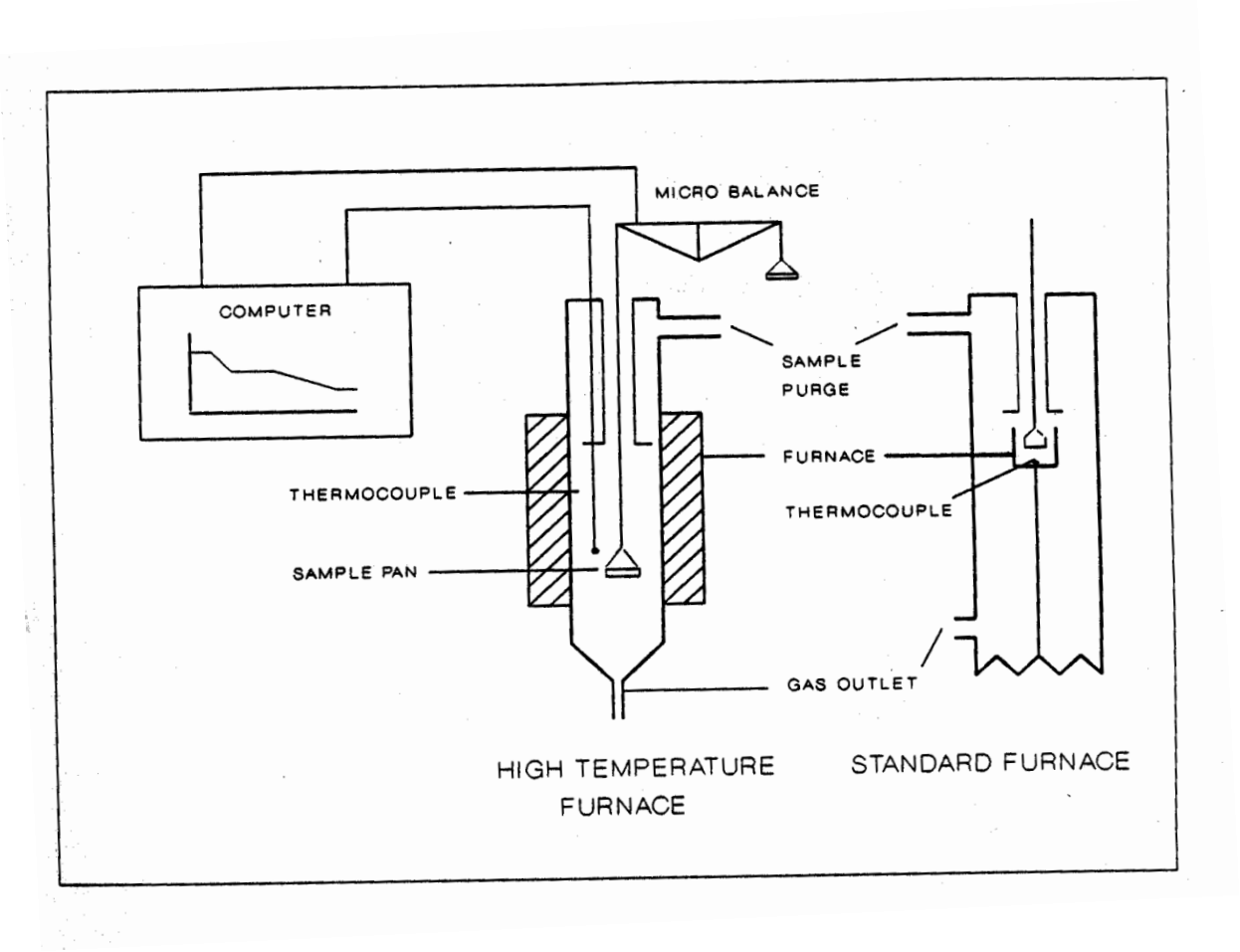

Figure 5.1: Schematic of the Layout of the Perkin Elmer TGA (Perkin Elmer Pyris TGA Software Presentation)

The machine used could not achieve very high temperatures, but for the purposes of this modelling study, a maximum temperature of 900°C was used. The heating rate was variable from values between 1°C/min up to 100°C/min. Specifications on the machine are given in Table 5.1 below.

Table 5.1: STA 6000 Specifications

Feature	***Tolerance***
Balance Sensitivity	10^{-3}mg
Balance Accuracy	0.1%
Temperature Range	25°C-1000°C
Heating Rate Range	0.1°C/min to 100°C/min
Temperature Precision	±2°C

Due to safety issues and to prolong the life of the furnace, the machine was operated at a maximum temperature of 900°C.

The purge gases, Nitrogen and Argon, were obtained from cylinders and the flow rate of 40ml/min was controlled automatically by the machine software. The gases could also be switched by the software. The machine is only able to operate under atmospheric conditions of 1 atm. It is important to note that atmospheric conditions in Johannesburg are significantly below 1 atm (≈0.9 atm), but these effects are considered negligible for purposes of this study.

The entire measuring process is automated and controlled by software. A typical pyrolysis run consist of entering the maximum final temperature, the heating rate and then introducing between 10-15mg of sample into the sample crucible. The crucible is then lowered into the furnace chamber and the run is started. The computer then controls the sample from then on. Data is logged in real time and the results are saved to a specified folder for later analysis. The software allows the operator to obtain mass change as a function of temperature or time. It also allows for the calculation of derivative information, delta Y and delta X onset and offset values.

A photograph of the TGA machine is shown in Figure 5.2.

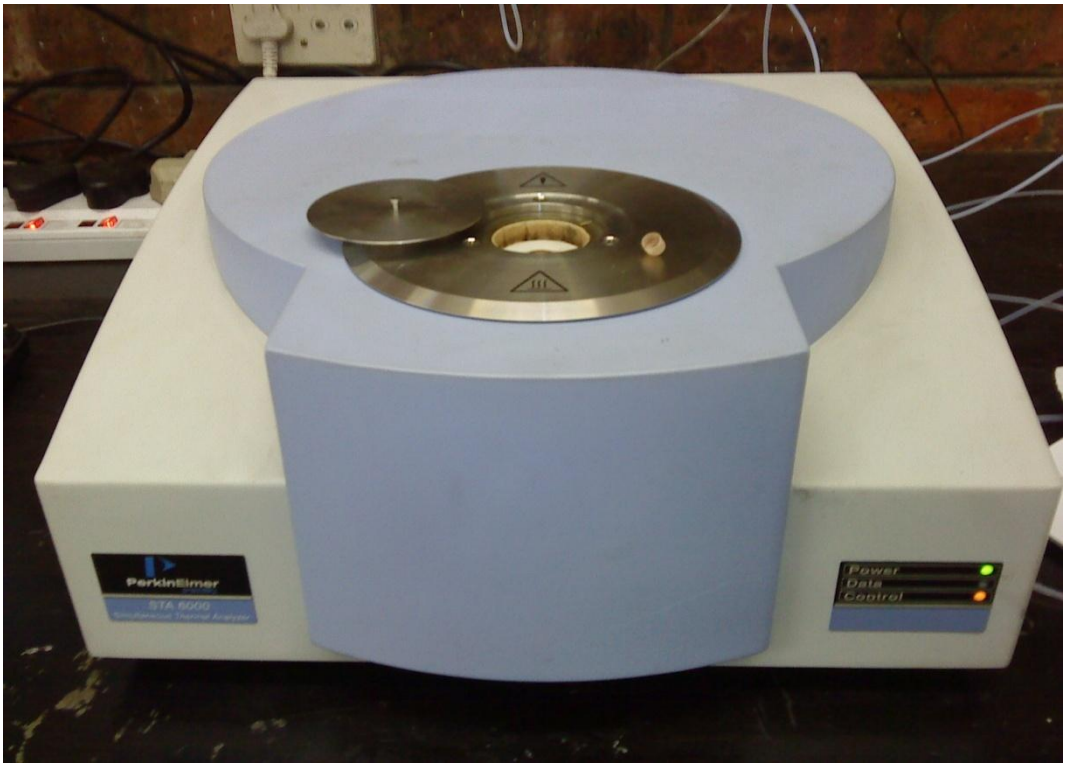

Figure 5.2: Perkin-Elmer STA 6000 Top-Loading TGA

5.2 Sample Preparation

In order to utilize the received coal in the TGA machine, sample preparation was carried out. The coal was received from a Witbank coalmine, housed at the Eskom Research and Innovation Centre (ERIC) for combustion trials. Biomass was collected from a local hardware store, in the form of sawdust and wood shavings from the cutting and preparation of wood for industrial uses. The coal and biomass were individually crushed using a Retch Cylindrical Crushing Mill. Sample was loaded into the crushing chamber, and the appropriate sieve blade was fitted over the crushing blades. The sample was then milled and the coal and biomass were crushed and sieved to 0.1mm. Only material remaining on the 0.1mm screen were collected to be used for experiments. The result of the milling process can be seen in Figure 5.3.

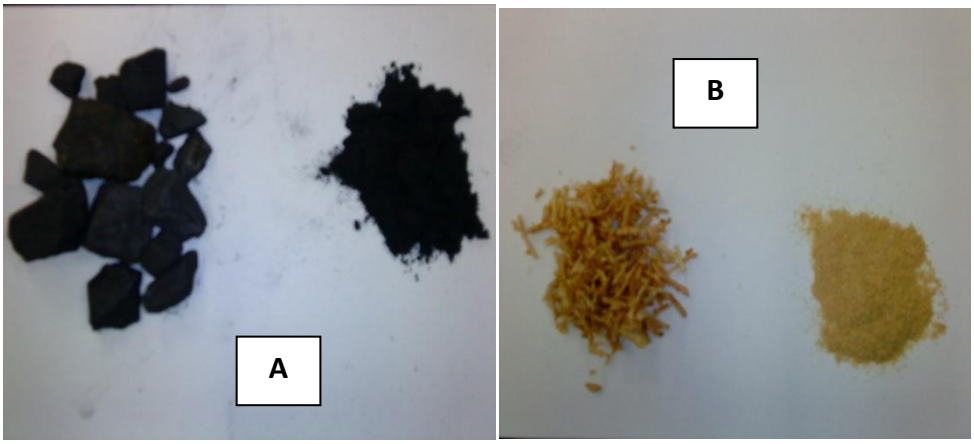

Figure 5.3: (A) Crushed Coal, (B) Crushed Sawdust Biomass

Samples were then prepared of raw coal, and raw biomass, and also samples of coal and biomass blends by incrementing biomass mass. Samples of 25% biomass, 50% biomass and 75% biomass were prepared on a mass basis by blending a known mass of coal with the appropriate mass of biomass in order to create the required mass concentration. This was done by creating a 10g parent sample for each concentration, and blending in the right mass proportions of biomass and coal to create the desired biomass concentrations.

The samples were thoroughly mixed by shaking the combined coal and biomass in a closed container, to ensure even distribution of the light biomass within the dense coal. Figure 5.4 shows the results of the blending process.

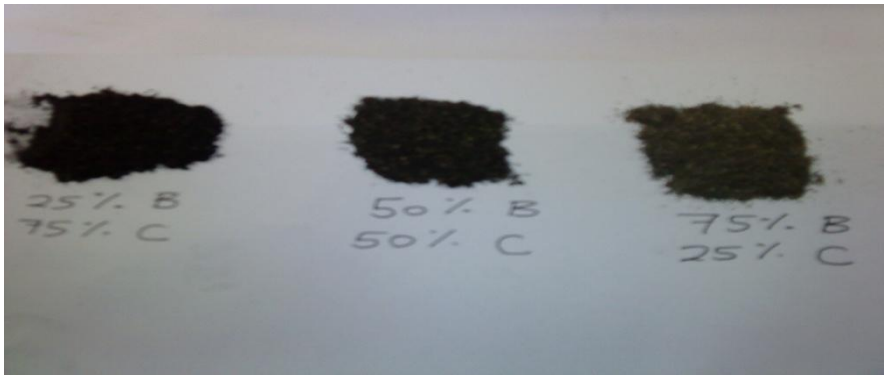

Figure 5.4: Results of Blending, B=Biomass, C=Coal

From Figure 5.4, it can be seen that as the concentration of biomass is increased, the resultant mixture takes on a lighter shade of grey.

5.3 Procedure

Once the coal and biomass were prepared, the samples could then be utilized in the experimental work. The experimental work required the determining of the key characteristics of the coal and biomass used, and in order to do this, the TGA was first used to perform a Proximate Analysis on the coal and then biomass.

5.3.1 Proximate Analyses

Once the samples were prepared, total volatile matter and fixed carbon measurements were required to compare the results obtained from the model and those obtained from the actual experimental work.

A Proximate Analysis was carried out on all samples, in order to determine the percentage of moisture, volatiles, fixed carbon and ash present in each sample.

This procedure consists of heating 10-15mg of sample in the TGA, under a nitrogen atmosphere to 110°C and then holding the sample at this temperature for 3 minutes. This step allows the surface moisture and some inherent moisture to be driven off from the sample. Next, the sample is heated from 110°C to 950°C, again under a nitrogen atmosphere in order to drive off the volatile matter. At 950°C, the software switches the gas from nitrogen to oxygen, and the sample is allowed to burn off until at 950°C, by holding it at this temperature for 3 minutes. This allows the remaining carbon to combust, leaving behind the ash. A diagrammatic result of a typical proximate analysis is given in figure 5.5.

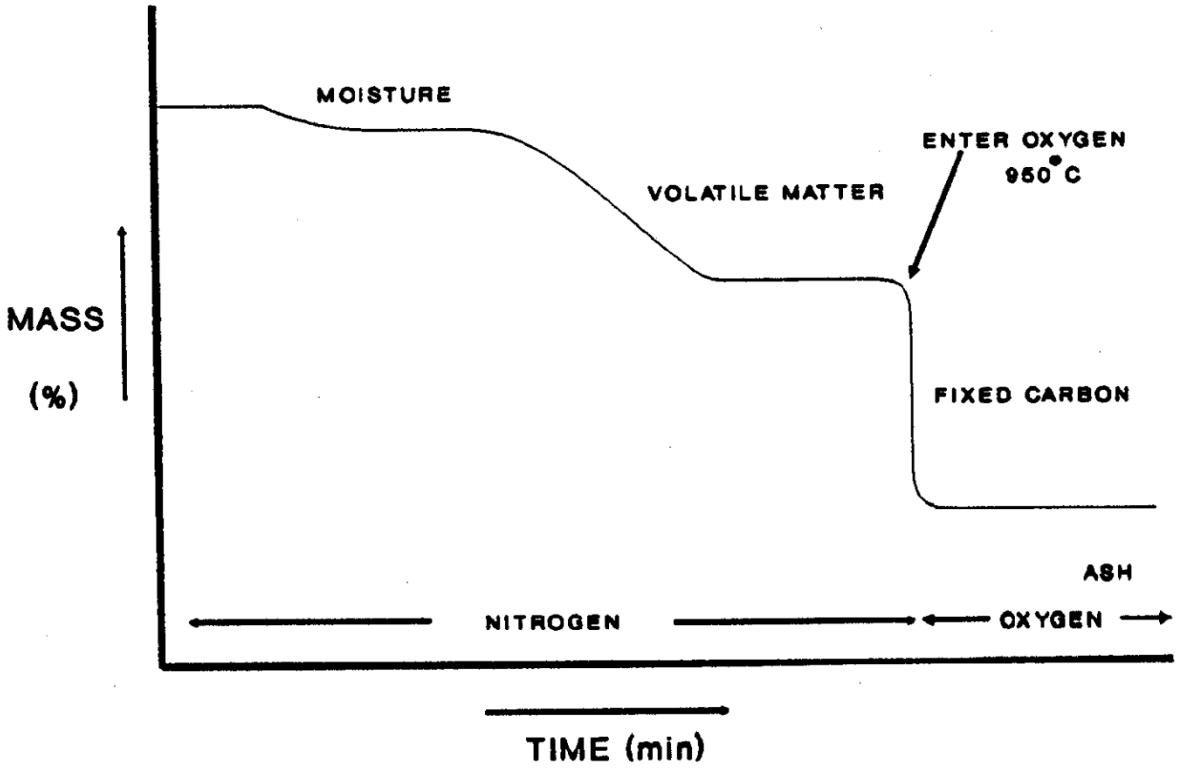

Figure 5.5: Result of Typical Proximate Analysis

By using the Pyris® software, one can easily calculate the amount of moisture, volatiles, fixed carbon and ash present in a sample.

Because ash and moisture contents of coals can vary between samples, the percentage of each product from the proximate analysis was expressed on a dry ash-free (daf) basis.

The daf values can be calculated as follows:

$$\%\text{daf volatile matter} = V/(V+FC) \quad (5.1)$$

$$\%daf\ fixed\ carbon = FC/(V+FC) \quad (5.2)$$

Where V is the volatiles as a percentage of the total coal mass and FC is the fixed carbon as a percentage of the total coal mass.

Once the proximate analysis was completed, representative samples were then run under pyrolysis conditions.

5.3.2 Pyrolysis Experiments

Samples were heated from ambient temperature to a final temperature of 900°C at varying heating rates. Since the only parameter needed to model the pyrolysis behaviour according to the DAEM is the heating rate, and mass loss at a given temperature, the other variables such as purge gas flow rate, pyrolysis atmosphere and initial and final temperature were all kept constant. These values are tabulated in Table 5.2.

Table 5.2: Pyrolysis Conditions for Experiments

Condition	Value
Initial Temperature	30°C
Final Temperature	900°C
Pyrolysis Atmosphere	Nitrogen only
Pyrolysis Purge Gas Flow Rate	40 ml/min
Pyrolysis Pressure	0.9 atmosphere

Samples were run, and a repeat run was done to confirm the results obtained. Since the only parameter varied was heating rate, samples were run at heating rates of 1°C/min, 5°C/min, 20°C/min, 40°C/min, 60°C/min and 80°/min. The two low values used were in order to obtain data when pyrolysis is carried out at nearly isothermal conditions, whilst the remaining heating rates were required for modelling information. A purge on the machine to clean out finely-settled particles from the sample pan, as well as a pre-warming to 110°C to drive off any trapped moisture within the machine, was carried out before and after each experiment was done.

A flow diagram of the experimental procedure and how the modelling process depends on it is given in figure 5.6.

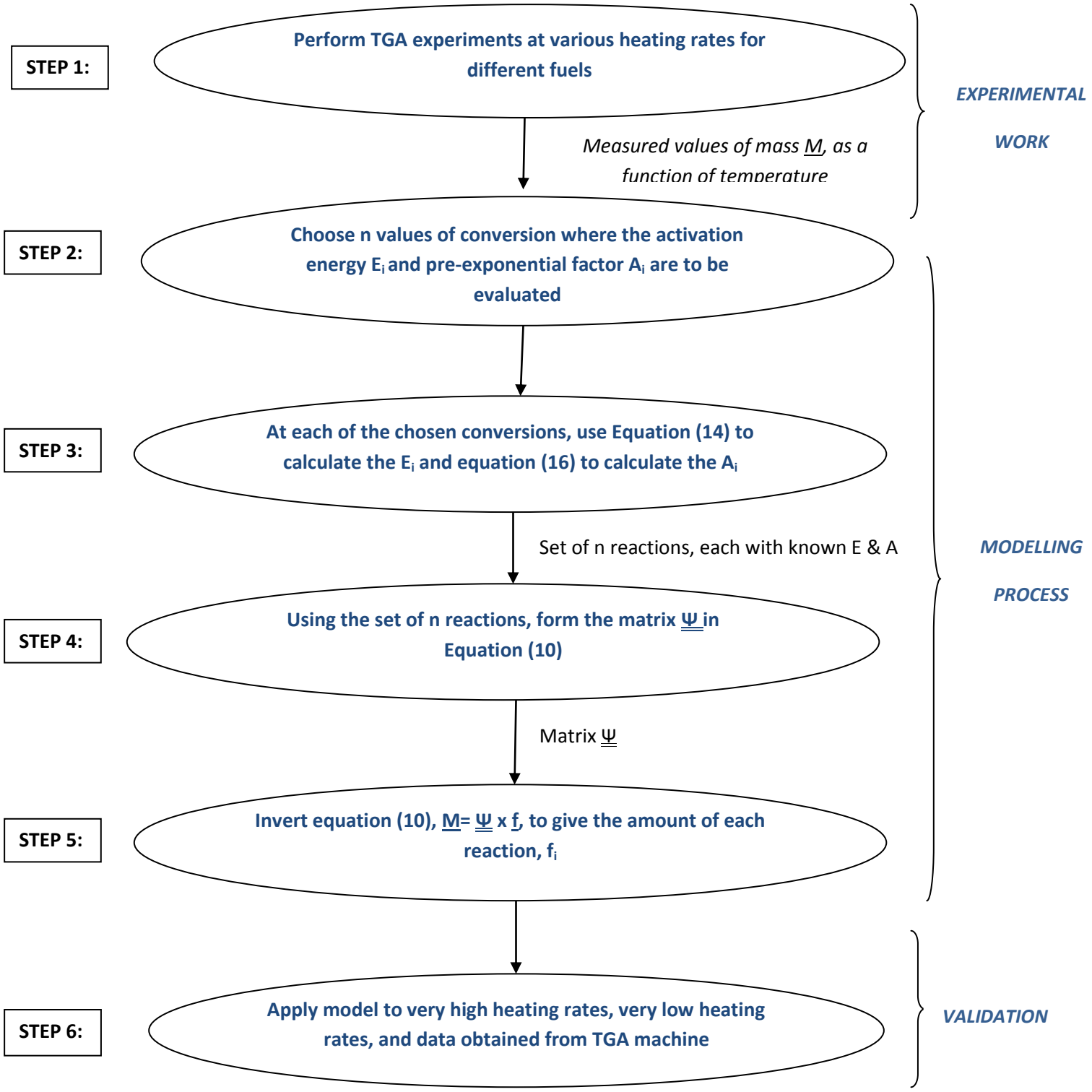

Figure 5.6: Flow Diagram of Experimental and Modelling Work

5.4 Pyrolysis Modelling

Once the data from the TGA experiments was obtained, it was collected and collated. The data can be seen in Appendix B. This data was then used with the algorithm to generate data. The algorithm was coded using a dedicated computer, using Matlab® 7.0. The code was written using the equations detailed in Chapter 4, Section 4.3.5, and can be seen in Appendix A. The results of the data and the algorithm can be seen in Chapter 6.

5.5 Summary

In this chapter, the experimental procedure as well as the apparatus was outlined. The manner in which samples were prepared, and the exact experimental procedure carried out on each sample was detailed. A flow diagram of the entire experimental procedure and how it ties in with the modelling aspect of the pyrolysis was also outlined.

Chapter 6: Results and Discussion

In this chapter, the results of the modelling exercise are given. Graphs are drawn for all relevant data, and the data is used to compare results obtained from the DAEM algorithm and the actual TGA data. The results are then discussed.

6.1 Proximate Analyses: Coal and Biomass

Figure 6.1 shows the results obtained for two independent runs for the proximate analysis of the coal. The coal sample weight was normalized and the procedure to determine the proximate analysis was carried out as mentioned in Section 5.3.

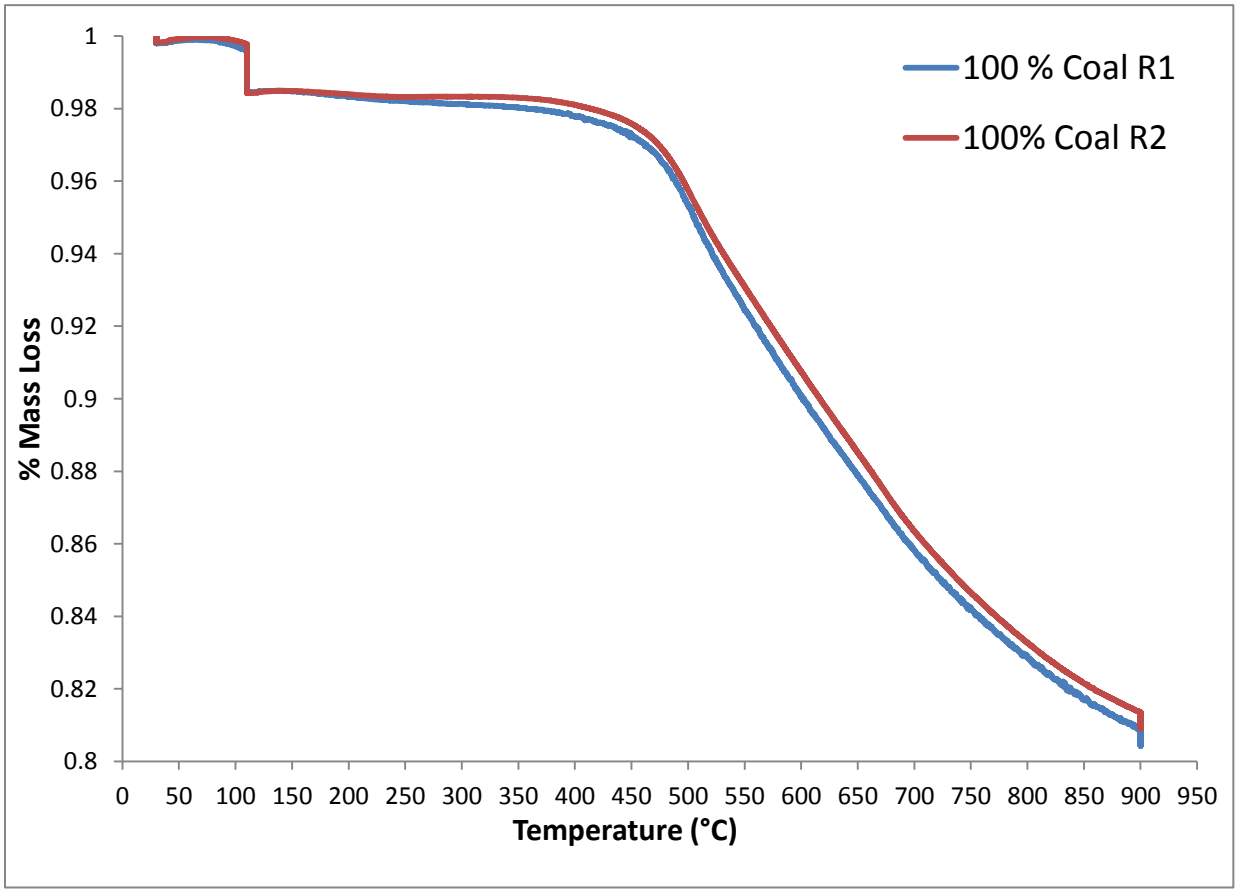

Figure 6.1: Results of Proximate Analysis for Medium Rank C Coal at 10 K/min

The slight variation in the two measurements is due such factors as sensitivity of the apparatus, or heterogeneity of the sample. These variations arose from differences in ambient temperature between sample analyses. The first sample was analysed, and immediately after the run was complete, the TGA was purged and cleaned before the next run could be done. Due to the size of the sample crucible and the geometry of the crucible, it is not possible to clean the sample crucible entirely, and some residue does tend to remain. It is possible that during the heating stage, heavy, tarry substances devolatilize from the sample and enter the gas phase. On cooling, these substances become dense again, and form a residue in the crucible cup (Gavalas, 1982). It is this residue that leads to slight over-calculations on subsequent runs. In order to mitigate these inter-experimental interactions, numerous runs were repeated until consistent results were obtained.

From the above results, and using the definition of proximate analysis given in Section 5.3, the average values for the proximate data on a *d.a.f.* basis can be calculated as given in Table 6.1 below. The relative error between Run1 and Run2 of the proximate exercise was found to be 0.94.

Table 6.1: Proximate Analysis Results for Medium Rank C Coal

Property	**Result**
Moisture	1.17 %
Volatiles	18.6 %
Fixed Carbon	61.2 %
Ash	18.9 %
daf Volatile Matter	**0.233**
daf Fixed Carbon	**0.767**

These values are typical of a Medium Rank 'C', South African Coal (Falcon 1988).

The same analysis was carried out on the biomass, to determine the amount of volatile matter and fixed carbon within the sawdust samples. The results are shown in Figure 6.2.

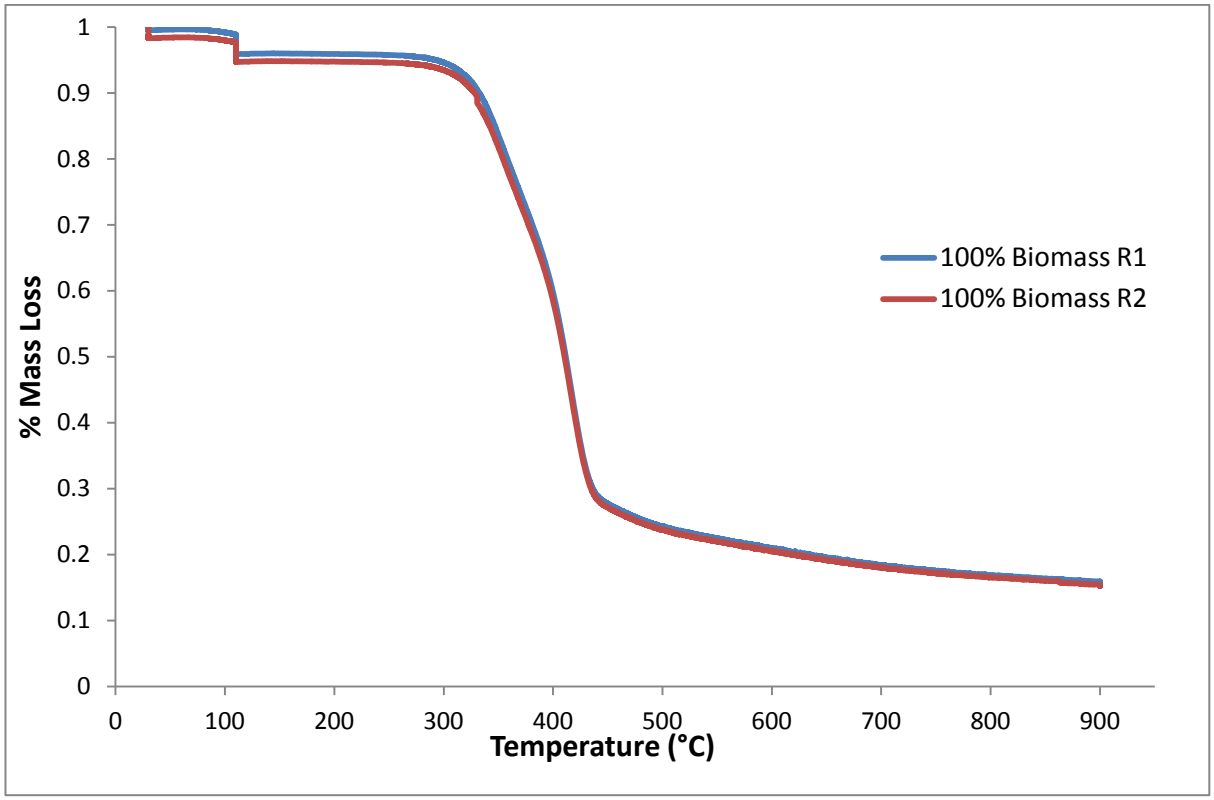

Figure 6.2: Results of Proximate Analysis for Biomass at 10 K/min

As can be seen from the results, the proximate analysis of biomass yields a smoother, much more accurate curve than that of coal for both runs. This is due largely to the absence of complex chemical structures within the biomass matrix (Diaz, 2006), and the presence of simple, highly-volatile components which decompose easily when exposed to high temperatures. The proximate results are tabulated in Table 6.2. The relative error between Run1 and Run2 of the proximate exercise was found to be 0.99.

Table 6.2: Proximate Analysis Results for Biomass Sawdust

PROPERTY	RESULT
Moisture	2.04%
Volatiles	70.4%
Fixed Carbon	16.5 %
Ash	11.0%
daf Volatile Matter	**0.810**
daf Fixed Carbon	**0.189**

It is important to note that while the biomass sample here does have rather high ash content, this is not abnormal for biomasses with a high concentration of alkali metals. The results of the proximate analysis are also within acceptable limits for typical biomass analyses carried out by many other researchers such as Maniatis et al. (2002) and Rostami et al. (2004), to name a few.

6.2 Application of the Modified DAEM to a Typical South African Medium Rank 'C' Coal

For purposes of this study, a typical South African Medium Rank 'C' Coal as detailed in Chapter 5, Section 5.2, was utilized. The sample was prepared as detailed in Chapter 5, Section 5.2, and then placed within the Thermogravimetric Analyzer. Data at various heating rates was obtained, and then used within the modified DAEM to produce the results in the following sections. The data was first tested, utilizing the same test methodology employed by Scott et al. (2006[a]), and can be seen in Appendix D.

6.2.1 Pyrolysis of Typical South African Medium Rank 'C' Coal

The results from the TGA experiments are shown in Figure 6.3.

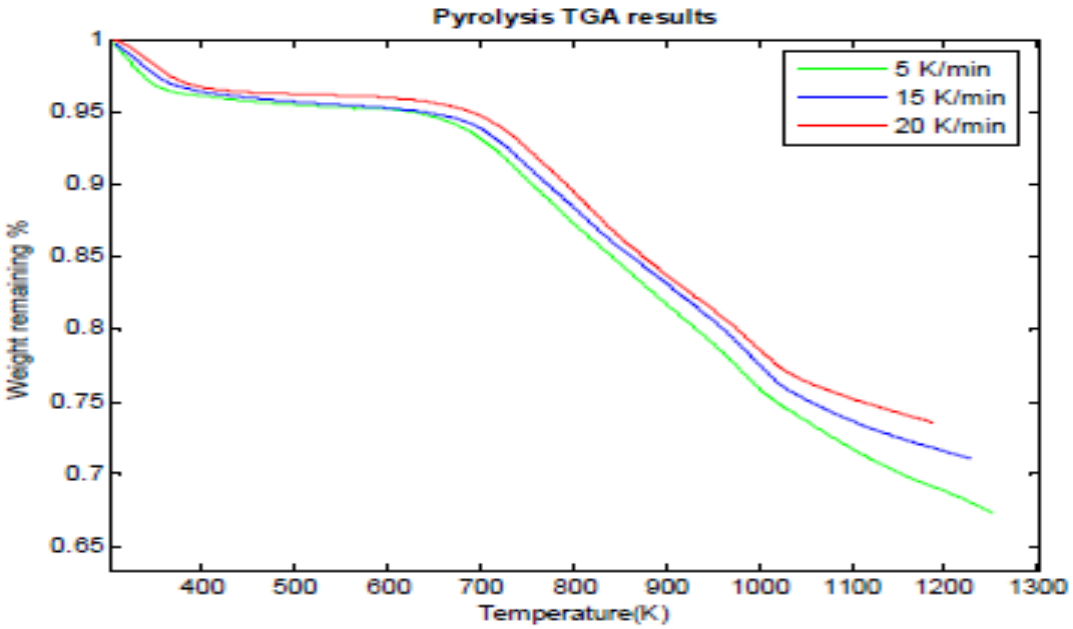

Figure 6.3: Results of TGA of Pyrolysis for Typical South African Medium Rank 'C' Coal

Three experiments were performed for purposes of this study, each at a different heating rate. Heating rates were varied from 5, 15 and 20 K/min for the experiments while all other parameters were kept constant. The results show the general trend that as heating rate increases, the height of the curve obtained increases, indicating a higher rate of mass loss as temperature increases. This is in accordance with Chern and Hayhurst (2004), who state that during devolatilization, the loss of mass is likely to be driven by the transmission of heat from the periphery of the particle, as well as heat transfer from the surrounding medium to the particle. Antal and Varhegyi (1995), on the other hand, as well as Howard (1981) state that effects attributed to heating rate can often be explained by other experimental factors, such as temperature gradients within the fuel particles and secondary reactions, in which the released volatile matter cracks to form char. From the results above, it can be seen that at a higher heating rate, more char is generated, indicating that heat transfer does indeed play an important factor in the devolatilization kinetics. The factors that influence internal and external mass and/or heat transfer within the particle has been discussed by Anderson (1963), and in light of the nature of pyrolysis, does not play a significant role in affecting the process.

An interesting result of the research is observed when looking at the data for the derivative mass loss versus temperature. The results of this are shown in Figure 6.4.

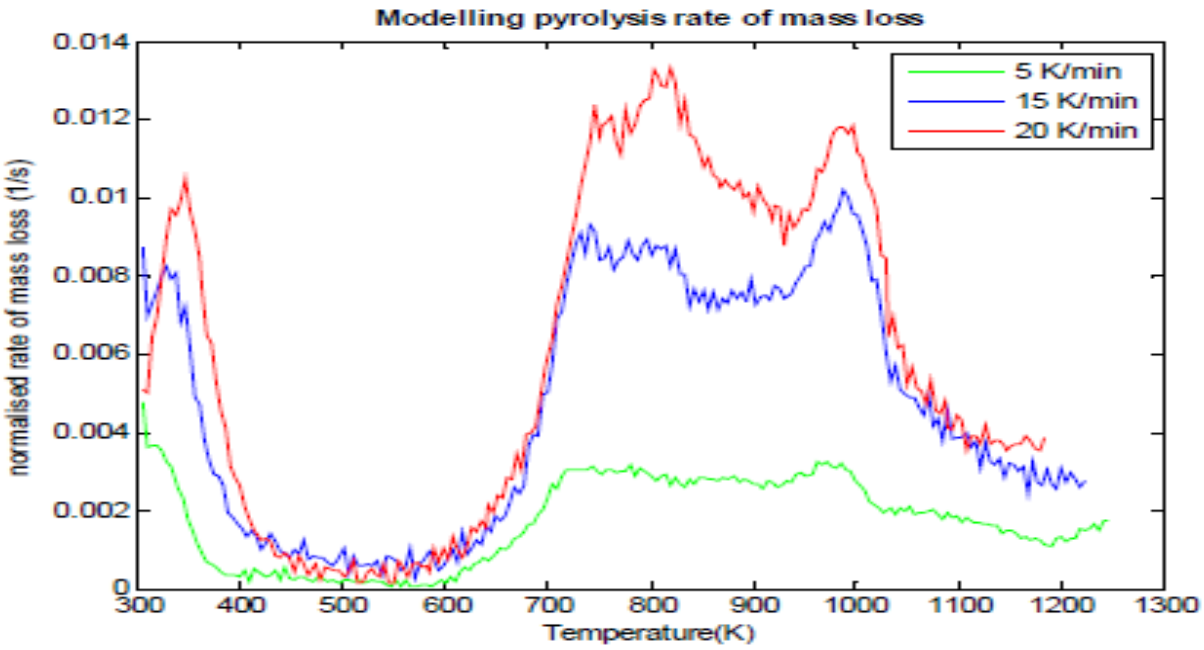

Figure 6.4: Derivative Mass Loss vs. Temperature for Pyrolysis Experiments

From the figure it can be seen that as the heating rate increases, the rate of mass loss increases. This is evident in the height of the peaks on the corresponding curves. It is also important to point out that each peak on the respective curves represents a dominating reaction occurring at that particular temperature interval. This finding is in agreement with work done by Arenillas et al. (2001), where the researchers report that as the heating rate increases, the mass loss profiles shift to a higher temperature, and the final mass is lower than that obtained at lower heating rates. Arenillas et al. (2001) associate this behavior to the effect of heating rate on secondary reactions of the primary pyrolysis products (tar and high molecular compounds). It can thus be deduced that the yield of char, gas and tar depends on the heating rate used during the pyrolysis process.

From the derivative information, the process of the pyrolysis process can clearly be seen. The high initial peak at the onset of the pyrolysis curve indicates the

initial heating of the particle and transfer of heat from the surrounding atmosphere to within the coal particle. This creates a temperature gradient, driving the breaking of the moisture bonds within the coal matrix, releasing the moisture trapped within the coal matrix. The temperature at which this occurs (between 370K and 390K) agrees with the boiling point of water, where moisture turns from liquid to vapour. This is however, not the intent of the study to quantify, as moisture content can be affected by factors such as sample storage conditions or even %relative humidity on day of experimentation. For purposes of this study, the effect of moisture before the onset of pyrolysis is the crucial pyrolysis zone will thus be ignored. As the temperature increases, the curve stabilizes, indicating that all moisture has been completely devolatilized, and at temperatures of around 700K, the optimal pyrolysis zone is reached. In this zone, there is a sufficiently large temperature gradient between the surroundings and the particle to completely break the bonds of the functional groups as discussed in Chapter 2, Section 2.3. At these high temperatures, radicals are formed and begin to devolatilize escaping through the porous coal particle. This continues to occur until all volatile organic species have escaped, resulting in the formation of the char.

From figure 6.4, it can also be seen that the behavior of the coal particle at the three different heating rates is fairly consistent, the only difference being the height of the peaks for each respective heating rate. This difference in height is of vital importance to industries that utilize coal in applications such as gasification or combustion. Where gasification is concerned, the maximum peak height for the coal sample at each representative heating rate indicates the maximum yield of volatiles devolatilized at that particular temperature. It can clearly be seen that as the heating rate increases, the mass of volatiles also increases, but the temperature at which this maximum yield occurs differs. An example can be seen in figure 6.4, where for the low heating rates of 5 and 10 K/min, respectively, the mass of volatiles is nearly doubled, while the temperature at which this occurs remains nearly constant, at approximately 320K, whereas for the higher heating rate of 15 K/min, the mass of volatiles released is nearly 20% greater than at the heating rate of 10 K/min, but the temperature at which this maximum occurs has shifted significantly to the right, at a temperature of approximately 370K. This is

counter-intuitive as the rate loss for lower heating rates is purely a result of non-isothermal heating. At lower heating rates, the fuel is held relatively longer at a certain temperature, thus in reality, the peak heights are nearly almost proportional to the heating rate.

In order to maximize char generation and volatiles release, it is crucial to industries to closely match their operating conditions to the behavior of the fuel. The necessity of a cleaner burning char is also mentioned by Pokothoane (2008), where he states that by completely devolatilizing the coal and generating a cleaner char, the resultant behavior of the char in the boiler during combustion results in lower operating temperatures and greater thermal efficiencies.

Since it has been established from the results of the hypothetical test scenarios in Section 6.2.1 that the modified DAE model is an effective tool for predicting the hypothetical scenarios put forward by Scott et al. (2006[a]), the model can now be tested on actual data obtained from the pyrolysis of a typical South African Coal.

The data obtained for the pyrolysis runs at three heating rates (5, 10 and 20 K/min) was input into the algorithm. The modified DAEM was then specified to run from the initial onset of the pyrolysis run to the end temperature, with a total of 100 possible reactions occurring during the pyrolysis. Figure 6.5 shows the results of the modified DAEM algorithm when using the data obtained from the pyrolysis experiments.

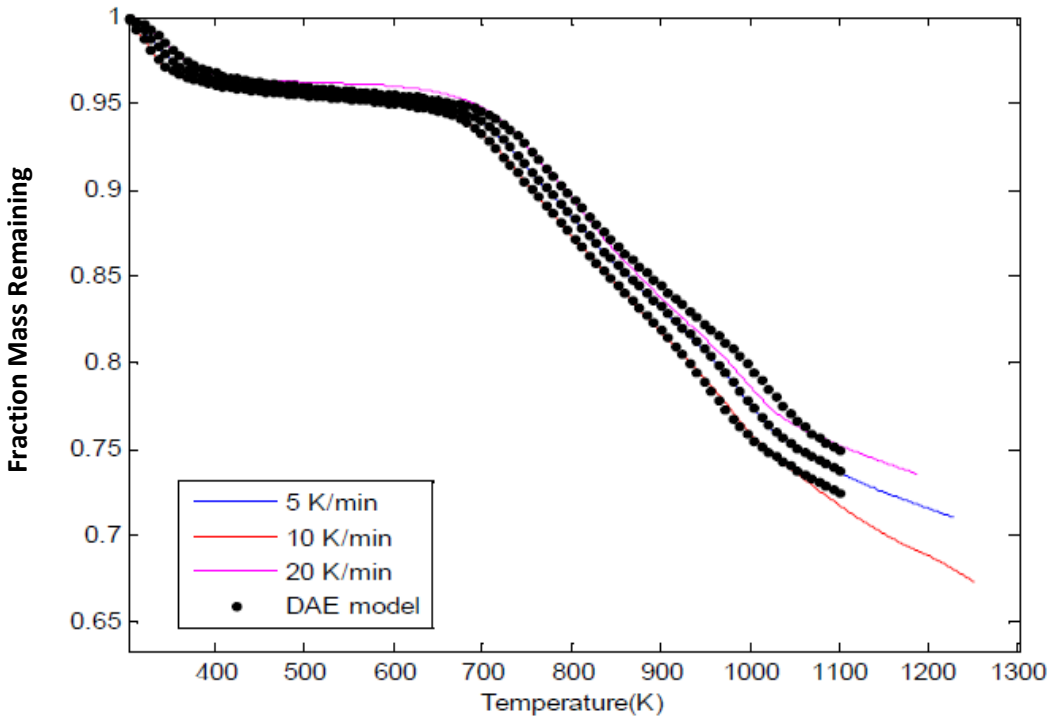

Figure 6.5: Results from DAEM for Pyrolysis Experiments of Coal

From the figure, it can clearly be seen that the model produces an excellent prediction of the pyrolysis of the coal at the three heating rates. The model utilises the information from the initial two thermogravimetric experiments of 5 and 10 K/min to formulate the matrix of all possible reactions and invert this matrix using equation (17) in Chapter 4, Section 4.2.5, and then predicts the pyrolysis behaviour of the fuel at the third heating rate of 20 K/min.

There is however, a discrepancy in the results obtained from the model and that of the actual TGA data on the pyrolysis curve at heating rate of 20 K/min. This is evident in the under-prediction of the devolatilization at the crucial pyrolysis zone temperatures of 550K-700K, and again the over-prediction of the behaviour of the coal towards the end of the curve during the char formation, at temperatures of 950K-1000K. The error analysis between the actual TGA data obtained and the use of the DAEM are tabulated in Table 6.3 below.

Table 6.3: Relative Error for DAEM vs. TGA

Heating Rate	*%Error*
5 K/min	0.996
10 K/min	0.961
20 K/min	0.687

This discrepancy is due largely to the occurrence of secondary reactions of the primary pyrolysis products. Arenillas et al. (2001) has noted that predominating conditions during the pyrolysis process influence phenomena such as coal fluidity, coal softening and swelling, which in turn affect the porosity and internal surface area of the resultant char. Thus, char reactivity depends on the thermal treatment undergone during coal devolatilization. Additionally, the pyrolysis variables control the product distribution of tar, char and gases, with ignition behaviour also being affected by the devolatilization process.

By looking at the derivative of the mass loss against time information, a clearer picture can be obtained of what occurs during the pyrolysis process. Figure 6.6 shows the results of the derivative information obtained for the three curves. The effect of the relative error between the DAEM and the actual TGA experiments can clearly be seen when looking at the predicted thermogram for the 20 K/min heating rate.

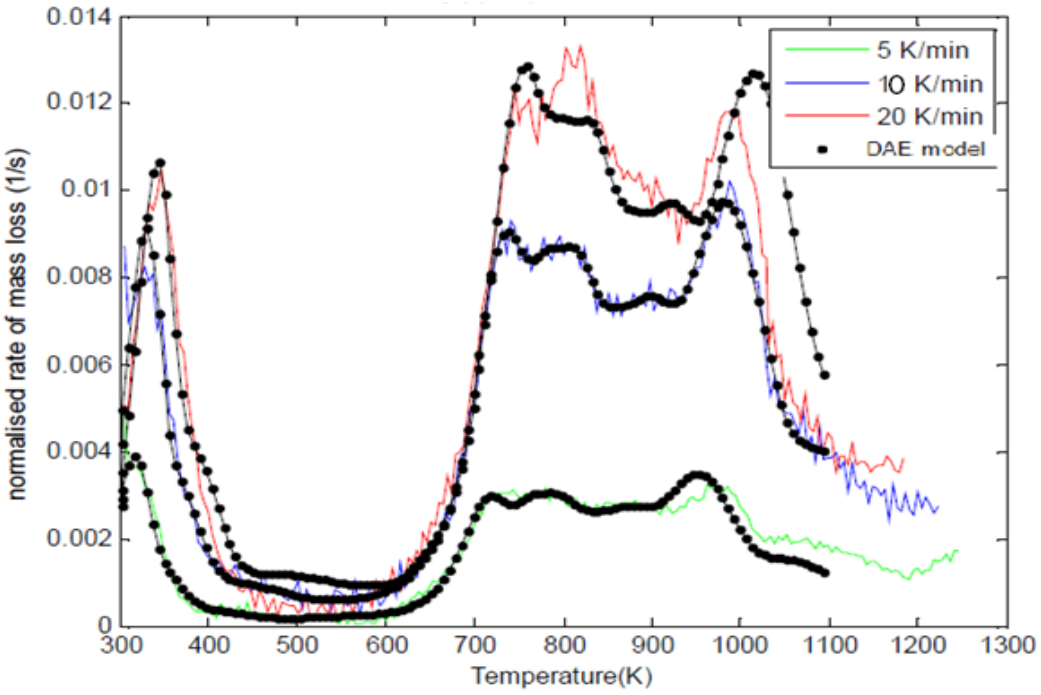

Figure 6.6: Comparison of Derivative Information from Actual TGA Experiments and Modified DAEM for Coal

From the figure, it can be seen that the modified DAEM is accurate at predicting the behaviour of the low heating rate pyrolysis curves of the 5 and 10 K/min heating rates, but when predicting the behaviour of the high heating rate of 20 K/min, the model fits the actual TGA data fairly well up until the crucial devolatilizing zone is reached. At temperatures above 750K, the model either under- or over- predicts the behaviour. This is can largely be attributed to the inherent nature of the type of coal used for the experiment, as confirmed by Antal & Varhegyi (1995) and Howard (1981), so much so that these effects could be caused by the occurrence of secondary reactions of the devolatilized radical species, which the model fails to capture.

This effect is witnessed by Navarro et al. (2008), who in their experiments, have shown that the DAEM is successful at predicting the pyrolysis profile curve for both coal and petcoke, at low heating rates, but starts to deviate at even modestly high heating rates of 20 K/min. Results from their work can be seen in Figure 6.7.

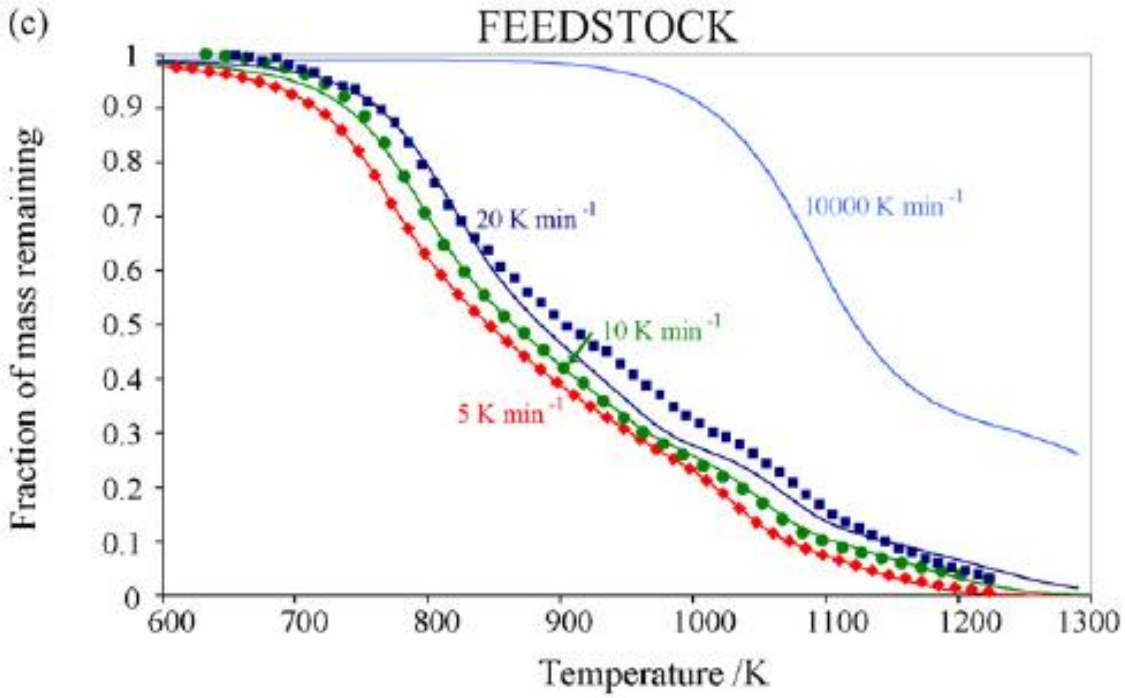

Figure 6.7: Comparison of DAEM vs. Actual TGA Data of Puertollano Coal, Navarro et al. (2008)

Navarro et al. (2008) has shown that when comparing experimental data to data obtained from DAEM predictions, the DAEM provides a near-perfect fit for the two heating rates of 5 and 10 K/min, respectively. However, for the heating rate of 20 K/min, Navarro et al. (2008) has shown that the DAEM is capable of predicting the exact starting temperature for pyrolysis, but for higher temperatures, the model under-predicts the fraction of mass remaining. Navarro et al. (2008) attributes this to the under-prediction of the maximum rate of mass loss, which occurs at around 800K, by the DAEM, to effects such as heat transfer and medium diffusion within the coal sample.

For the heating rate of 20 K/min, the results from the modified DAEM matrix inversion are shown graphically in Figure 6.8.

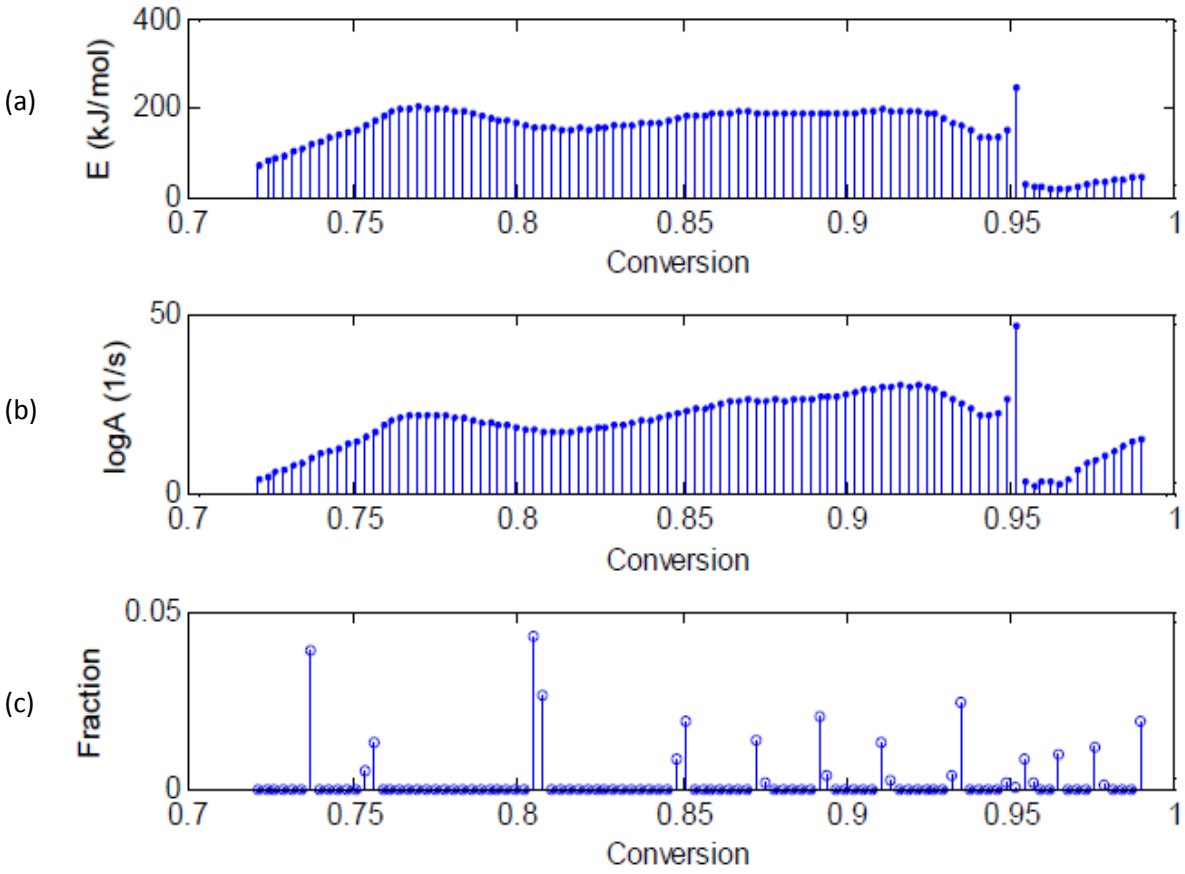

Figure 6.8: Results of Pyrolysis at 20 K/min

(a) Activation Energy vs. Conversion, (b) Pre-exponential Factor vs. Conversion, (c) Mass Fraction of Each Reaction vs. Conversion

The results above are presented in the same style as Scott et al. (2006[a]), and show the activation energy, pre-exponential factor and mass fraction of each reaction, calculated by the modified DAEM at each value of the fraction of mass remaining. Figure 6.8 (c) shows the amounts allocated to each reaction by the matrix inversion. From (c), it can be seen that a majority of the reactions have been allocated a zero mass fraction, indicating that those reactions do not occur at the specified interval. The activation energy and pre-exponential factor are also consistent with the results of the hypothetical scenario proposed by Scott et al (2006[a]).

The results of the matrix inversion are shown in Table 6.4.

Table 6.4: Activation Energy and Pre-Exponential Factors for Coal Pyrolysis Dominating Reactions

Fraction	Activation energy (kJ/mol)	Pre-exponential factor (s^{-1})
0.019	45.24	7.10E+06
0.001	35.624	1.00E+05
0.011	33.161	0.00E+00
0.009	17.731	0.00E+00
0.008	29.442	0.00E+00
0.001	250.574	3.06E+20
0.001	154.339	4.58E+11
0.024	160.969	1.34E+11
0.004	169.901	4.96E+11
0.002	197.028	1.17E+13
0.013	198.424	1.20E+13
0.003	187.822	6.53E+11
0.021	188.803	6.36E+11
0.002	189.241	2.36E+11
0.014	190.419	2.37E+11
0.019	182.198	1.71E+10
0.008	177.568	7.35E+09
0.026	155.575	4.17E+07
0.043	158.688	5.62E+07
0.013	171.262	4.27E+07
0.005	161.149	1.08E+07
0.039	118.867	0.00E+00
0.71	73.011	0.00E+00

From the table, it can be seen that even though the modified DAEM algorithm was made to run with the possibility of 100 reactions, only 23 reactions return an actual mass loss during the matrix inversion, indicating that the remaining reactions do not occur.

The results obtained from the application of the modified DAEM to the pyrolysis of a typical South African coal, indicate that the model is suitable for predicting pyrolysis behaviour at low heating rates, where the devolatilization process occurs as a series of single, first-order reactions provided no secondary reactions occur

which would otherwise tend to interfere with the prediction behaviour generated by the model.

The modified DAEM is also successful in automatically determining the number of reactions occurring, and the mass of each specie devolatilized, as well as the Activation Energy and Pre-exponential Factor, during each reaction by inverting the matrix of Equation (17) in Chapter 4, Section 4.2.5.

At higher heating rates, the model tends to either under- or over-predict the pyrolysis behaviour, owing to the possible occurrence of secondary reactions from the resultant devolatilized radicals. This observation arises due to the occurrence of secondary reactions, as reported by Scott et al. (2006[b]), who suggests that the presence of secondary reactions causes volatile matter cracking resulting in the generation of solid carbon. This observation was also described by Navarro et al. (2008), who attributed the lack of the DAEM to predict the precise pyrolysis profile of both coal and petcoke at even modest heating rates of 20 K/min to the unique nature of these fuels, and the manner in which they undergo thermal decomposition.

The model is also accurate at providing first-hand information about the behaviour of a coal at a high heating rate provided all secondary reactions and other possible experimental factors, such as temperature gradients within the fuel particle, are excluded. The derivative information provides a clear indication of how the coal behaves, and also shows how the modified DAEM fares in predicting the behaviour of the coal.

6.3. Application of the Modified DAEM to Coal-Biomass Blends

Owing to the interesting results obtained from the application of the modified DAEM to the pyrolysis of South African Coal, it was of interest to investigate the use of the modified DAEM in predicting the kinetics of devolatilization of biomass and

coal-biomass blended samples. Scott et al. (2006[b]) applies the modified DAEM to two samples of dried sewage sludge. Sludge A was a digested sludge and Sludge B was an undigested sludge. The results of his work are shown in Figure 6.9.

From the figure, it can be seen that Scott et al. (2006[b]) performed the same routine test work on the sludge samples, by initially performing two TGA experiments at the two heating rates of 10 and 20 K/min respectively, and then using this data, then inputs it into the algorithm to determine the behavior of the sludge at a higher heating rate. He then compares the results obtained from the modified DAEM and results of the actual TGA experiment performed on the two sludge samples at the high heating rate of 40 K/min.

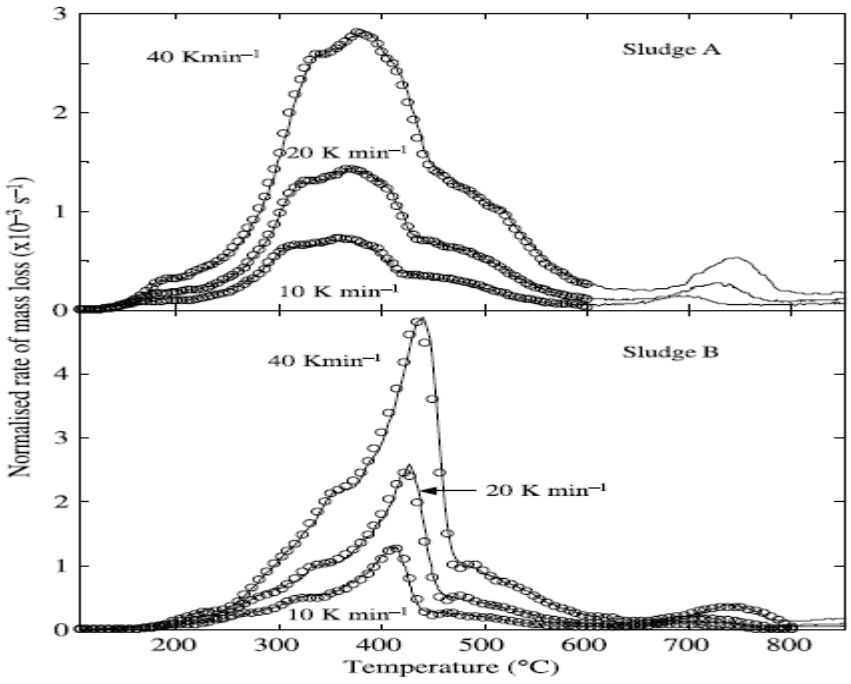

Figure 6.9: Comparison of the Measured Rate of Mass Loss with Those Predicted by the Modified DAEM (circles) (Scott et al. (2006[b]))

The figure shows that the results obtained from the algorithm provide an accurate and precise prediction of the behavior of the biomass samples.

Scott et al. (2006[b]) then uses the output from the modified DAEM to compute the kinetics of the pyrolysis, and this result is shown in Figure 6.10.

The results obtained by Scott et al. (2006[b]) are postulated for 100 possible first-order reactions. Many of these postulated reactions are automatically turned to zero by the algorithm upon the matrix inversion, signifying that that particular reaction does not occur.

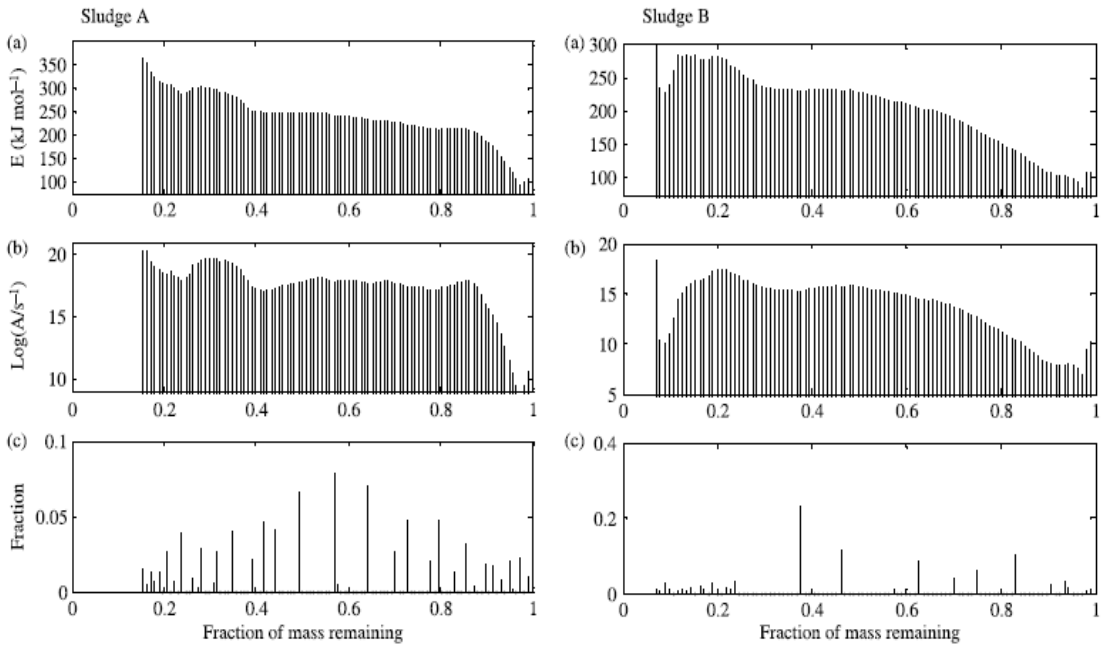

Figure 6.10: Results from the Modified DAEM for the Kinetic Parameters of the Pyrolysis of Sewage Sludge (Scott et al. (2006[b]))

The algorithm generated 100 candidate reactions by evaluating the (a) Activation Energy and (b) Pre-exponential Factor at 100 values of fractional mass remaining; (c) Shows the fraction of volatile material assigned to each of these reactions

It can also be observed from the experiments that for Sludge A the kinetic parameters appear fairly constant, while for Sludge B, the results are slightly more varied. Scott et al. (2006[b]) attributes this to the nature of Sludge B, which is undigested, and thus has a significant amount of cellulosic material. By using the modified DAEM, Scott et al. (2006[b]) is able to show how for both the digested and undigested sludge, the recovered kinetic parameters are nearly indistinguishable

from the actual, experimental measurements, thus confirming the validity of the model to predict the pyrolysis behavior of biomass.

6.3.1 Pyrolysis of Sawdust Biomass

As in the case for coal, TGA experiments were performed at three heating rates for the sawdust. The heating rates chosen varied from 10, 25 and 100 °C/min. The results of the TGA runs can be seen in Figure 6.11.

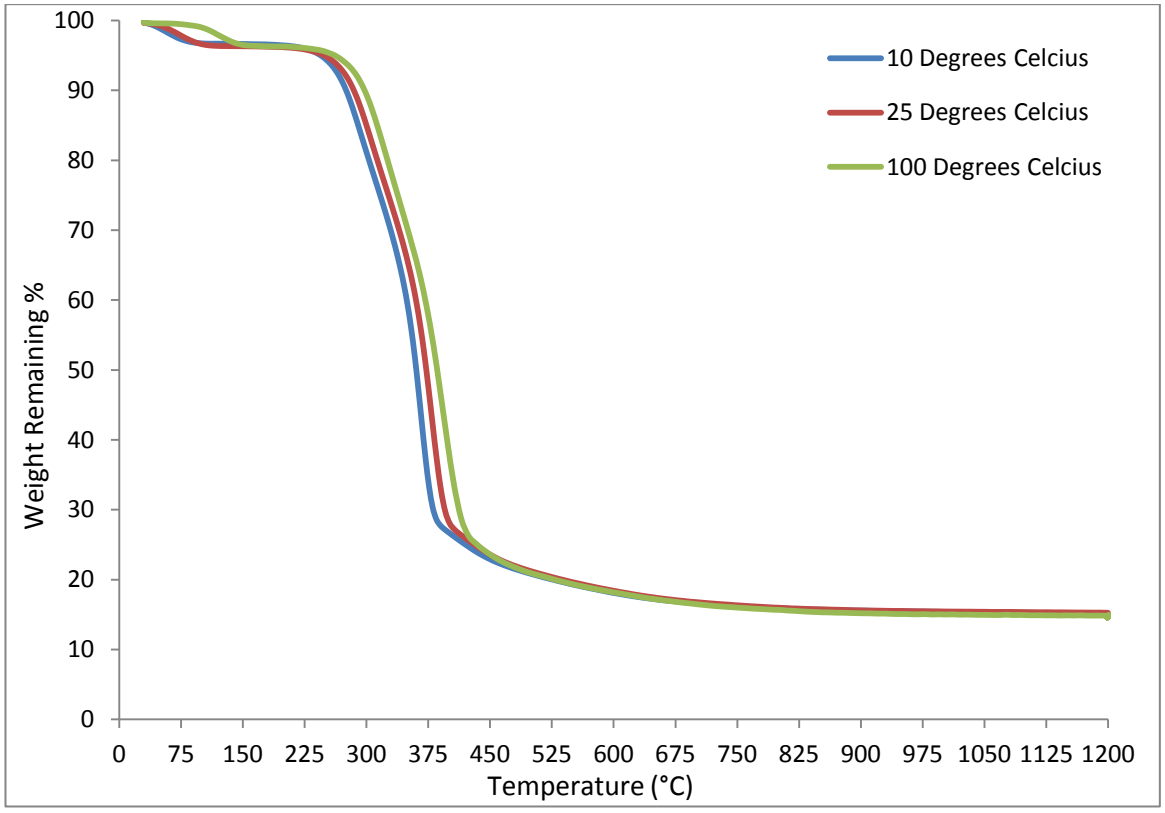

Figure 6.11: Results of TGA of Pyrolysis for Biomass in the Form of Sawdust

From Figure 6.11, it can be seen that as the heating rate increases, the rate of mass loss also increases. Again, this is in agreement with the works by Chern and Hayhurst (2004). It is also important to note that there is no significant difference

between the pyrolysis of biomass at 10 K/min and 25 K/min, as the curves lie nearly on top of each other, indicating that at the onset of pyrolysis for these low heating rates, the behavior of the fuel is nearly identical for both heating rates. As the pyrolysis zone is reached, at temperatures above 300°C, the curves begin to move apart, indicating the effect of heat transfer on the production of pyrolysis products. At temperatures above 400°C, it can be seen that all curves lie neatly on top of each other, indicating a uniform distribution of pyrolysis products (Diaz, 2006). These products are all devolatilized and the char is completely formed at temperatures above 450°C. Further heating beyond this results in no further pyrolysis products being devolatilized.

Again, as in Section 6.3.1, the derivative information gives a more insightful idea of the pyrolysis of the fuel. In Figure 6.12, the pyrolysis results for the biomass can be seen at the three different heating rates.

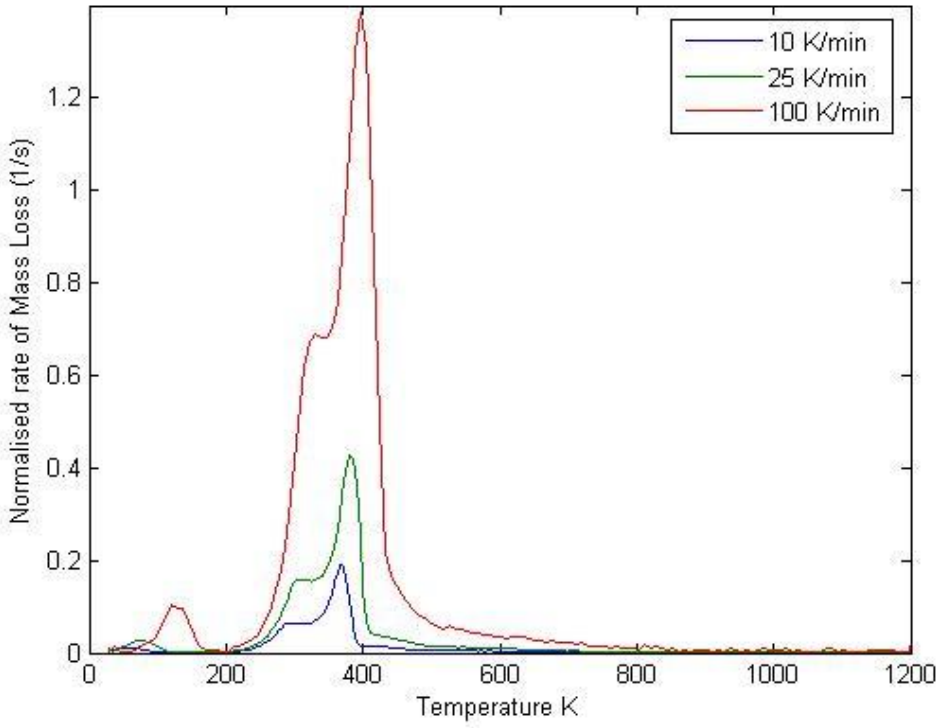

Figure 6.12: Derivative Mass Loss vs. Temperature for Biomass Experiments

The figure above clearly shows the distinct behavior of biomass during the pyrolysis process. The initial peak at the onset of pyrolysis due to moisture loss can be seen. The mass of moisture within this particular sample is not as great as

that of the coal samples analyzed earlier. Although the Proximate Analyses results completed in Section 6.1 show that the level of moisture within the coal is less than that of biomass, (1.17% for coal and 2.04% for biomass), it is however due to the conditions under which the samples were stored, and since the moisture is released around 100°C, is not critical to the pyrolysis step of the fuel.

The temperature at which the pyrolysis process begins to occur is also significantly lower, starting at just after 200 K. This is nearly 100 degrees lower than the onset of pyrolysis for coal, and the mass of volatiles is quickly devolatilized, indicating that by temperatures of around 450 K, the biomass sample is already completely devolatilized, and the char is generated. For the higher heating rates, the mass of volatiles obtained is also greatly increased, indicated by the large change in peak height for the 100 K/min curve when compared to that of the 10 or 25 K/min curves. When the data obtained from the pyrolysis of biomass is compared to that of coal, it can also be seen that while the maximum yield of volatiles for coal varies with temperature for a specific heating rate, the maximum yield of volatiles for biomass is largely uniform, and occurs at a specific temperature for all heating rates. This is due largely to the material that comprises the biomass, largely cellulosic matter (Diaz, 2006), that devolatilizes easily due to its non-complex nature.

The pyrolysis profile obtained for the sawdust is not uncommon in the literature, and numerous authors have shown that for biomass, the general pyrolysis profile is nearly similar across all mediums. Lee & Fasina (2009) have shown that the pyrolysis profile for switchgrass at various heating rates, is similar in appearance, with only the amount of volatiles released increasing, as heating rate is increased. The results of their work can be seen in Figure 6.13.

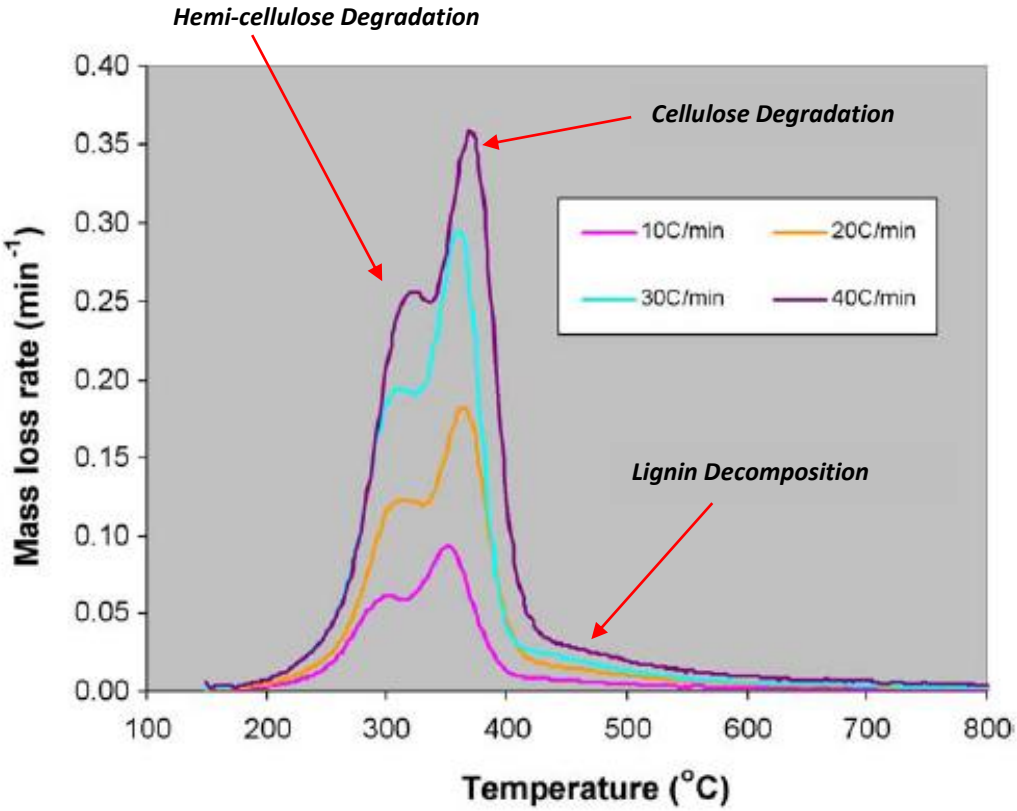

Figure 6.13: Pyrolysis Profile of Switchgrass at Different Heating Rates (Lee & Fasina, 2009)

The authors note that the behavior of switchgrass is not uncommon to other types of biomass analyzed in the literature. According to Lee & Fasina (2009), as typically found in biomass thermogravimetric studies, all the thermograms produced two overlapping peaks: a single peak and a shoulder peak on the left of the single peak.

Based on studies that have been carried out on biomass feedstocks by Tsamba et al. (2006) and Sorum et al. (2001), to name but a few, the shoulder at the left side corresponds to hemi-cellulose decomposition while the higher temperature peak represents the degradation of cellulose. The flat tailing section of the DTG curves at higher temperatures corresponds to the decomposition of lignin since the pyrolysis of lignin has been found to occur over a wide temperature range. The temperature at which the highest mass loss rate was obtained increased with increasing heating rate. The values of the mass loss rates are within the range that has been obtained for other biomass wastes (olive kernel, forest residue, cotton residue, rice husk, cotton straw coconut and cashew nut shells).

The results of the modeling exercise are shown for biomass in Figure 6.14.

The data generated using the modified DAEM, was obtained by specifying 120 reaction points. From Figure 6.21, it can be seen that the algorithm is again accurate at predicting the pyrolysis behaviour of biomass. Here, the data for the 100 K/min curve was generated using the data for the 10 and 25 K/min, respectively.

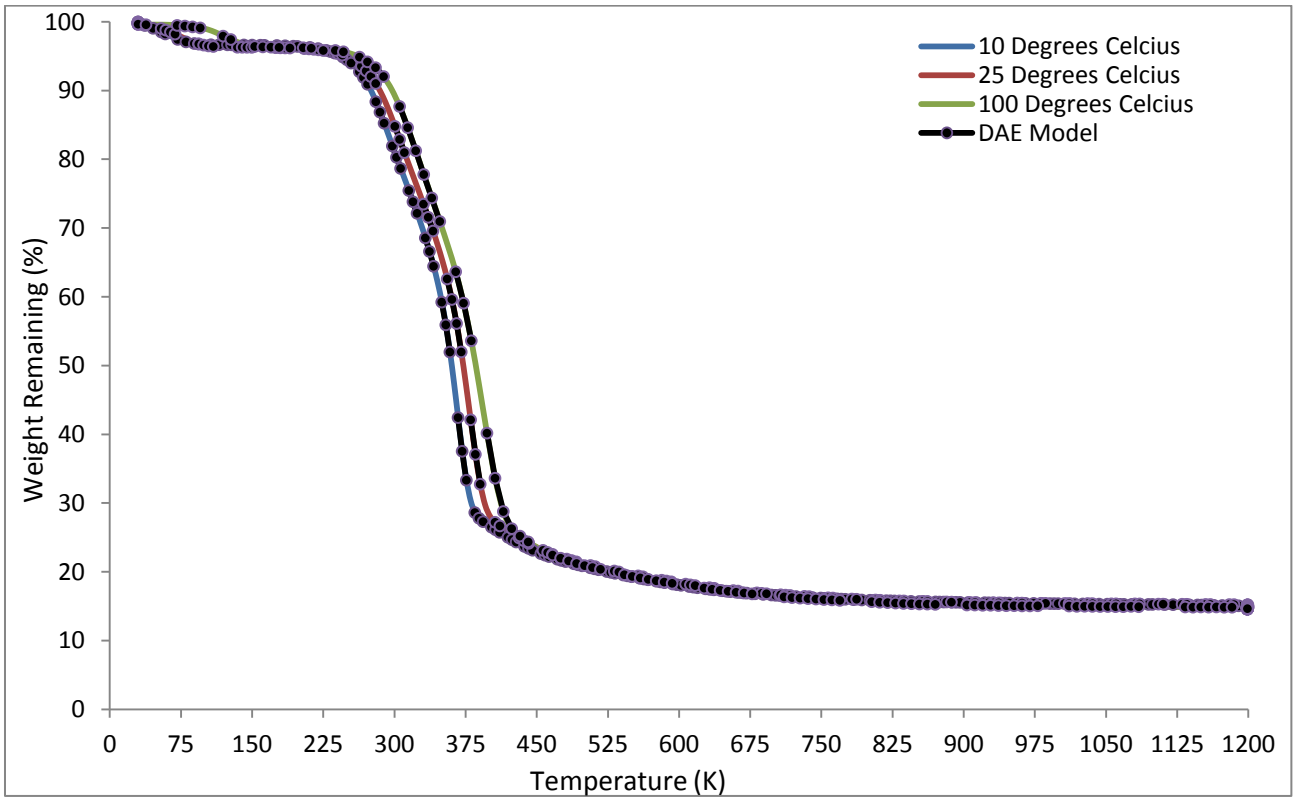

Figure 6.14: Results from DAEM for Pyrolysis Experiments of Biomass

It is important to note that due to the less complex nature of the compounds that comprise the biomass, there is also not a great amount of under- or over-estimation of the results. This agrees with findings by Scott et al. (2006[b]), who found that biomass is generally well suited to thermo-gravimetric kinetic modelling exercises, due to the absence of complex secondary reactions.

These results are confirmed by looking at the derivative information for the biomass at the three heating rates. This can be seen in Figure 6.15.

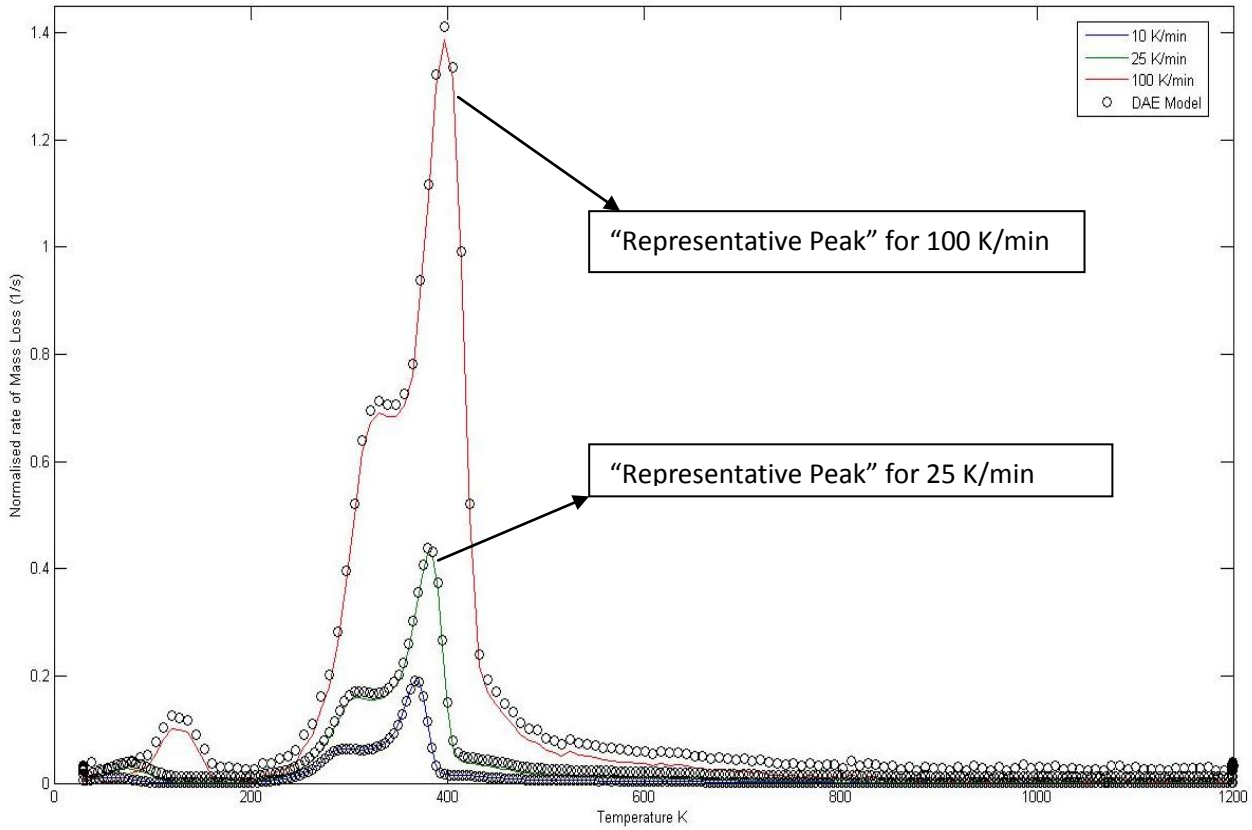

Figure 6.15: Comparison of Derivative Information from Actual TGA Experiments and Modified DAEM for Biomass

From the figure, the results of the DAEM at predicting the pyrolysis behavior of biomass can clearly be seen. At the low heating rates of 10 and 25 K/min, the algorithm gives a near perfect result, however, for the higher heating rate of 100 K/min, the model gives a slight over-prediction. This is explained by Scott et al. (2006[a]), and arises largely due to numeric issues in the computer software when the matrix inversion of equation (17) is carried out. Despite the slight over-calculation due to numerical issues in the matrix inversion algorithm, the model still gives a clear and accurate prediction of the biomass fuel even at the high heating rate of 100 K/min. This is was not the case for the coal sample, where the presence of secondary reactions gave rise to larger over- and under- predictions at the higher heating rate.

The height of the largest peak also indicates the maximum volatiles yield for the sample at the given heating rate. The area under this curve can be analyzed, and

the result of this analysis gives the total mass of the volatiles devolatilized in the temperature interval in question. Work carried out by Lester et al. (2007), has shown that during the pyrolysis of biomass, there appears to be a common peak in all biomass, and even coal-biomass blended samples, as volatile evolution occurs. This was demonstrated in Figure 6.13 above. For purposes of this research, this maximum peak on the pyrolysis curve for biomass will henceforth be termed the 'representative peak'. The curve obtained for the derivative study appears to be similar in shape to the curve obtained by Scott et al. (2006[b]) for the undigested sludge. Scott et al. (2006[b]) attributes the shape of the curve obtained for the sludge to the presence of cellulosic material. Owing to the nature of the biomass used in this study, it can be assumed that the biomass sawdust behaves in a similar manner to the undigested sewage sludge under pyrolysis conditions. This is because undigested sludge comprises more cellulosic material that remains chemically unaltered by bacteriological action. The differing results obtained by Scott et al. (2006[b]) for the digested sludge indicate the chemical alteration of some of the constituents of the biomass, thus resulting in the metabolic products of these micro-organisms on the digestible parts of the sludge.

The underlying characteristic of biomass pyrolysis can best be described by the review given by Sinha et al. (2000) as follows:

The reaction products of pyrolysis are a combination of the products expected from the separate pyrolysis of each of the three major constituents, which are Cellulose, Hemi-cellulose and Lignin. The pyrolysis characteristics of the individual constituents, cellulose, hemicellulose and lignin can best be described as follows:

Cellulose

Cellulose is a glucon polymer consisting of linear chains of B(1,4) d-glucopyranose units. Its average molecular weight is 100,000. Aggregation of these linear chains within the microfibrils provides a crystalline structure that is highly inert and inaccessible to chemical reagents. Cellulose components normally constitute 45-50% of dry wood. Shafizadeh (1982) has studied the pyrolysis of cellulose as the temperature of the sample increased. At temperatures less than 300°C, the

dominant process is the reduction in degree of polymerisation. In the second step, at temperatures above 300°C, there is formation of char, tar and gaseous products. The major component of tar is laevoglucosan that vaporizes and then decomposes with increasing temperature.

Hemi-cellulose

Hemi-cellulose is a mixture of polysaccharides mainly composed of glucose, mannose, galactose, xylose, arabinose, 4-0 methylglucuronic acid and galacturonic acid residues. Generally, it is of much lower molecular weight than cellulose and is amorphous in structure unlike cellulose. Its content varies from 20 to 40%. According to Soltes & Elder (1981), hemi-cellulose is thermally most sensitive and decomposes in the temperature range 200oC to 260oC. This decomposition may occur in two steps; decomposition of the polymer into soluble fragments and/or conversion into monomer units that further decomposes into volatile products. As compared to cellulose, hemi-cellulose gives rise to more volatiles, less tar and char. The components of tar are organic acids such as acetic acid, formic acid and a few furfural derivatives.

Lignin

Lignin is amorphous in nature and a random polymer of substituted phenyl propane units that can be processed to yield aromatics. It is considered as the main binder for agglomeration of fibrous components. The lignin component in biomass varies between 17 and 30%. According to Soltes & Elder (1981), lignin decomposes when heated between 280°C and 500°C. Char is the more abundant constituent in the products of lignin pyrolysis with a yield of 55%. A liquid product known as pyroligneous acid consists of 20% aqueous components and 15% tar residue on dry lignin basis. The aqueous portion is composed of methanol, acetic acid, acetone and water. The tar residue consists mainly of homologous phenolic compounds. The gaseous products represent 10% of the lignin and are composed of methane, ethane and carbon monoxide.

The kinetic data for the pyrolysis of sawdust can be seen in Table 6.5.

Table 6.5: Activation Energy and Pre-Exponential Factors for Biomass Pyrolysis Dominating Reactions

Fraction	Activation Energy (kJ/mol)	Pre-exponential Factor (s^{-1})
R_1: Cellulose	209	$1.13x10^{15}$
R_2: Hemi-cellulose	86.8	$5.28x10^{5}$
R_3: Lignin	17.3	0.0154

The data obtained in table 6.4 above, show the results of the kinetic modelling exercise on the three dominating reactions for biomass pyrolysis. This data is also compared to data from the literature, and the results can be seen in Table 6.6 below.

Table 6.6: Activation Energy and Pre-Exponential Factors for Pyrolysis of Four Different Biomass Samples (Conesa & Domene, 2011)

TYPE OF BIOMASS	ESPARTO GRASS	STRAW	Forest Pruning Waste	Agricultural Pruning Waste
E_1 **(kJ/mol)**	171.8	162.1	103.2	295.9
E_2 **(kJ/mol)**	150.4	239.6	199.4	130.6
E_3 **(kJ/mol)**	229.3	181.6	125.9	102.5
A_1 **(s^{-1})**	$2.33x10^{3}$	$5.05x10^{3}$	558.33	$5.48x10^{7}$
A_2 **(s^{-1})**	$2.82x10^{16}$	$5.08x10^{19}$	$6.1x10^{14}$	$2.4x10^{10}$
A_3 **(s^{-1})**	$9.12x10^{18}$	$1.41x10^{17}$	$2.6x10^{10}$	$9.32x10^{10}$

Where 1 describes the Activation Energy and Pre-exponential Factor for Cellulose decomposition, 2 for that of Hemi-cellulose and 3 for Lignin

As can be seen from table 6.6, the values for Activation Energy and Pre-exponential factor for the 4 types of biomass as quoted by Conesa & Domene (2011), for the three dominating reactions are varying, and show how susceptible biomass is to differing thermal decomposition conditions. The Activation Energy values vary from 103 to 296 kJ/mol, while the pre-exponential factor is orders of magnitude different across the various samples tested. More conclusive work needs to be done to compile a database of kinetic data for various biomass fuels undergoing pyrolysis. Typical data available in literature is usually relevant to the specific geographic location of the researcher, or the precise experimental conditions under which the data was obtained, and while the data serves as a

means of a reasonable comparison, it is not indicative of the behaviour of a biomass sample studied under different experimental conditions.

6.3.2 Pyrolysis of Coal-Biomass Blends

The results of the pyrolysis of coal-biomass blends are presented. The samples were prepared as detailed in Chapter 5, Section 5.2, and then analyzed at the same heating rates of 10, 25 and 100 K/min, respectively. Figure 6.16 shows the results for the three pyrolysis runs performed on the TGA.

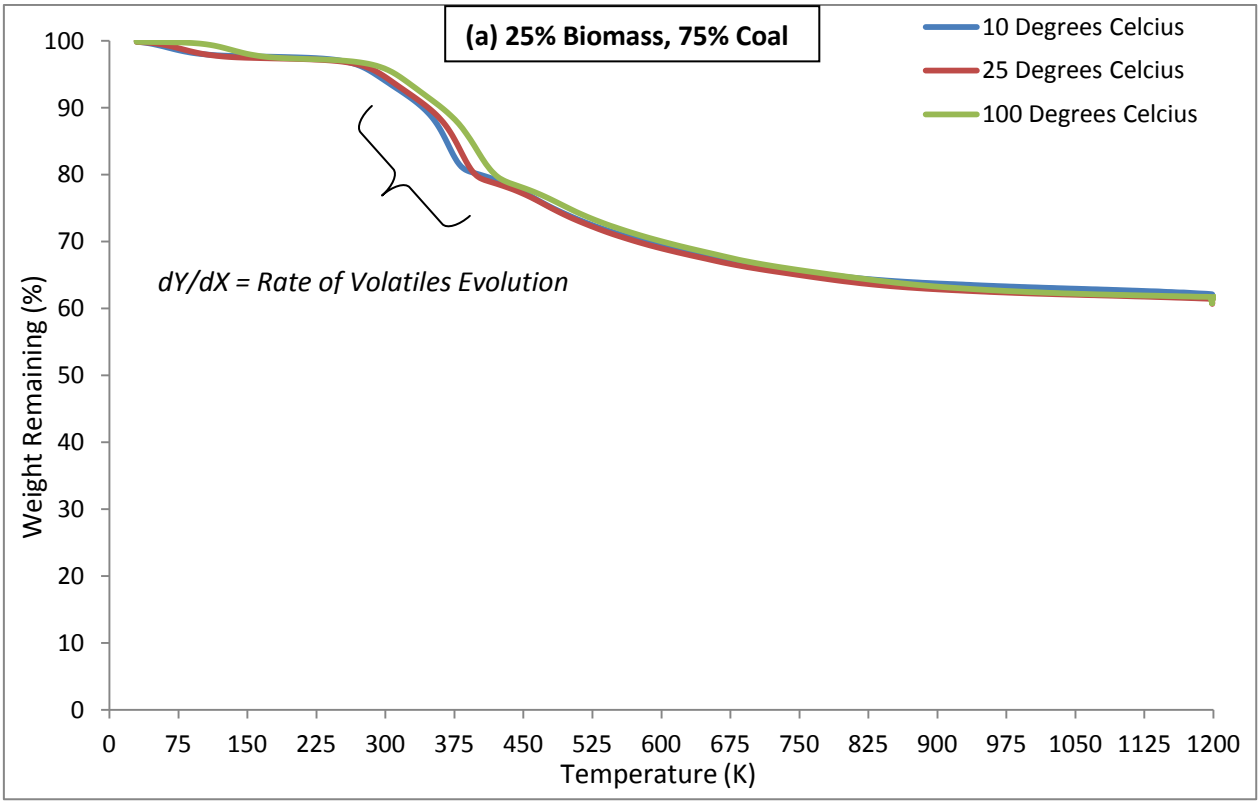

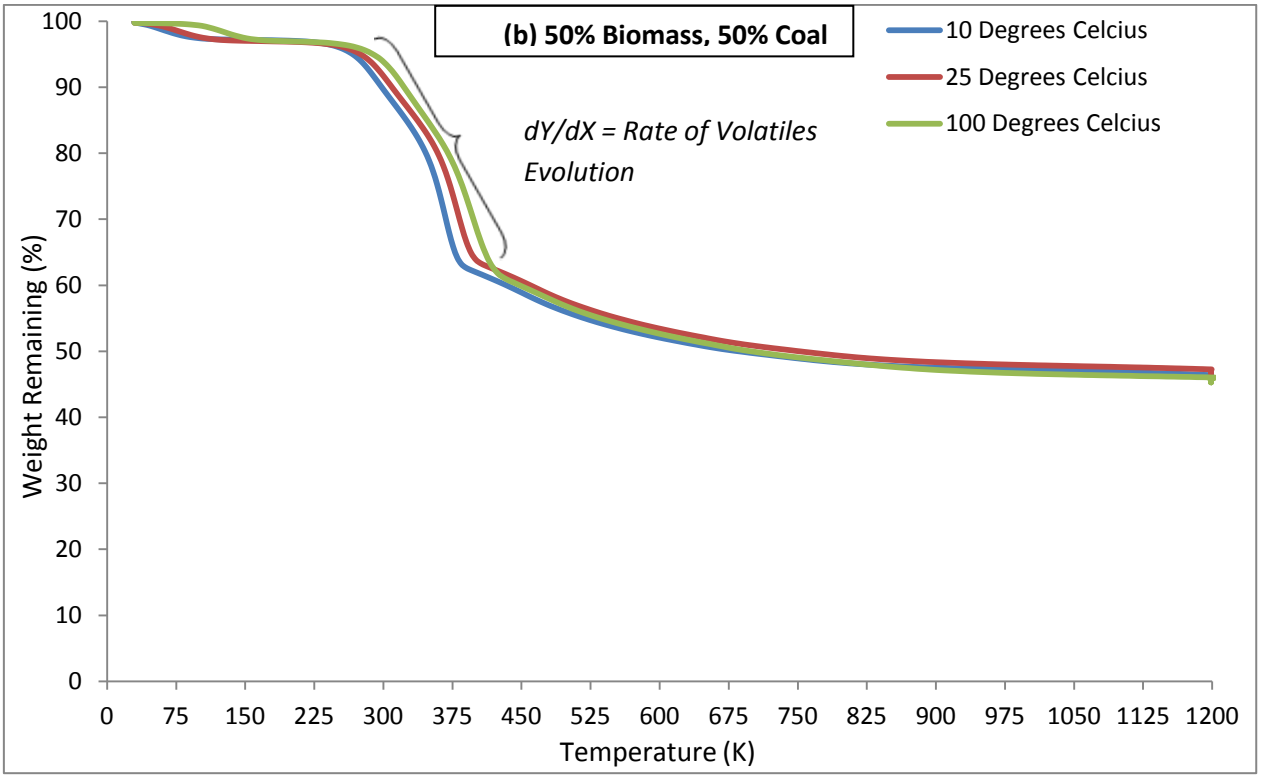

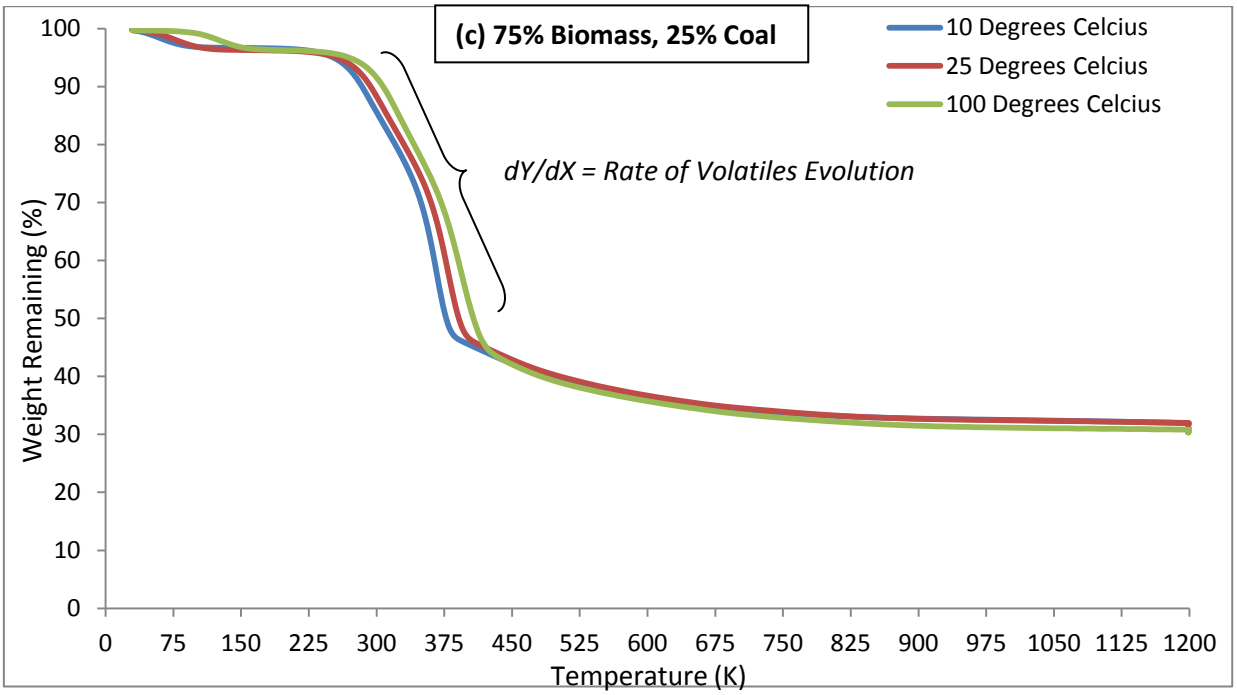

Figure 6.16: Pyrolysis Results for Coal-Biomass Blends

(a) Pyrolysis results of 25% Biomass and 75% Coal Blend
(b) Pyrolysis results of 50% Biomass and 50% Coal Blend
(c) Pyrolysis results of 75% Biomass and 25% Coal Blend

From the results, it can be seen that at the lower mass proportion of biomass (25%), the sample behaves nearly the same as coal, while at the higher biomass concentrations, the sample tends to devolatilize more completely, leaving behind a lighter char. This is evident in looking at the mass remaining for the three samples. For all the samples tested, the char is generated at around 400K, with the total mass loss varying, depending on the biomass concentration. For the 25% biomass sample, the total mass loss of the sample is approximately 35% of the original sample size, while for the 50% biomass sample, the mass loss is 45%, and for the 75% biomass sample this loss is 65% of the original sample size. This shows that as the mass of biomass increases in a coal biomass blend, the mass of volatiles released also increases. This could be due to the simple, cellulosic nature of the biomass material, which devolatilizes fairly easily, while the more complex coal constituents require more time and energy to break down chemical bonds. This leads to the investigation of any interaction between the coal and biomass pyrolysis products during the devolatilization process, and is discussed in Section 6.4.3.

The major difference between the three samples occurs during the crucial pyrolysis zone, denoted by the change in slope of the curve between the temperatures of 225 K and 400 K. The slope of the curve increases significantly as the biomass concentration increases, indicating a smaller fraction of complex volatiles devolatilizing from the sample. This is confirmed by Scott et al. (2006[b]), who noted that due to the cellulosic nature of the biomass, the sample is less likely to generate heavy, tar-like products from the pyrolysis process.

The results are better illustrated by observing the derivative information for the mass loss for the three coal-biomass samples as shown in Figure 6.17.

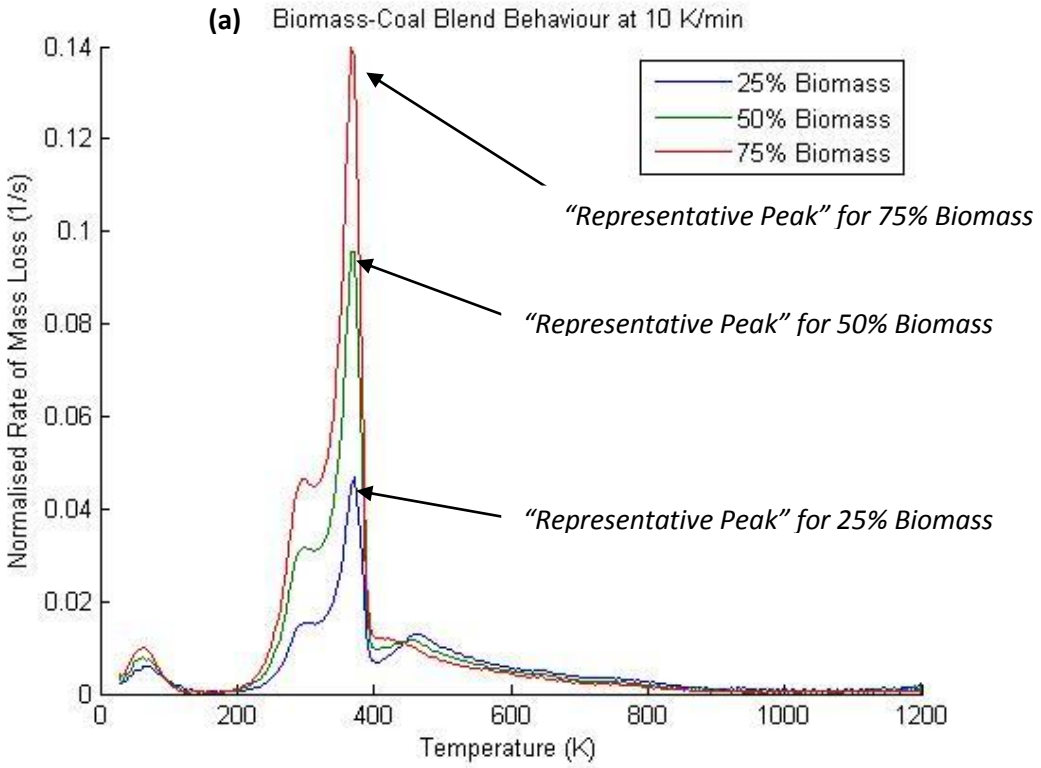
(a) Biomass-Coal Blend Behaviour at 10 K/min
25% Biomass
50% Biomass
75% Biomass
"Representative Peak" for 75% Biomass
"Representative Peak" for 50% Biomass
"Representative Peak" for 25% Biomass
Normalised Rate of Mass Loss (1/s)
Temperature (K)
0.14
0.12
0.1
0.08
0.06
0.04
0.02
0
0
200
400
600
800
1000
1200

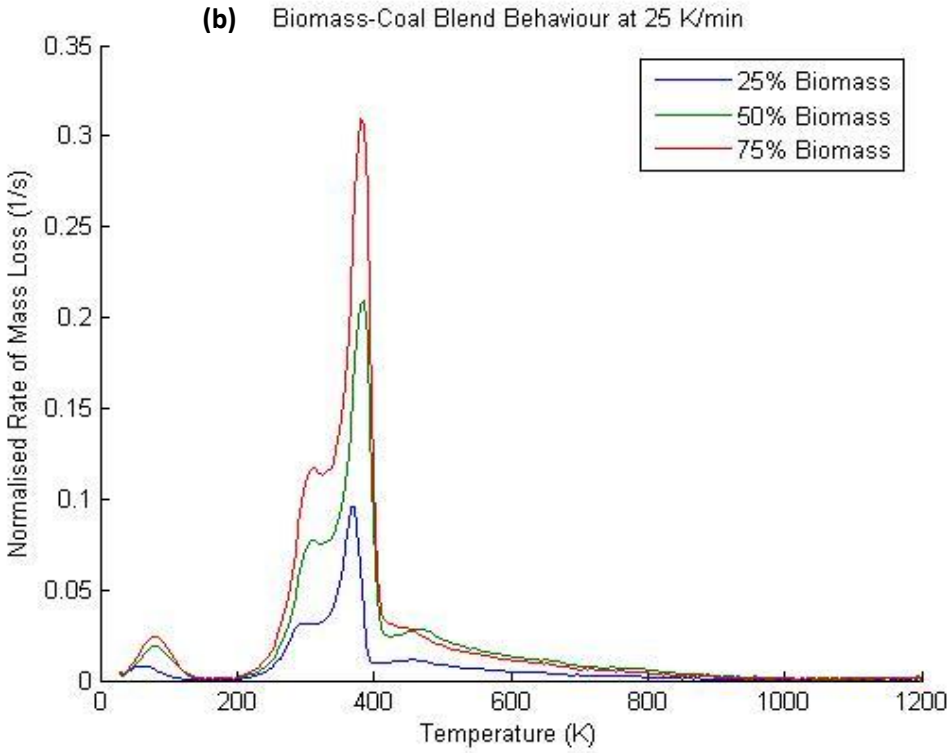
(b) Biomass-Coal Blend Behaviour at 25 K/min
25% Biomass
50% Biomass
75% Biomass
Normalised Rate of Mass Loss (1/s)
Temperature (K)
0.35
0.3
0.25
0.2
0.15
0.1
0.05
0
0
200
400
600
800
1000
1200

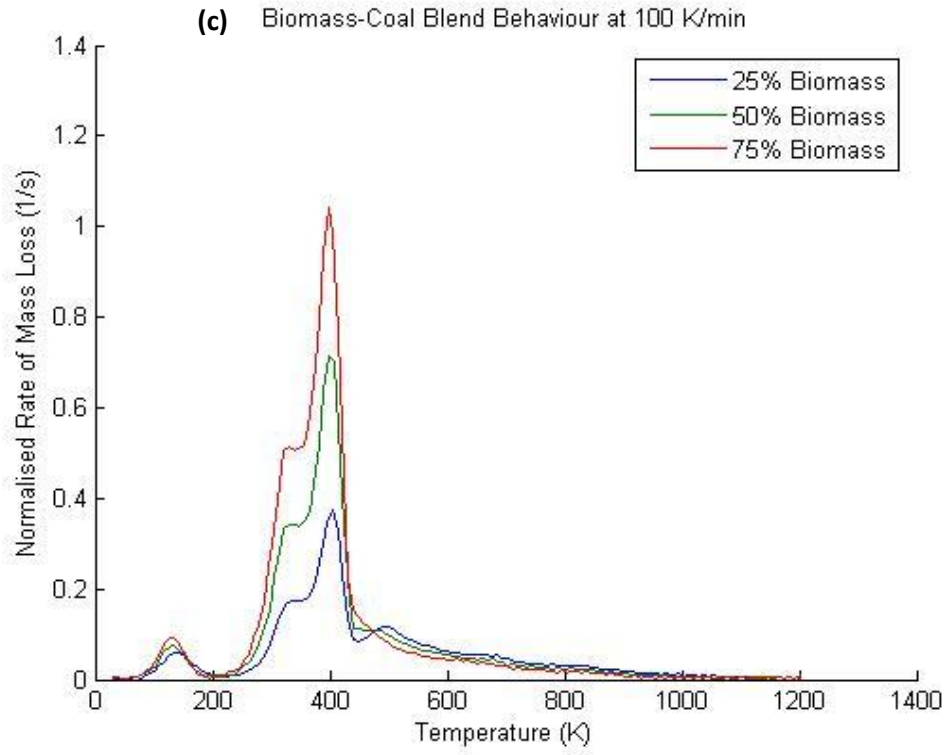

Figure 6.17: Comparison of Coal-Biomass Blends at Different Heating Rates

(a) Pyrolysis results of 25% Biomass and 75% Coal Blend at 10 K/min
(b) Pyrolysis results of 50% Biomass and 50% Coal Blend at 25 K/min
(c) Pyrolysis results of 75% Biomass and 25% Coal Blend at 100 K/min

The figure shows the results for the normalized rate of mass loss as a function of temperature for the three samples at the different heating rates. From the figure, it can be seen that the same general shape is obtained for the pyrolysis profile of a coal-biomass blended sample. It can also be observed that as the biomass concentration increases, the rate of mass loss increases, indicating that even for a constant heating rate, the rate at which volatiles are evolved from a coal-biomass blended sample, depends to some extent on the concentration of biomass or coal present in the sample. Another interesting observation from the results is the dependence of rate of mass loss on heating rate. At the low heating rate of 10 K/min, the maximum rate of volatiles yield, indicated by the maximum height of the representative peak, is approximately 0.14 s^{-1}, while for the increasing heating rate of 25 K/min, this peak height increases to 0.3 s^{-1}, and for the highest heating rate of 100 K/min, this peak height increases to 1.05 s^{-1}. This represents an increase in rate of exponential proportions for increasing heating rate. This result

was observed by Lester et al. (2007), who identified this increase in peak height as the representative peak, and used the Area Under Curve (AUC) analysis to determine any relationship between the concentration of biomass in a blended sample and the area under the representative peak.

6.3.3 Interaction of Coal and Biomass in a Coal-Biomass Blend

Due to the nature of the results obtained from the pyrolysis of coal and biomass blends, it was of interest to the research to investigate the interaction of coal and biomass in a blend during the pyrolysis process, and ascertain whether the presence of one component in the blend influences the behavior of the other. Figure 6.18 shows the results for the derivative mass loss as a function of temperature for the three coal-biomass blended samples, this time, keeping the mass concentrations of biomass constant, while varying the heating rates.

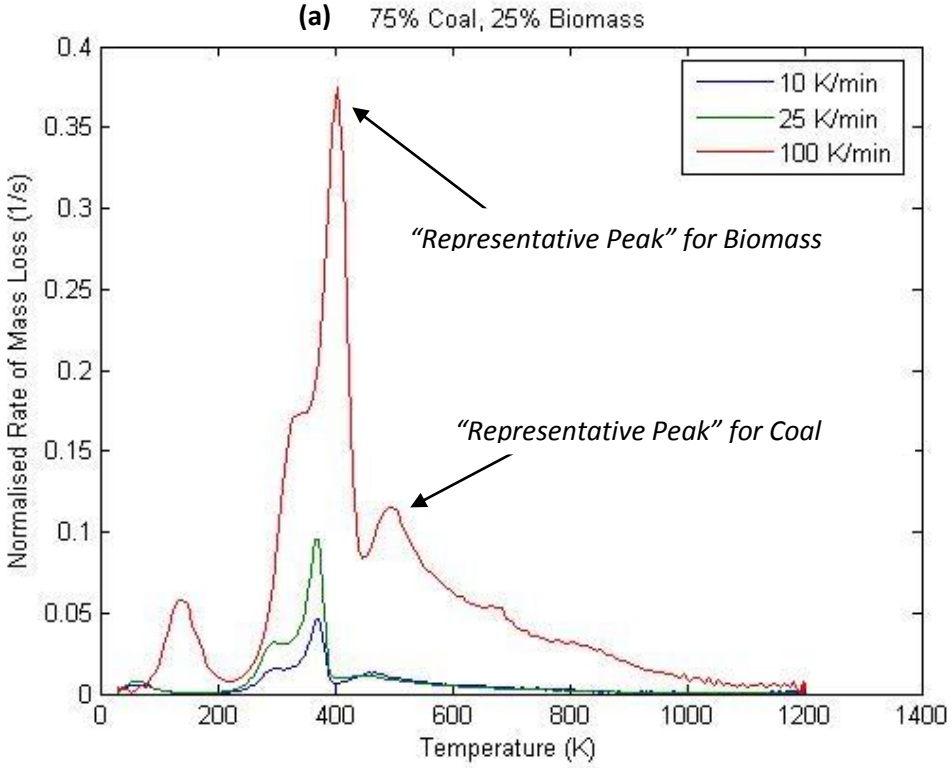

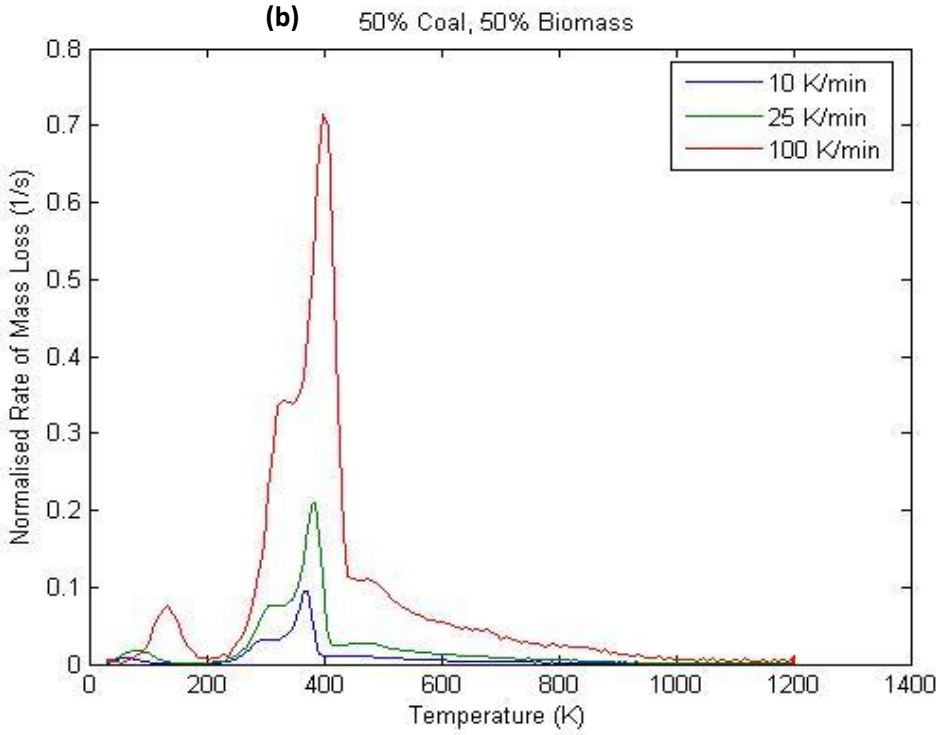

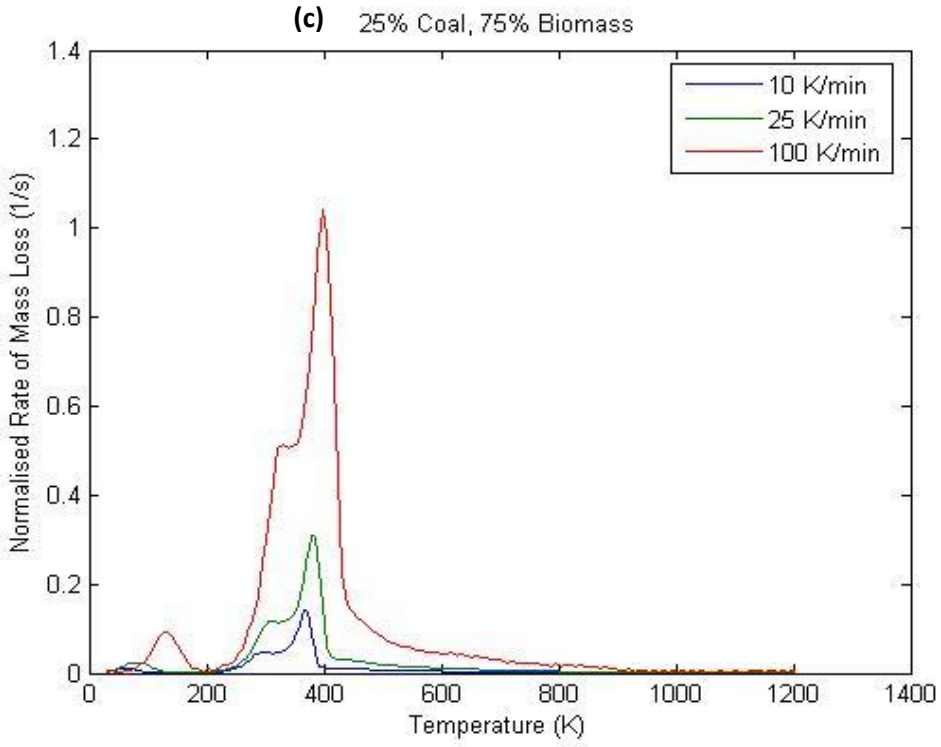

Figure 6.18: Comparison of Coal-Biomass Blends at Mass Concentrations of Biomass

(a) Pyrolysis results of 25% Biomass and 75% Coal Blend
(b) Pyrolysis results of 50% Biomass and 50% Coal Blend
(c) Pyrolysis results of 75% Biomass and 25% Coal Blend

The figure clearly shows the behavior of the coal and biomass for the various heating rates. In Figure 6.18 (a), it can be seen that at the low mass concentration of 25% biomass, the curve gives a clear indication of the separate behavior of the coal and biomass within the sample. For the two low heating rates, of 10 and 25 K/min, respectively, this can be noticed by the slight peak occurring at temperatures around 450K. This would not be noticeable, unless a higher heating rate was used, where the distinction can clearly be seen. The peak of the coal pyrolysis is clearly seen as a separate peak from that of the biomass, indicating that no interaction between the coal and biomass constituents occurs. This can be explained by the fact that the biomass consists of mostly cellulosic components that devolatilize easily, and well before the pyrolysis of coal begins to occur. For a 50-50 blend of coal and biomass the same behavior can be seen, as shown in Figure 6.18 (b), where the representative peak of the coal pyrolysis process peaks at a temperature of around 450K. At the higher biomass concentration of 75%, as seen in Figure 6.18 (c), this effect is not clearly noticeable, and the sample appears to behave as though it were pure biomass.

6.4 Area under Curve Analysis

Another interesting result observed when looking at the representative peak information for coal and biomass blended samples of Figures 6.12 and 6.14, is the somewhat directly proportional relationship between the area under the curve of the representative peak, and the biomass concentration, at a given heating rate. From Figure 6.14, it can be seen that the representative peak for 25% Biomass, reaches a maximum at approximately 0.04 s^{-1}, while for 50% Biomass the curve peaks at 0.95s^{-1}, and at 75% Biomass, the curve peaks at 0.14 s^{-1} .This indicates a somewhat linear relationship between the area under the curve of the representative peak, and the concentration of biomass within a coal-biomass sample. For this exercise, TGA runs were conducted for each blended sample at the heating rate of 50 K/min, and the results can be seen in Figure 6.19 below.

In order to calculate the area under the representative peak for the three biomass samples, it was first necessary to single out the representative peak in question, and integrate underneath the curve to obtain the area. This is where the modified DAEM can be a useful tool to researchers. The modified DAEM can be successfully used to obtain pyrolysis profile curves of coal, biomass and blends, at extremely low, nearly isothermal rates, quickly and reliably, without having to wait for experimental apparatus. Running simulations under these conditions in a laboratory can be extremely time consuming, whereas the modified DAEM can quickly and accurately predict the pyrolysis profiles for these extreme conditions, in a matter of minutes. The results of the representative peaks used for this research are shown in Figure 6.19.

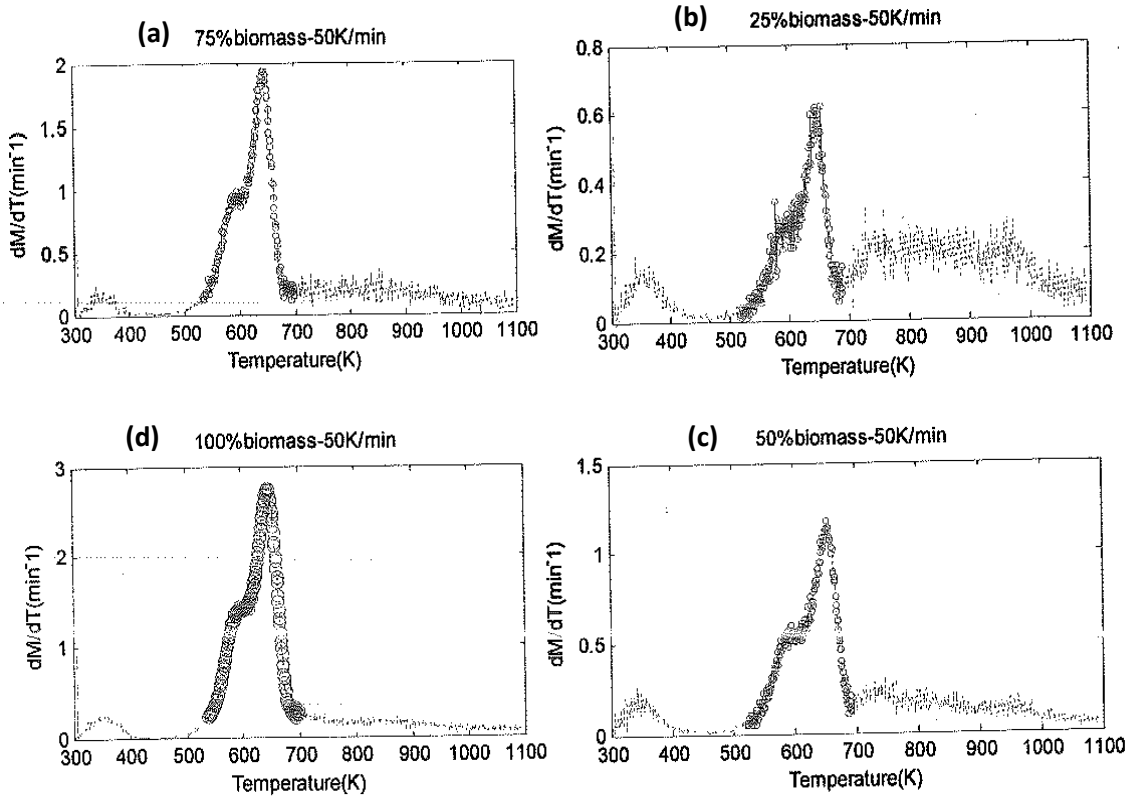

Figure 6.19: Selection of Representative Peak for Area under Curve Analysis

(a) DAEM Results for 75% Biomass Blend at 50 K/min
(b) DAEM Results for 25% Biomass Blend at 50 K/min
(c) DAEM Results for 50% Biomass Blend at 50 K/min
(d) DAEM Results for 100% Biomass Blend at 50 K/min

The figure shows the application of the modified DAEM to the pyrolysis profile for the 25%, 50%, 75% and 100% biomass samples at the constant heating rate of 50

K/min. The dotted segment indicates the selection of the representative peak for the four samples. This representative peak, for purposes of this study, is defined as the peak indicating the maximum yield of volatiles for a given fuel, in a given temperature interval. i.e In this example, the representative peak for this heating rate of 50 K/min, occurs in the temperature interval of 500 – 700 K.

However, from the figure, it can be seen that the start and end of the curve that comprises the representative peak, is not clearly defined, as can be seen by the presence of the slight 'bump' on the left side of the peak, and the turning point on the right side of the peak. This can be improved by making use of the modified DAEM, and generating the pyrolysis profiles for these samples at extremely low heating rates. This results in higher resolution images of the pyrolysis process, and allows for nearly isothermal kinetic data to be easily obtained. The results of the high resolution, near-isothermal pyrolysis profiles for the four samples can be seen in Figure 6.20.

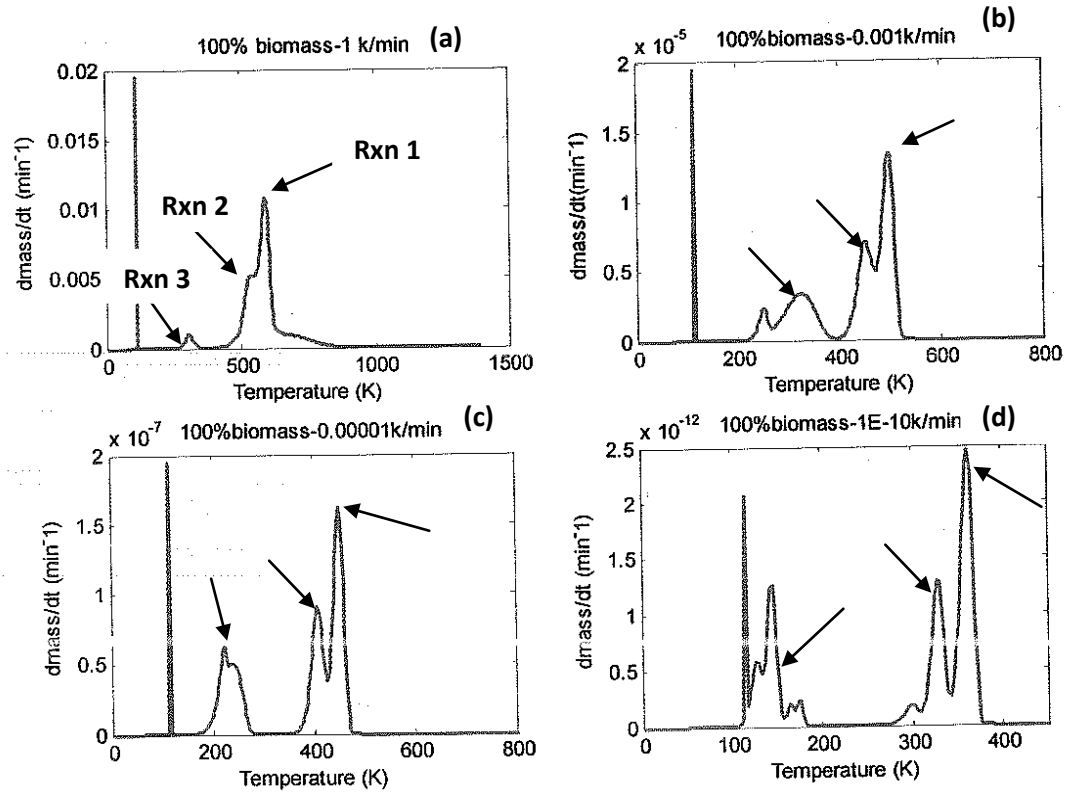

Figure 6.20: High Resolution Pyrolysis Profiles at Near-Isothermal Conditions

(a) DAEM Results for 100% Biomass at 1 K/min

(b) DAEM Results for 100% Biomass at 0.001 K/min
(c) DAEM Results for 100% Biomass at $1x10^{-5}$ K/min
(d) DAEM Results for 100% Biomass at $1x10^{-10}$ K/min

From the figure, it can be seen that as the heating rate is gradually decreased, the representative peak, which as described in Section 6.3.1, represents a dominating reaction at that particular temperature, begins to separate out into the individual components that compromise that dominating reaction. This is indicated by the arrows on the figure, to enable one to clearly view the separation of the dominating reactions, into its constituent reactions. Figure 6.20 (a) shows that for 100% Biomass at 1 K/min, there appears to be only three dominating reactions, indicated by the three peaks. At a heating rate of 0.001 K/min, Figure 6.20 (b), the third reaction suddenly separates and becomes two individual reactions. As the heating rate is lowered furthered, to $1x10^{-5}$, Figure 6.20 (c), the second reaction begins to separate from the main, representative peak, and at the extremely low, nearly isothermal heating rate of $1x10^{-10}$ K/min, Figure 6.20 (d), the representative peak is clearly defined, and separated from the other reactions. It is also interesting to note that the third reaction has now separated into five more reactions, indicating the effectiveness of the modified DAEM at predicting these dominating reactions, even at such low heating rates. The results of the continual lowering of the heating rate until the representative peak has been completely isolated can be seen in Figure 6.21.

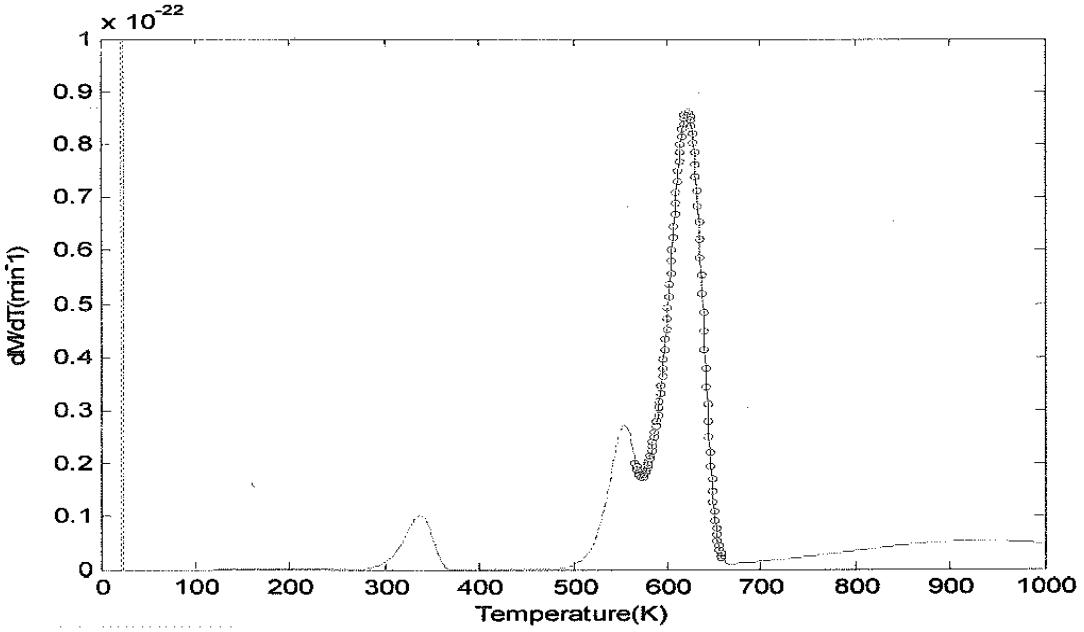

Figure 6.21: Isolation of Representative Peak for 100% Biomass at Heating Rate of $1x10^{-22}$ K/min

It can be seen that at a heating rate of $1x10^{-22}$ K/min, a sufficiently smooth and fairly continuous function for the representative peak can be obtained. Had this been carried out in a laboratory scale TGA, the time taken to generate the data would far exceed the time taken to generate the data using the modified DAEM. Once the representative peak has been sufficiently singled out from other dominating and interacting reactions, the area under the curve (AUC) can be determined using traditional mathematical techniques. This technique involves identifying the representative peak, and assumes that the curve is continuous and symmetrical about the abscissa of bisection. The result of the AUC analysis can be seen in Figure

(a)

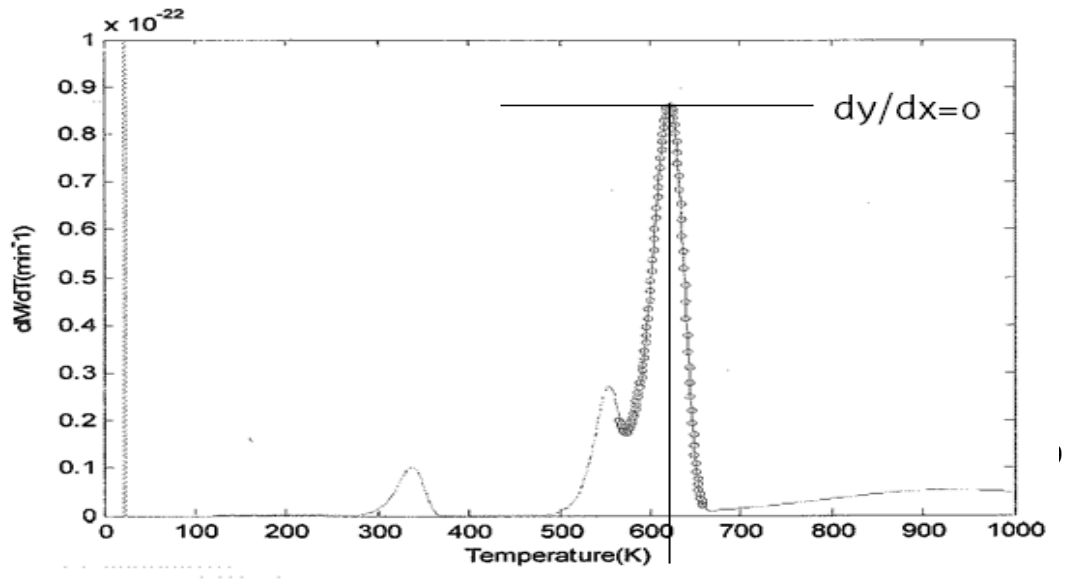

6.22.

(b)

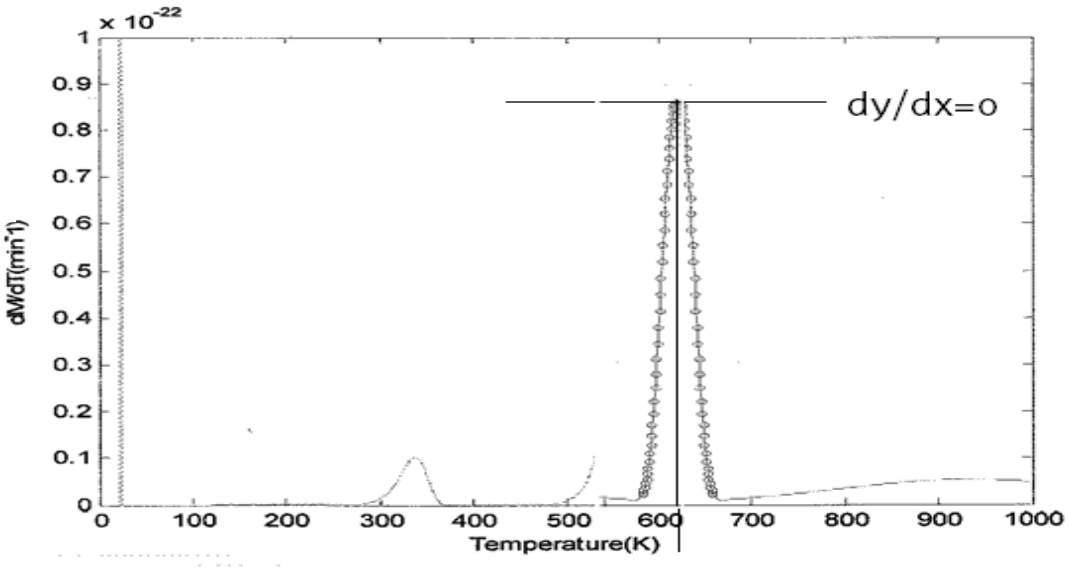

Figure 6.22: AUC Analysis for 100% Biomass

(a) Identification of the turning point and construction of perpendicular bisector for 100% Biomass (b) Reflection of the curve about the line x= perpendicular bisector, in order to duplicate the RHS of the curve

From the figure, it can be seen that in order to correctly isolate the representative peak, mathematical analyses had to be carried out. Firstly, the turning point of the representative peak was identified, by analyzing the derivative information, and observing the point at which the second derivative equates to zero. This indicates the point at which the tangent to the curve intersects at that point. Once this was identified, the perpendicular bisector to the derivative at this point was constructed; this can be seen in Figure 6.22 (a). The figure also shows that the right hand side of the representative peak is better defined, in terms of starting and end points, and the left hand side is not so easy to ascertain, due to the interaction of the second reaction, denoted by the peak on the left hand side of the representative curve of Figure 6.22 (a). In order to overcome this, it was assumed that the function describing the representative peak is smooth and continuous but more importantly, nearly Gaussian, allowing for the use of traditional mathematical techniques for curve analyses. It must be noted that this technique, while not entirely accurate, provides a reasonable estimate of the area under the curve, but should be used with caution. Once the perpendicular bisector was constructed, the right hand side of the curve was reflected across this line, to give a fair representation of the entire

representative peak, independent from the interaction of any other reactions. This can be seen in Figure 6.22 (b). The representative peak is now clearly defined, and the area under the curve can be easily obtained using traditional integration techniques. The area under the representative peak was calculated using the *TRAPZ* command in Matlab® 7.0. The results of the AUC integration for the three heating rates for the biomass-blended samples are shown in Tables 6.7, 6.8, 6.9 and 6.10. The results are displayed alongside the results obtained using the DAEM at the respective heating rates for the best approximation of the AUC, using the *TRAPZ* command in Matlab® 7.0.

Table 6.7: AUC Results for Heating Rate of 10 K/min

Sample Blend	Area Under Curve of Representative Peak	Mass % of Biomass
100% Biomass	2.01	1
75% Biomass	1.382	0.75
50% Biomass	0.869	0.5
25% Biomass	0.561	0.25
0% Biomass	0	0

Table 6.8: AUC Results for Heating Rate of 25 K/min

Sample Blend	Area Under Curve of Representative Peak	Mass % of Biomass
100% Biomass	2.21	1
75% Biomass	1.64	0.75
50% Biomass	1.02	0.5
25% Biomass	0.796	0.25
0% Biomass	0	0

Table 6.9 AUC Results for Heating Rate of 100 K/min

Sample Blend	Area Under Curve of Representative Peak	Mass Fraction of Biomass
100% Biomass	3.96	1
75% Biomass	2.63	0.75
50% Biomass	1.72	0.5
25% Biomass	1.47	0.25
0% Biomass	0	0

Table 6.10 AUC Results for Heating Rate of 10^{-22} K/min

Sample Blend	Area Under Curve of Representative Peak	Mass % of Biomass
100% Biomass	1.343	1
75% Biomass	0.959	0.75
50% Biomass	0.564	0.5
25% Biomass	0.297	0.25
0% Biomass	0	0

From the results, it can be seen that as the heating rate increases, the area under the curve of the representative peak also increases. This increase is almost linear. The combined results of the AUC analysis for the three different heating rates can be seen in Figure 6.23.

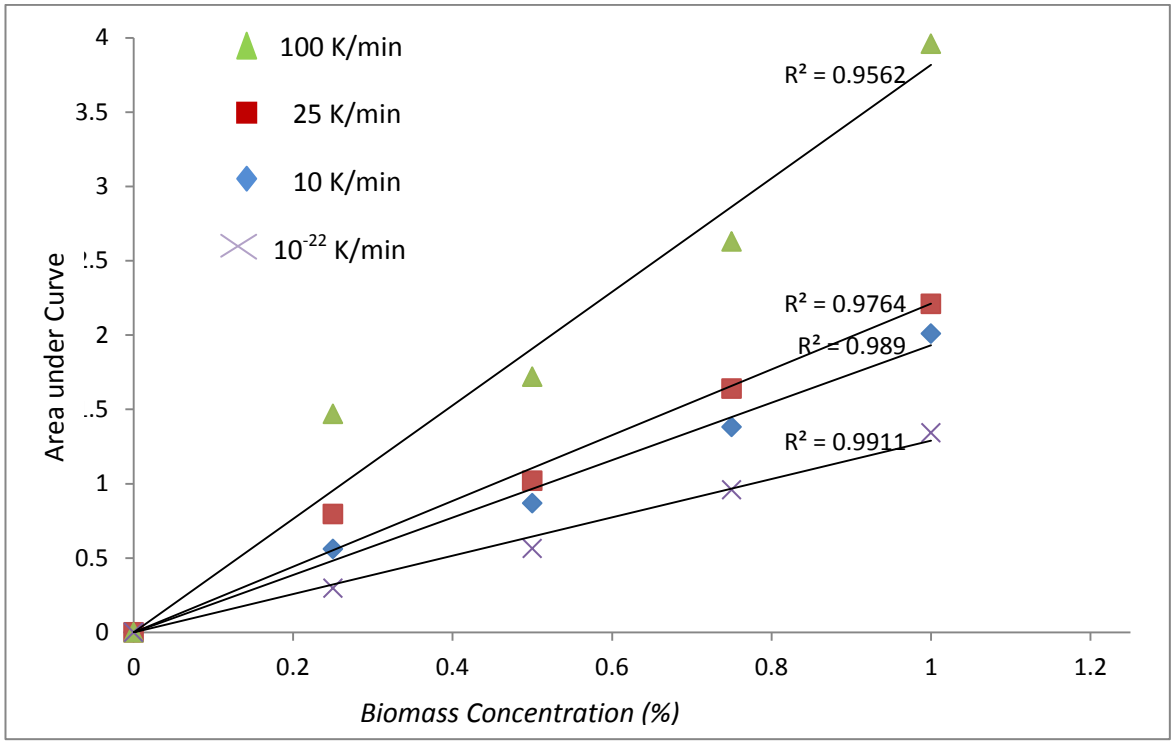

Figure 6.23: AUC Analysis for Biomass Blends at Various Heating Rates

From the figure, it can be seen that nearly all blend proportions of biomass lie on a straight line. The relative error of the experimental points is considerably small, and can be corrected by better analysing the start and end points of the representative peak curve. It can also be seen from the figure that the relative error increases as the heating rate increases. At the low heating rate of 10^{-22} K/min, the AUC analysis for the representative peak gives a relative error of 0.99, whilst at the slightly higher heating rate of 10 and 25 K/min, this error increases to 0.989 and 0.976, respectively. For the high heating rate of 100 K/min, this error increases even further to 0.956, with nearly all the points lying outside the straight line, only the start and end points actually forming what looks like a linear relationship. This is indicative that as heating rate increases, the relationship between biomass concentration present in a blend, and the heating rate might not actually be linear.

The outlying points are due largely to numerical issues arising from the points which were chosen as the end points for the representative peak. It cannot be simply assumed that the representative peak begins and ends at the x-axis, but for simplicity

sake, this was assumed during the integration. A proper analysis of the beginning and tail ends of the representative peak will yield a more accurate result.

This information can be a useful tool in determining the concentration of an unknown sample. By constructing the AUC vs. Biomass Concentration curve at the same constant heating rate, if the unknown sample lies on the line representing the biomass concentration, then the mass of biomass present in the unknown sample can easily be determined. This is also useful when conducting experiments or using fuels that require high heating rates, where representative peaks can otherwise be diluted, and not clearly seen. By slowing the heating rate down using the DAE model, the representative peak can be easily identified. This result depends largely on the type of biomass used, the TGA machine in which the pyrolysis experiments were conducted, and the non-interaction of the biomass with the coal present in the blend. Better numerical techniques will also yield a more accurate result. In this instance, the *TRAPZ* command in Matlab ® 7.0, uses the trapezoidal rule to determine the area under the curve. A more robust technique such as Simpson's rule or multi-point Gaussian Quadrature can yield a better result, but the results obtained here are sufficient to show that there exists a linear relationship between AUC and biomass concentration in a coal-biomass blended sample.

6.5 Summary

This chapter showed that the results from the modelling exercise indicate that the modified form of the DAEM is an effective tool for determining the pyrolysis profiles of coal, biomass and blends of coal and biomass, at various constant heating rates. The model is also effective at determining the behaviour of a fuel undergoing pyrolysis, provided no secondary reactions within the fuel or between the devolatilized products and fuel occur. The DAEM can successfully predict the behaviour of a fuel undergoing pyrolysis at high heating rates, not uncommon to industry, provided secondary reactions are accounted for. The model is an effective tool for the generation of high resolution images, obtained at nearly isothermal conditions, where dominating reactions can be clearly separated and accounted for.

This has a major advantage over traditional isothermal techniques, as results are obtainable quickly, and the results obtained are accurate. The differences in the pyrolysis profiles for coal and biomass were shown, and the behaviour of these two fuels was shown to differ, due largely to the constituents that comprise the particular fuel. Since biomass is comprised of largely cellulosic material, it devolatilizes easily with three noticeable and distinct reactions, while coal, on the other hand, is comprised of various aliphatic and aromatic groups that devolatilize at their own unique rate and temperature. This drew the conclusion that it is necessary in industry, to match the correct operating conditions for industrial boilers or gasifiers, with respect to heating rate, to the type of fuel being used.

The chapter also highlighted the important result of utilizing a blend of coal and biomass, in order to achieve a larger yield of volatiles, as well as an improved heat transfer mechanism for the transference of heat to the coal particles. This allows the speeding up of the pyrolysis reactions of the coal constituents due to an increase in available heat.

Lastly, the chapter highlighted the use of the DAEM in generating high resolution images for the isolation of the representative peak, in order to show that a linear relationship exists for the area under the representative peak, and the mass of biomass within the sample. This can be utilised as an effective tool in determining the mass concentration of biomass in an unknown coal-biomass blended sample.

Chapter 7: Conclusion

This chapter concludes the research presented, by highlighting key findings from the modeling process. Future groundwork is also laid for further work, and this is outlined in recommendations for future work.

7.1 Global Conclusions

The results of the modeling exercise have shown the versatility of the DAEM as a model to quickly obtain data about the pyrolysis profile for coal, and biomass, as well as coal-biomass blends. To this end, the following important information was discussed:

- Chapter one outlined the importance of the research, and showed the necessity for a robust model which can quickly, and reliably predict the pyrolysis profile for coal, biomass and coal-biomass blends. The context of the research was set, and the measurable aims and objectives of the research were outlined.

- Chapter two discussed the mechanism of pyrolysis, where it occurs, and more importantly, how pyrolysis can be a useful tool in determining numerous characteristics of fuels, such as volatiles content, aliphatic content, aromatic content, etc. A thorough description of thermo-gravimetric analyses was given, along with a discussion about why TG- analyses are the preferred method for analyzing kinetic data for fuels. The different types of TG machines are discussed, and a comparison of each is given. An in-depth discussion of how South African coal was formed, and the underlying geological history that led to its unique formation is presented. This

chapter sought to understand the inherent nature of coal, so that modeling exercises can be easily understood

- Chapter three showed the many conditions that affect the pyrolysis process, and how these conditions affect the behavior of coal and biomass during thermal decomposition. Numerous examples of research carried out by various authors is given, and their work is used as basis for understanding the behavior of South African coal during the pyrolysis modeling exercise. The different types of biomass are also shown, and more importantly, the future biomass will play in the South African Renewable Energy program. Different biomass-to-energy conversion technologies are discussed, and focus is given to technologies that use pyrolysis as a means for energy conversion.

- Chapter four provides a historical examination of the development of numerous modeling techniques, developed over time by numerous researchers. As technology became more accessible, and mathematical techniques more advanced, so too, did models for predicting thermal decomposition become more and more accurate. The success of the modified form of the DAEM at providing an easier, faster way for calculating the Activation Energy and Pre-exponential Factor as compared to the traditional DAEM was shown. The earlier DAEM utilized a complex numerical integration technique requiring considerable amount of time and processing power. The modified DAEM was also shown to work effectively to model the pyrolysis behaviour of coal, biomass and blends of coal and biomass as the model requires only data from TGA experiments, and calculates the kinetics independent of sample composition. This provides an advantage of the DAEM as a means of providing a model-free approach to determining the Activation Energy (A) for any sample undergoing pyrolysis.

- Chapter four also showed that the results from the modelling exercise indicate that the modified form of the DAEM is an effective tool for determining the pyrolysis profiles of coal, biomass and blends of coal and biomass, at various constant heating rates. It is important to note, that the model is only successful at predicting pyrolysis behaviour at fairly low heating rates, as at high heating rates, secondary reactions tend to dominate, resulting in incorrect predictions for pyrolysis of coal. The model is an effective tool for the generation of high resolution images, obtained at nearly isothermal conditions, where dominating reactions can be clearly separated and accounted for. This has a major advantage over traditional isothermal techniques, as results are obtainable quickly, and the results obtained are accurate. The differences in the pyrolysis profiles for coal and biomass were shown, and the behaviour of these two fuels was shown to differ, due largely to the constituents that comprise the particular fuel. Since biomass is comprised of largely cellulosic material, it devolatilizes easily with three noticeable and distinct reactions, while coal, on the other hand, is comprised of various aliphatic and aromatic groups that devolatilize at their own unique rate and temperature.

- Chapter six highlighted the important result of utilizing a blend of coal and biomass, in order to achieve a larger yield of volatiles as witnessed in the literature by Pokothoane (2008), where the researcher noted that co-firing of coal and biomass in a pulverized burner, resulted in a synergistic effect, enhancing the combustion characteristics of the fuel. Lastly, the chapter highlighted the use of the DAEM in generating high resolution images for the isolation of the representative peak, in order to show that a linear relationship exists for the area under the representative peak, and the mass of biomass within the sample. This can be utilised as an effective tool in determining the mass concentration of biomass in an unknown coal-biomass blended sample.

It is important to note, that a key finding of the modelling exercise has shown the importance of in industry of matching the correct operating conditions for industrial boilers or gasifiers, with respect to heating rate, to the type of fuel being used. This key conclusion was shown from the modelling pyrolysis profiles, where, as the heating rate increased, the rate of volatiles evolution was changed, and the temperature at which devolatilization occurred also changed. Current research has shown how utilizing a blend of coal and biomass can help increase the rate of volatiles devolatilized during the combustion process, as the biomass has shown to exhibit independent behaviour of the coal, resulting in earlier devolatilization, thus allowing more heat transfer to occur to the coal substrate. This essentially allows industries to combust coal more effectively, with better, cleaner energy yields.

By using the DAEM to slow the heating rate to extremely low magnitudes, the pyrolysis profile behaves nearly isothermal, allowing for the generation of high-resolution images, from which the representative peak can clearly be singled out. This representative peak depicts the reaction dominating at a specific temperature interval, and can be used, in the case of a coal-biomass blend, to determine the biomass concentration, by carrying out the Area Under Curve analysis technique. This technique has shown to display a linear relationship between Area Under the Curve of the representative peak, and the biomass concentration in the blend.

Ultimately, the purpose of this research was to show that the Distributed Activation Energy Model, as described by Scott et al. (2006[a]) is effective at determining the pyrolysis behaviour of South African coal, biomass and coal-biomass blends. This was duly accomplished, and the groundwork now is to lay the foundation for future work into more extensive research for gasification and combustion technologies.

7.2 Recommendations

The use of the DAEM for kinetic modelling of fuels undergoing pyrolysis was shown to be successful, provided secondary reactions can be accounted for. To this end, it is the recommendation of the author to further investigate the following avenues of research to enhance the use of the DAEM as the preferred model for kinetic studies of coal and biomass:

- The use of the DAEM to better predict secondary reactions, and account for these in the model. This would require a more robust description of the thermal decomposition kinetics, as well as better numerical techniques to analyze them. Future work in this field will result in the DAEM being more capable of predicting true and accurate profiles for fuels undergoing pyrolysis, at any heating rate.

- Applying the DAEM to combustion studies. Ultimately, combustion and gasification are the preferred technologies for coal-to-energy and biomass-to-energy processes. Combustion is a much more complex process, and the presence of secondary reactions is invariably possible. A robust DAE model will successfully predict the combustion profiles for coal or biomass, and this information will be invaluable to industries, as matching operating conditions to the combustion behaviour of the fuel will become relatively easy, from a simple modelling exercise.

Interest has already been shown in some of these recommendations, and work by authors such as Sakhele (2010), has shown that the DAEM is capable of predicting the combustion profiles of coal at very low heating rates, but for heating rates greater than 20 K/min, the model under-predicts the profile. The author has attributed this to numerous secondary reactions, which occur when devolatilized components come into contact with evolved hydrogen atoms, in the presence of oxygen. While Sakhele (2010) has shown that modelling

combustion is possible, using the DAEM, more work needs to be done in better describing these secondary reactions.

7.3 Summary

This chapter highlighted the conclusions from the research. Key learning's from the modelling exercise are given. Each chapter is analysed, and the main conclusions are drawn. Ultimately, the research concludes with the proposed aim of showing that the DAEM is an effective tool for the kinetic modelling of the pyrolysis of coal, biomass, and coal-biomass blends. Future recommendations are given for further work in expanding the area of research.

References

Anderson, J.B., *A Criterion for Isothermal Behaviour of a Catalyst Pallet*, Chemical Engineering Science, 18, (1963), 147-150.

Antal, M.J., Grønli, M.G., *The Art, Science and Technology of Charcoal Production*, Industrial & Engineering Chemistry Research, 42, (2003), 1619-1640.

Antal, M.J., Varhegyi, G., *Cellulose Pyrolysis Kinetics Revisited* Industrial Engineering and Chemical Research, 34, 1995, 703-717.

Anthony, D.B., Howard, J.B., *Coal Devolatilization and Hydrogasification*, A.I.Ch.E. Journal, 22, (1976), 625-655.

Anthony, D.B., Howard, J.B., Hottel, H.C., Meissner, H.P., Fifteenth Symposium (International) on Combustion, The Combustion Institute, Pittsburgh, (1974), 1303-1317.

Arenillas, A., Rubiera, F., Pevida, C., Pis, J.J., *A Comparison of Different Methods for Predicting Coal Devolatilization Kinetics*, Journal of Analytical and Applied Pyrolysis, 58-59, (2001), 685-701.

Badzioch, S. and Hawksley, P.G.W., *Kinetics of Thermal Decomposition of Pulverized Coal Particles*, Ind. Eng. Chem. Process Des. Dev., 9, (1970), p. 521.

Badzioch, S., *Thermal Decomposition*, ibid, Vol. 31 (4), (1967), 193-218.

Berkowitz, N., *Coal Science and Technology 7*, *The Chemistry of Coal*, Elsevier, New York, (1985), 223.

Berndesa G, Hoogwijk M, van den Broek R., *The Contribution of Biomass in the Future Global Energy Supply: A Review of 17 Studies*. Biomass and Bioenergy, 25, (2003), 1–28.

Biagini, E., Lippi, F., Petarca, L., Tognotti, L., *Devolatilisation Rate of Biomasses and Coal–Biomass Blends: An Experimental Investigation*, Fuel 81, (2002), 1041–1050.

Braun, R.L., Burnham, A.K., *Analysis of Chemical Reaction Kinetics Using a Distribution of Activation Energies and Simpler Models*, Energy and Fuels, 1, (1987), 153-161.

Bridgwater, A.V., *Biomass Fast Pyrolysis*, Bio-Energy Research Group, Aston University, Birmingham, UK, (2002).

Braudel, F., *The Structures of Everyday Life*, Vol. 1, (1981).

Burnham, A.K., Braun, R.L., *Global Kinetic Analysis of Complex Materials*, Energy and Fuels, 13, (1999), 2-27.

Burnham, A.K., Braun R.L., Gregg, H.R., Samoun, A.M., *Comparison of Methods for Measuring Kerogen Pyrolysis Rates and Fitting Kinetic Parameters*, Energy and Fuels, 1, 1987, 452-458.

Chern, J.S., Hayhurst, A.N., *Does a Large Coal Particle in a Hot Fluidised Bed Lose its Volatile Matter According to the Shrinking Core Model*?, Combustion and Flame, 139, 2004, 208-221.

Church, R., *The History of the British Coal Industry*, Vol. 3, 1830-1913, Oxford, UK: Clarendon Press, (1986).

Coats A.W., Redfern J.P., *Kinetic Parameters from Thermogravimetric Data,* Nature, 201, (1964), 68.

Conesa, J.A., Domene, A., *Biomass Pyrolysis and Combustion Kinetics Through n-th Order Parallel Reactions*, Thermochimica Acta, (2011), Universidad de Alicante Press.

Deane, P., *The First Industrial Revolution*, New York: Cambridge University Press, (1965).

Deng, N., Zhang, Y., Wang, Y., *Thermo-gravimetric Analysis and Kinetic Study on Pyrolysis of Representative Medical Waste Composition*, Waste Management, 28, (2007), 1572-1580.

Diaz, C.J.G., *Understanding Biomass Pyrolysis Kinetics: Improved Modelling Based on Comprehensive Thermokinetic Analysis*, PhD. Thesis, Universitat Politècnica de Catalunya, (2006).

Freeman, E.S., Carroll J., *The Application of Thermoanalytical Techniques to Reaction Kinetics: The Thermogravimetric Evaluation of the Kinetics of the Decomposition of Calcium Oxalate Monohydrate,* J. Phys. Chem., 62, (1958), 394.

Friedman, H., *Kinetics of Thermal Degradation of Char-forming Plastics from Thermogravimetry*, J. Polym. Sci., Part C, 6, (1964), 183.

Feng, B., Bhatia, S.K., *On the Validity of Thermogravimetric Determination of Carbon Gasification Kinetics*, Chemical Engineering Science **57** (2002), pp. 2907–2920.

Falcon, R.M.S., *A Brief Review of the Origin, Formation and Distribution of Coal in Southern Africa*, Mineral Deposits of Southern Africa, I & II, Geological Society of South Africa, (1986), 1879-1899.

Falcon, R.M.S., Ham, A.J., *The Characteristics of Southern African Coals*, J. S.Afr. Inst. Min. Metall., Vol. 88, No, 5, (1988), 145-161.

Gavalas, G.R., *Coal Pyrolysis*, New York: Elsevier Scientific Publishing Company, (1982).

Gavrikov, V.V., Mozgovay, E.D., Belan, Z.G., *Effect of Particle Size and Pre-Heating on Plastic Properties of Coal Mass*, Coke and Chemistry USSR, No. 1, (1967), p. 7.

Gómez-Barea , A., Arjona, R.,. Reaction-diffusion Model of TGA Gasification Experiments for Estimating Diffusional Effects, Fuel, 84 (12-13), (2005), pp 1695-1704.

Gray, D., Cogoli, G.C., Essenhigh, R.H., *Problems in Pulverized Coal and Char Combustion*, Am. Chem. Soc., 131, (1974), 72-91.

Hall, D.O., Overend, R.P., *Biomass: Regenerable Energy*, Hall, D.O. and Overend, R.P. (Eds.), John Wiley & Sons, (1987), p.469–473.

Hoogwijk M, Faaij APC, van den Broek R, Berndes G, Gielen D, Turkenburg W., *Exploration of the Ranges of the Global Potential of Biomass for Energy*. Biomass and Bioenergy, 25, (2003), 119–133.

Howard, J.B., *Fundamentals of Coal Pyrolysis and Hydrogasification*, In: Elliot, M.A. (Ed.), Chemistry of Coal Utilisation, Wiley, New York, (1981), 665-785.

Howard, J.B., Peters, W.A., Serio, M.A, *Coal Devolatilization Information for Reactor Modelling*, EPRI AP-1803, Massachusetts Institute of Technology,, Cambridge, MA, (1981).

Jones, J.F., Schmid, M.R., Eddinger, R.T., *Fluidized-bed Pyrolysis of Coal*, Chem. Eng. Progr., 60, No. 6, (1964), 69-73.

Jüntgen, H., *Review of the Kinetics of Pyrolysis and Hydropyrolysis in Relation to the Chemical Constitution of Coal,* Fuel, 63, (1984), 731-737.

Jüntgen, H., Van Heek, K.H., *Recent Results on the Kinetics of Coal Pyrolysis and Hydropyrolysis and their Relationship to Coal Structure*, Paper Presented to the Meeting on Coal Fundamentals, (1977), Stoke Orchard.

Kaltschmitt, M., Dinkelbach , L. *Biomass for Energy in Europe—Status and Prospects*. University of Stuttgart, Germany, (1997), 537 pp.

Kimber, G. M., Gray, M. D., *Comparison of Evolution of Heteroatoms from Coal and Petroleum Based Electrode Cokes*, *Am. Chem. Soc. Sym. Ser*.; **21**; (1976), 445-450.

Klass, D.L., *Biomass for Renewable Energy, Fuels, and Chemicals*, Academic Press, San Diego, CA, (1998), p.651.

Kobayashi, H., Howard. J.B., Sarofim, A.F., *Sixteenth Symposium (International) on Combustion*, The Combustion Institute, Pittsburgh, (1977), 427-436.

Lee, S-B., Fasina, O., *TG-FTIR Analysis of Switchgrass Pyrolysis*, Journal of Analytical and Applied Pyrolysis, 86, (2009), 39-43.

Lester, E., Gong, M., Thompson, A., *A Method for Source Apportionment in Biomass/Coal Blends Using Thermogravimetric Analysis*, J. Anal. Appl. Pyrolysis, 80, (2007), 111-117.

Lewellen, P.C., *The Rapid Devolatilization of Lignite*, U.R.O.P. Report, Chem. Eng. Dept., Massachusetts Institute of Technology, (1973).

Loisson, R., Cauvin, F., *Pyrolyse Rapid de Charbon*, Chim. Ind. (Paris), 91, (1964), 269-273.

Mahalingam, R., *Evolution of Tars and Gases during Devolatilization of Coal in a Fixed Bed Reactor*, PhD Thesis, Department of Chemical Engineering, Washington State University, (1985).

Maniatis, K., Palz, W., Spitzer, J., Kwant, K., Helm, P., Grassi, A., *Thermal Conversion of Biomass into Secondary Products: The Case of Gasification and Pyrolysis*, Twelfth European Biomass Conference, Amsterdam, Netherlands. (2002), 38-44.

Matsumoto, J., Nakata, T., *The Energy System Analysis and Forecasts of the Republic of South Africa*, In Proceedings of the Industrial & Commercial Use of Energy (ICUE) Conference, (2007) Cape Town.

Miura, K., *A New and Simple Method to Estimate f(E) and k(E) in the Distributed Activation Energy Model*, Energy and Fuels, 9, (1995), 302-307.

Miura, K., Maki, T., *A Simple Method for Estimating f(E) and k(E) in the Distributed Activation Energy Model from Three Sets of Experimental Data*, Energy and Fuels, 12, (1998), 864-869.

Morgan, P.M., *An Experimental and Modelling Study of Coal Pyrolysis in a Lurgi Gasifier*, M.Sc. Dissertation, University of the Witwatersrand Press, (1991).

Navarro, M.V., Aranda, A., Garcia, T., Murillo, R., Mastral, A.M., *Application of the Distributed Activation Energy Model to Blends Devolatilization*, Chemical Engineering Journal, 142, (2008), 87-94.

Ozawa, T., *A New Method of Analysing Thermogravimetric Data*, Bull. Chem. Soc. Jpn., 38, (1965), 1881-1886.

Ollero, P., Serrera, A., Arjona, R., Alcantarilla, S., *Diffusional Effects in TGA Gasification Experiments for Kinetic Determination*, Fuel 81, (2002), 1989-2000.

Peters, W., Bertling, H., *Kinetics of the Rapid Degasification of Coals*, Fuel, 44, (1965), 317-331.

Pitt, G.J., *The Kinetics of the Evolution of Volatile Products from Coal*, Fuel, 41, (1962), 264-274.

Please, C.P., McGuinness, M.J., McElwain, D.L.S., *Approximations to the Distributed Activation Energy Model for the Pyrolysis of Various Coals*, Combustion and Flame, 133, (2003), 107-117.

Plumstead, E.P., *Coal in Southern Africa*, Johannesburg: Witwatersrand University Press, (1957).

Pokothoane, P., *Analyses of Co-firing Biomass with SA Coal in Pulverised Coal Boilers*, PhD. Candidate, University of the Witwatersrand Press, (2008).

Rostami, A.A., Hajalgol, M.R., Wrenn, S.E., *A Biomass Pyrolysis Sub-model for CFD Applications*, Fuel, 83, (2004), 1519-1525.

Sakhele, K., *Modelling Pyrolysis and Combustion Using the DAEM*, Final Year Research Report, University of the Witwatersrand Press, (2010).

Salisbury, F.B., Ross, C.W., *Plant Physiology*, Wadsworth Publishing Co., Inc., Belmont, (1992).

Scott, S.A., Dennis, J.S., Davidson, J.F., Hayhurst, A.N., *An Algorithm for Determining the Kinetics of Devolatilisation of Complex Solid Fuels from Thermogravimetric Experiments*, Chemical Engineering Science, 61, (2006[a]), 2339-2348.

Scott, S.A., Dennis, J.S., Davidson, J.F., Hayhurst, A.N., *Thermogravimteric Measurements of the Kinetics of Pyrolysis of Dried Sewage Sludge*, Fuel, 85, (2006[b]), 1248-1253.

Shafizadeh, F., *Introduction to Pyrolysis of Biomass* , Journal of Analytical and Applied Pyrolysis, (1982), **3**: 283-305.

Sinha, S., Jhalani, A., Ravi, M.R, Ray, A., *Modeling of Pyrolysis in Wood: A review*. J Solar Energy Soc., India, (2000), 10(1): 41-62.

Smoot, L.D., Smith, P.J., *Coal Combustion and Gasification*, New York: Plenum Press, (1985).

Soltes, E.J., Elder, T.J., Organic *Chemicals from Biomass*, Pyrolysis, (1981), CRC Press: 63-95.

Snyman, C.P., Barclay, J., *The Coalification of South African Coal*, Int. J. Coal Geology, 13, (1989), 375-390.

Snyman, C.P., Botha, W.J., *Coal in South Africa*, J. Afr. Earth Science, Volume 16, Issues 1-2, (1993), 171-180.

Solomon, P.R., *Relationship between Coal Structure and Thermal Decomposition Products*, Am. Chem. Soc., Div. Fuel Chem. Preprints, Vol. 24, No. 2, (1979), p. 184.

Solomon, P.R., *Characterization of Coal and Coal Thermal Decomposition*, Chapter III Report, Advanced Fuel Research Inc., East Hartford, CN., (1980).

Sorum, L., Grønli, M.G., Hustad, J.E. , *Pyrolysis Characteristics and Kinetics of Municipal Solid Wastes*, Fuel, 80, (2001), 1217-1227.

Sprouse, K.M., Schuman, M.D., *Predicting Lignite Devolatilization with the Multiple Parallel and Two-Competing Reaction Models*, Combust. Flame, 43,(1981), 265-271.

Suurberg, E.M., Peters, W.A., Howard, J.B., in Oblad (Ed), *Thermal Hydrocarbon Chemistry, Advances in Chemistry Series*, No. 183, Am. Chem. Soc., New York, (1979), 239-257.

Suurberg, E.M., Sc.D. Thesis, Massachusetts Institute of Technology, (1977).

Tromp, P.J.J., *Slow and Rapid Pyrolysis of Coal*, PhD Thesis, University of Amsterdam, (1987), 6-39.

Tsamba, A.J., Yang, W., Blasiak, W., *Pyrolysis Characteristics and Global Kinetic of Coconut and Cashew Nut Shells*, Fuel Processing Technology, 87, (2006), 523-530.
Vuthaluru, H.B., *Investigations into the Pyrolytic Behaviour of Coal/Biomass Blends Using Thermogravimetric Analyses*, Bioresource Technology, 92, (2003), 187-195.

Walker, P.L., Jnr., *Coal Gasification- University Contribution to the Story of Devolatilization*, Catalysis and Active Sites, Paper Presented at the Symposium on Advances in Coal Utilization Technology, Sponsored by the Institute of Gas Technology, (1979).

Ward, R.C., *Coal Geology and Coal Technology*, Blackwell Scientific Publications, Melbourne, Australia, (1984), p. 345.

Warren, W. B., *Carbonization of Typical Bituminous Coals*, Ind. Eng. Chem., *30,* (1938), 136.

Wendt, J.O.L., *Fundamental Coal Combustion Mechanisms and Pollutant Formation in Furnaces*, Progr. Energy Combust. Sci., Vol. 6, No. 201, (1980).

Williamson, I. A., *Coal Mining Geology,* London: Oxford University Press, (1967).

Wiser, W.H., Hill, G.R., Kertamus, N.J., *Kinetic Study of the Pyrolysis of a High-Volatile Bituminous Coal*, Ind. Eng. Chem. Proc. Des. Dev., Vol. 6, (1967), p.133.

Wiser, W.H., *Prep. Am. Chem. Soc*., Div. Fuel Chem., Vol. 20, (1975), p.122.

Yaman, S., *Pyrolysis of Biomass to Produce Fuels and Chemical Feedstocks,* Energy Convers. Manage., (2004), 45, p.651–671.

Appendix A: Matlab® Source Code

This appendix gives details of the Matlab® Source Code used in the modelling exercise.

The source code is presented in three parts:

- Source Code for Hypothetical Scenario, where the fuel decomposes by seven first-order reactions. This was outlined by Scott et al. (2006[a]), and is shown in Section 6.2.1 of Chapter 6.
- Source Code for Gaussian Distribution Test. This was also outlined by Scott et al. (2006a), and is shown in Section 6.2.1 of Chapter 6.
- Source code for the modelling of the pyrolysis process, using the DAEM. This was carried out using the equations (16) to (24) in Section 4.3.5 of Chapter 4.

All code was written using Matlab®7.0.

A1: Source Code for Hypothetical Scenario

```
 clc
clear all
Ea=200; % Assign any random activation energy
A=5E16; % Assign any random pre-exponential factor;
R=0.008314; % Universal gas constant
B=[15 45 10000]; % Heating rates
%_____________________________________________________________________
n=50;% Choose number of reactions
Tn=linspace(490,800,n); % Temperatures corresponding to each reaction
x1 = exp(-((((A*R).*(Tn.^2))/(B(1)*Ea)).*(1-(((2*R).*Tn)/Ea))).*exp(-Ea./(R.*Tn)));
%X=1-alpha mass of fuel remaining for heating rate 1
x2 = exp(-((((A*R).*(Tn.^2))/(B(2)*Ea)).*(1-(((2*R).*Tn)/Ea))).*exp(-Ea./(R.*Tn)));
%for heating rate 2
x3 = exp(-((((A*R).*(Tn.^2))/(B(3)*Ea)).*(1-(((2*R).*Tn)/Ea))).*exp(-Ea./(R.*Tn)));
%_____________________________________________________________________
%plotting of the mass remaining as a function of temperature
plot(Tn,x1,'m',Tn,x2,'g',Tn,x3,'r')
title(' Hypothetical combustion thermogravimetric experiment','FontWeight','bold')
xlabel('Temperature(K)');ylabel('Weight % remaining'); axis([490,800,0,1]); Hold on
legend('15 K/min','45 K/min','10000 K/min',3)
%_____________________________________________________________________
% The DAEM model for the dummy reactions
U=linspace(0.9999,0.001,n); % Assign random conversions to 100 reactions
% Solve for temperatures corresponding to the allotted number of reactions
%This will be done by solving between the dummy curve and the DAEM curve
```

```
for i=1:n
T1(i)=fzero(@(T)(U(i)-exp(-((((A*R).*(T.^2))/(B(1)*Ea)).*(1-(((2*R).*T)/Ea))).*exp(-
Ea./(R.*T)))),500);
T2(i)=fzero(@(T)(U(i)-exp(-((((A*R).*(T.^2))/(B(2)*Ea)).*(1-(((2*R).*T)/Ea))).*exp(-
Ea./(R.*T)))),500);
T3(i)=fzero(@(T)(U(i)-exp(-((((A*R).*(T.^2))/(B(3)*Ea)).*(1-(((2*R).*T)/Ea))).*exp(-
Ea./(R.*T)))),500);
end;
% Parameters for the hypothetical reactions
T0=490; % Initial temperature of the fuel
E0=200; % Initial guess activation energy
%_____________________________________________________________________
for j=1:n
Ti1=T1(j);
Ti2=T2(j);
% Activation energy
E(j)=fzero(@(E)(((1/B(1))*(T0*exp(-E/(R*T0))-(E/R)*expint(E/(R*T0))-Ti1*exp(-
E/(R*Ti1))+(E/R)*expint(E/(R*Ti1))))...
-((1/B(2))*(T0*exp(-E/(R*T0))-(E/R)*expint(E/(R*T0))-Ti2*exp(-
E/(R*Ti2))+(E/R)*expint(E/(R*Ti2))))),E0);%activation energy
%Pre-exponential
A(j)=-B(1)/(T0*exp(-E(j)/(R*T0))-(E(j)/R)*expint(E(j)/(R*T0))-Ti2*exp(-
E(j)/(R*Ti2))+(E(j)/R)*expint(E(j)/(R*Ti2)));
end;
E % Activation energy
A %Pre-exponential factor
%_____________________________________________________________________
%determining the mass initial mass fraction
42
%
T=linspace(500,900,n); % temperatures to evaluate model
chm1=zeros(n+1);% generate zero matrix
chm1(:,end)=1; % 1 's in the end of each row
chm1(1,:)=1; % 1's in column this corresponds to 100 % mass remaining
for k=1:n;
for z=1:n;% for the columns
chm1(k+1,z)=exp((-A(z)/B(1)).*quad(@(T)exp(-E(z)./(R*T)),T0,T1(k)));
end
end
chm1;
M1=[1 U]'; % matrix of mass remaining
f1=lsqnonneg(chm1,M1)
%_____________________________________________________________________
%CHI MATRIX FOR HEATING RATE 0ne
chm2=zeros(n+1);
chm2(:,end)=1;
chm2(1,:)=1;
for k=1:n;
for z=1:n;% for the columns
chm2(k+1,z)=exp((-A(z)/B(1))*quad(@(T)exp(-E(z)./(R*T)),T0,T(k)));
end
end
chm2;
S2=chm2*f1;
Te2=[T0 T]';
plot(Te2,S2,'.b')
%_____________________________________________________________________
%CHI MATRIX FOR HEATING RATE two
```

```
chm3=zeros(n+1);
chm3(:,end)=1;
chm3(1,:)=1;
for k=1:n;
for z=1:n;% for the columns
chm3(k+1,z)=exp((-A(z)/B(2))*quad(@(T)exp(-E(z)./(R*T)),T0,T(k)));
end
end
chm3;
S3=chm3*f1;
Te3=[T0 T]';
plot(Te3,S3,'.b')
%--------------------------------------------------------------------------
%CHI MATRIX FOR HEATING RATE three
chm4=zeros(n+1);
chm4(:,end)=1;
chm4(1,:)=1;
for k=1:n;
for z=1:n;% for the columns
chm4(k+1,z)=exp((-A(z)/B(3))*quad(@(T)exp(-E(z)./(R*T)),T0,T(k)));
end
end
chm4;
43
S4=chm4*f1;
Te4=[T0 T]';
plot(Te4,S4,'.b')
% deriv=-diff(S4)./diff(Te4)
% plot(T,deriv)

legend('15 K/min','45 K/min','10000 K/min','DAE Model',3)
```

A2: Source Code for Gaussian Distribution Test

```
clc
clear all
o=1.001;%order of reaction
R=8.314E-3;%kj/mol.K
Ac=6E16;%/min, assumed pre-exponential factor
%a Gaussian distribution of activation energies is used with:
Em=225;%mean activation activation energy,kJ/mol
d=25;%standard deviation,kJ/mol
Emin=50;%minimum AE to use for distribution
Emax=400;%maximum AE to use for the distribution
%fe=quad(@(E)(1/(d*(2*pi)^0.5))*exp(-(E-Em).^2/(2*d^2)),Emin,Emax);%fe=1 by definition
B=[20 30 10000];%heating rates to use
Te=linspace(380,1200,300);%temperatures to generate the reaction
for i=1:length(B)
for j=1:length(Te)
Tr=Te(j);
```

```
W(i,j)=quad(@(E)(((1-(1-o)*(Ac*R*Tr^2./(B(i)*E)).*exp(-E/(R*Tr)).*(1-(2*R*Tr./E))).^(1/(1-
o)))).*...
((1/(d*sqrt(2*pi))).*exp(-(E-Em).^2/(2*d^2))),Emin,Emax);%weight% remaining
end
end
W;
%--------------------------------------------------------------------------
n=100;%number of reactions to use in the model
X=linspace(0.99,0.001,n);% evenly spaced conversions to use for the model
Ta1=(interp1q(flipud(W(1,:)'),flipud(Te'),flipud(X')));
Ta1=(flipud(Ta1))';%interpolated temperatures for heating rate one
Tb1=(interp1q(flipud(W(2,:)'),flipud(Te'),flipud(X')));
Tb1=(flipud(Tb1))';%interpolated temperatures for heating rate two
%Tcheck=[X' Ta1' Tb1']%to check whetether the interpolated data is consistent
%--------------------------------------------------------------------------
%DAEM for hypothetical reactions
T0=379;%initial temperature of fuel
E0=200;% guess for activation energy
xi=1-exp(-1);%conversion to evaluate the pre exponential factor
for j=1:n
44
Ti1=Ta1(j);
Ti2=Tb1(j);
E(j)=fzero(@(E)((R*Ti1^2/(B(1)*E))*exp(-E/(R*Ti1))*(1-(2*R*Ti1/E)))-...
((R*Ti2^2/(B(2)*E))*exp(-E/(R*Ti2))*(1-(2*R*Ti2/E))),E0);%activation energy
A(j)=(1/(1-o))*(1-xi^(1-o))*(B(1)*E(j))/(R*Ti1^2*exp(-E(j)/(R*Ti1))*(1-
(2*R*Ti1/E(j))));%preexponential
factor
end
E;%
A;%
%--------------------------------------------------------------------------
%chi matrix to determine the initial mass fractions of the reactions
cm=zeros(n+1);% generate zero matrix
cm(:,end)=1;
cm(1,:)=1;
for k=1:n;%generates the rows
for z=1:n;%generates the columns
cm(k+1,z)=(1-(1-o)*(A(z)*R*Ta1(k)^2/(B(1)*E(z)))*exp(-E(z)/(R*Ta1(k)))*(1-
(2*R*Ta1(k)/E(z))))^(1/(1-o));
%exp((-A(z)/B(1))*quad(@(T)exp(-E(z)./(R*T)),T0,Tb1(k)))
end
end
cm;%chi matrix
M=[1 X]'; % vector of mass remaining
f=lsqnonneg(cm,M);%fractions of reactions
%--------------------------------------------------------------------------
% Predicting the reactions
T=linspace(385,1150,n);%temperatures to evaluate the model
Tt=[T0 T]';% temperatures for the plot
for i=1:length(B)%to predict for the heating rates
cm=zeros(n+1);%generate chi matrix
cm(:,end)=1;
cm(1,:)=1;
for k=1:n;
for z=1:n;
cm(k+1,z)=(1-(1-o)*(A(z)*R*T(k)^2/(B(i)*E(z)))*exp(-E(z)/(R*T(k)))*(1-
(2*R*T(k)/E(z))))^(1/(1-o));
```

```
end
end
cm;
Y(:,i)=cm*f;%predicted weight% remaining for the ith heating rate
% plot(Tt,Y(:,i),'.k');
end
% legend('20 K/min','30 K/min','10000 K/min','DAE model',4);
%Y
%here u can generate the chi matrix with more points in order to predict
%rate of mass loss
Ef=linspace(Emin,Emax,100);
for k=1:length(Ef)
Einf=Ef(k);
cmf(k)=quad(@(E)(1/(d*(2*pi)^0.5))*exp(-(E-Em).^2/(2*d^2)),Emin,Einf);
45
end
cmf;
Y(:,1);
Y(:,2);
Y(:,3);
subplot(1,2,1)
plot(Te,W(1,:),'b',Te,W(2,:),'g',Te,W(3,:),'r');hold on
plot(Tt,Y(:,1),'.k');
plot(Tt,Y(:,2),'.k');
plot(Tt,Y(:,3),'.k');
title('Gaussian distribution test')
xlabel('Temperature(K)');ylabel('fraction of mass remaining'); axis([379,1200,0,1]);
legend('20 K/min','30 K/min','10000 K/min','DAE model',4);
subplot(1,2,2)
r1=-diff(W(1,:))./diff(Te);
r2=-diff(W(2,:))./diff(Te);
r3=-diff(W(3,:))./diff(Te);
Te(end)=[];
plot(Te,r1,'b');hold on
plot(Te,r2,'g');
plot(Te,r3,'r');
d1=-diff(Y(:,1))./diff(Tt);
d2=-diff(Y(:,2))./diff(Tt);
d3=-diff(Y(:,3))./diff(Tt);
Tt(end)=[];
plot(Tt,d1,'.k');
plot(Tt,d2,'.k');
plot(Tt,d3,'.k');
title('Gaussian distribution test')
xlabel('Temperature(K)');ylabel('Normalised rate of mass loss (1/s)'); axis([379,1200,0,1]);ylim([0
0.007])
legend('20 K/min','30 K/min','10000 K/min','DAE model',4);
hold off
drvr=-(B(3)/60)*diff(W(3,:))./diff(Te);%derivative for the reaction
drvr=[0 drvr 0];
Tdr=[T0 Te];
plot(Tdr,drvr)
```

A3: Source Code for Pyrolysis Modelling

```
clc
clear all
%matrices with pyrolysis experimental results
a=result('a');b=result('b');c=result('c');
format long
%to convert to fraction and kelvin
a(:,1)=a(:,1)+273;a(:,2)=a(:,2)/100;%at 50 K/min
b(:,1)=b(:,1)+273;b(:,2)=b(:,2)/100;%at 15 K/min
c(:,1)=c(:,1)+273;c(:,2)=c(:,2)/100;%at 5 K/min
%--------------------------------------------------------------------------
Xa=a(:,2);%weight% remaining for a
Ta=a(:,1);%temperatures for a
Xmina=Xa(end);
Xb=b(:,2);%weight% remaining for b
Tb=b(:,1);%temperatures for b
Xminb=Xb(end);%
Xc=c(:,2);
Tc=c(:,1);
Xminc=Xc(end);
B=[5 10 20];
%--------------------------------------------------------------------------
Tbb=linspace(Tb(1),Tb(end),300);%
Xbb=interp1(Tb,Xb,Tbb);
% plot(Tbb,Xbb,'.k');
Tcc=linspace(Tc(1),Tc(end),300);%
Xcc=interp1(Tc,Xc,Tcc);
% plot(Tcc,Xcc,'.k');
%--------------------------------------------------------------------------
n=100;%number of reactions to use in the model
X=linspace(0.989,Xminc+0.01,n);% evenly spaced conversions to use for the model
Tb1=(interp1q(flipud(Xbb'),flipud(Tbb'),flipud(X')));
Tc1=(interp1q(flipud(Xcc'),flipud(Tcc'),flipud(X')));
Tb1=(flipud(Tb1))';
Tc1=(flipud(Tc1))';
%--------------------------------------------------------------------------
%DAEM for hypothetical experiment
R=8.314E-3;%kj/mol.K
B=[5 10 20];
T0=303;%initial temperature of fuel,K
E0=200;% initial guess for activation energy for fzero
for j=1:n
Ti1=Tb1(j);
Ti2=Tc1(j);
E(j)=fzero(@(E)(((1/B(1))*(T0*exp(-E/(R*T0))-(E/R)*expint(E/(R*T0))-Ti1*exp(-
E/(R*Ti1))+(E/R)*expint(E/(R*Ti1))))...
47
-((1/B(2))*(T0*exp(-E/(R*T0))-(E/R)*expint(E/(R*T0))-Ti2*exp(-
E/(R*Ti2))+(E/R)*expint(E/(R*Ti2))))),E0);%activation energy
A(j)=-B(1)/(T0*exp(-E(j)/(R*T0))-(E(j)/R)*expint(E(j)/(R*T0))-Ti2*exp(-
E(j)/(R*Ti2))+(E(j)/R)*expint(E(j)/(R*Ti2)));%preexponential factor
end
E% activation energy
A;% preexponential factor
%--------------------------------------------------------------------------
%chi matrix to determine the initial mass fractions of the reactions
```

```
cm=zeros(n+1);% generate zero matrix
cm(:,end)=1;
cm(1,:)=1;
for k=1:n;
for z=1:n;% for the columns
cm(k+1,z)=exp((-A(z)/B(2))*quad(@(T)exp(-E(z)./(R*T)),T0,Tc1(k)));
end
end
cm;
M=[1 X]'; % vector of mass remaining
f=lsqnonneg(cm,M);%fractions of reactions
%-------------------------------------------------------------------------
%Recovering the reactions
T=linspace(304,1100,n);%temperatures to evaluate the model at each heating rate
%first heating rate-----------------------------------------------------
cm1=zeros(n+1);%chi matrix
cm1(:,end)=1;
cm1(1,:)=1;
for k=1:n;
for z=1:n;% for the columns
cm1(k+1,z)=exp((-A(z)/B(1))*quad(@(T)exp(-E(z)./(R*T)),T0,T(k)));
end
end
cm1;
%need to recover the reaction
Y1=cm1*f;
T1=[T0 T]';
% plot(T1,Y1,'.k','Markersize',5)
%second heating rate----------------------------------------------------
cm2=zeros(n+1);% generate zero matrix
cm2(:,end)=1;
cm2(1,:)=1;
for k=1:n;
for z=1:n;% for the columns
cm2(k+1,z)=exp((-A(z)/B(2))*quad(@(T)exp(-E(z)./(R*T)),T0,T(k)));
end
end
48
cm2;
%need to recover the reaction
Y2=cm2*f;
T2=[T0 T]';
% plot(T2,Y2,'.k','Markersize',5)
%need to predict at the third heating rate-------------------------------
cm3=zeros(n+1);% generate zero matrix
cm3(:,end)=1;
cm3(1,:)=1;
for k=1:n;
for z=1:n;% for the columns
cm3(k+1,z)=exp((-A(z)/B(3))*quad(@(T)exp(-E(z)./(R*T)),T0,T(k)));
end
end
cm3;
%need to recover the reaction
Y3=cm3*f;
T3=[T0 T]';
cm4=zeros(n+1);% generate zero matrix
cm4(:,end)=1;
```

```
cm4(1,:)=1;
for k=1:n;
for z=1:n;% for the columns
cm4(k+1,z)=exp((-A(z)/10000)*quad(@(T)exp(-E(z)./(R*T)),T0,T(k)));
end
end
cm4;
Y4=cm4*f;
T4=[T0 T]';
subplot(1,2,1)
plot(Tb,Xb,'-r');hold on
plot(Tc,Xc,'-b');
plot(Ta,Xa,'-m')
plot(T1,Y1,'.k')
plot(T2,Y2,'.k')
plot(T3,Y3,'.k')
plot(T4,Y4,'g')
legend('5 K/min','10 K/min','20 K/min',3);
title('Pyrolysis thermogravimetric experiment results','FontWeight','bold')
xlabel('Temperature(K)');ylabel('Weight remaining %'); axis([303,Tb(end)+50,Xminb-0.04,1]);
subplot(1,2,2)
plot(Ta,Xa,'-m');hold on
plot(Tb,Xb,'-r');
plot(Tc,Xc,'-b');
plot(T1,Y1,'.k')
plot(T2,Y2,'.k')
plot(T3,Y3,'.k')
legend('5 K/min','10 K/min','20 K/min','DAE model',4);
title('Modelling pyrolysis thermogravimetric experiment','FontWeight','bold')
xlabel('Temperature(K)');ylabel('Weight remaining %'); axis([303,Tb(end)+50,Xminb-0.04,1]);
```

Appendix B: Experimental Results

This section contains the results obtained from the experimental procedure, as outlined in Chapter 5.The graphs obtained, represent the actual experimental data for the pyrolysis of the fuel, at the given heating rate.

B1: Experimental Results for Coal

Figure B1 below shows the results of the thermal decomposition profile obtained via a top-loading TGA, for a coal sample at a heating rate of 10, 25 and 100°C/min, respectively.

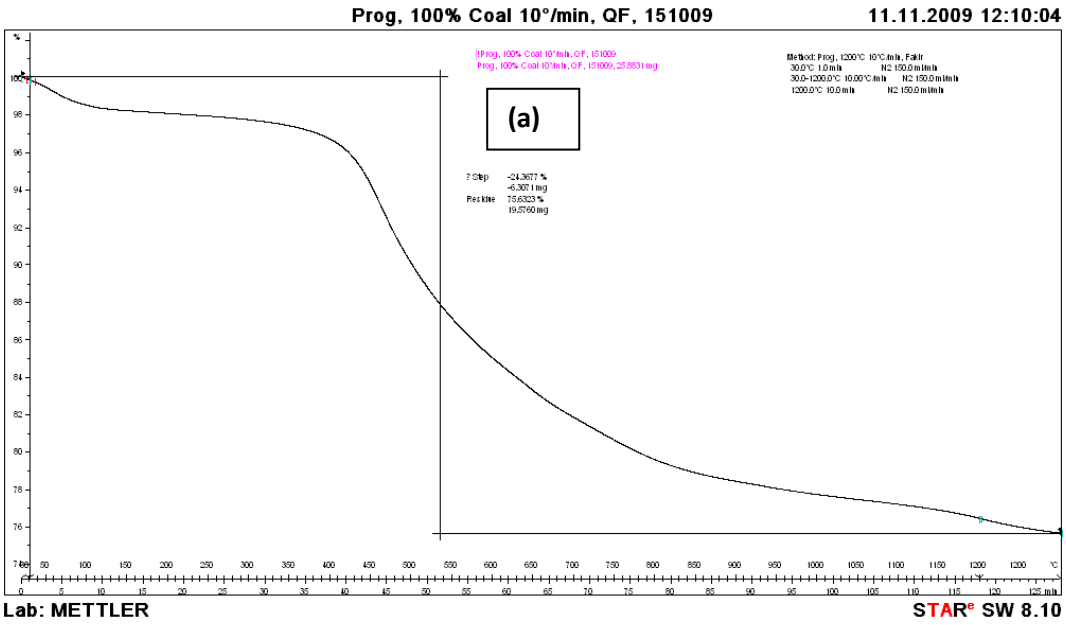

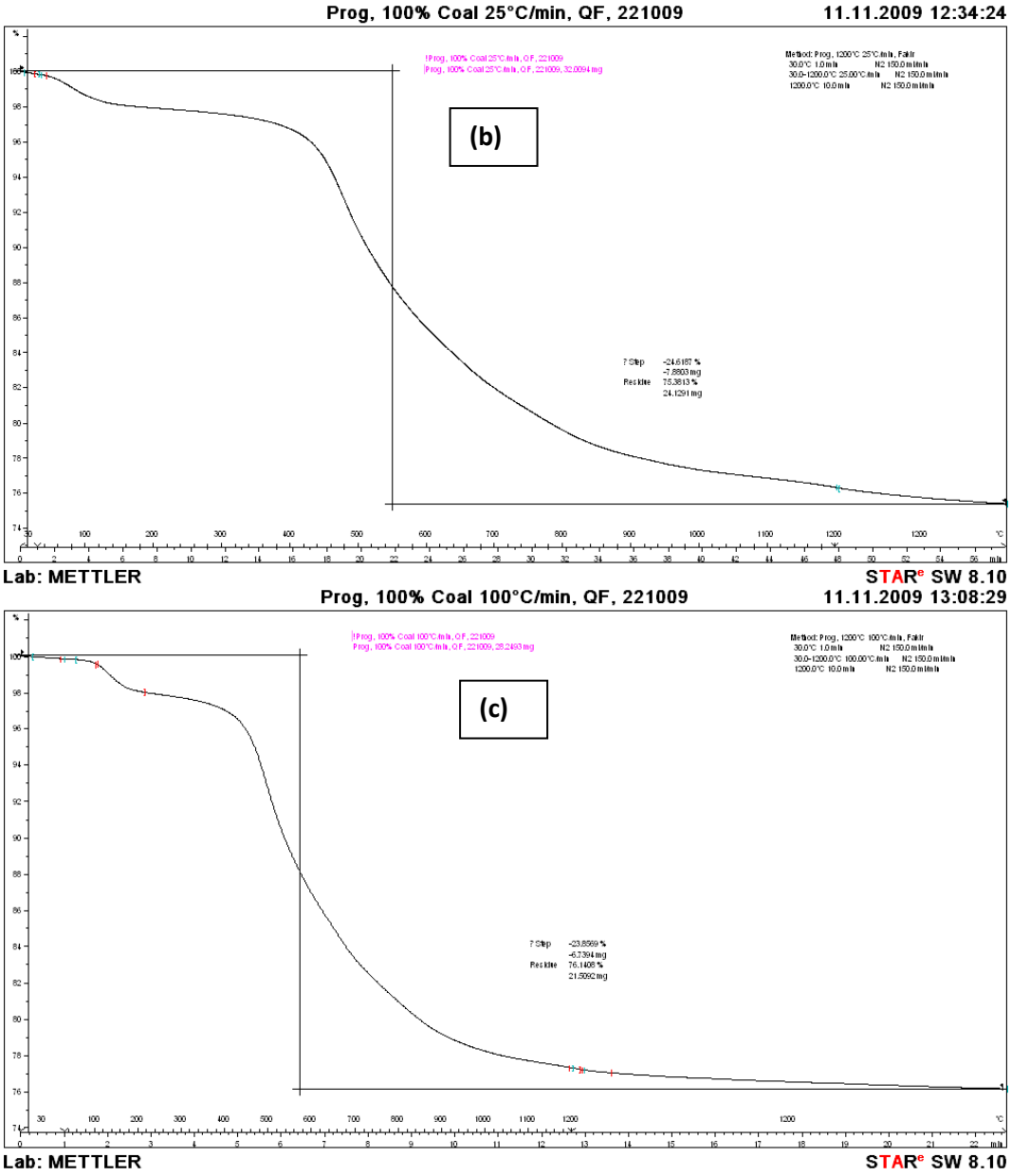

Figure B1: Pyrolysis Results from TGA Experiments at Three Heating Rates

(a) Pyrolysis profile for coal at 10°C/min
(b) Pyrolysis profile for coal at 25°C/min
(c) Pyrolysis profile for coal at 100°C/min

B2: Experimental Results for Biomass

Figure B2 below shows the results of the thermal decomposition profile obtained via a top-loading TGA, for a sawdust (biomass) sample at a heating rate of 10, 25 and 100°C/min, respectively.

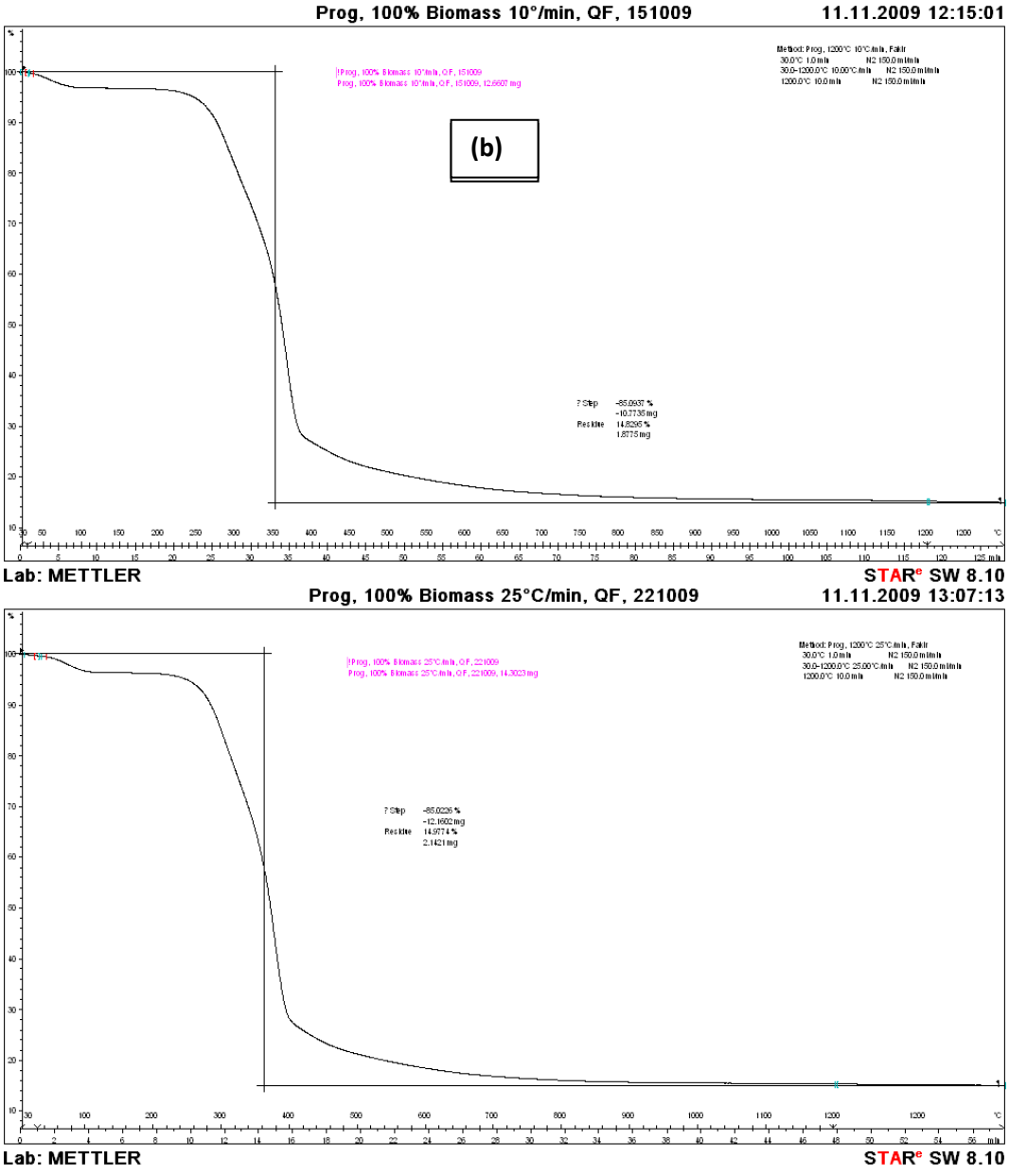

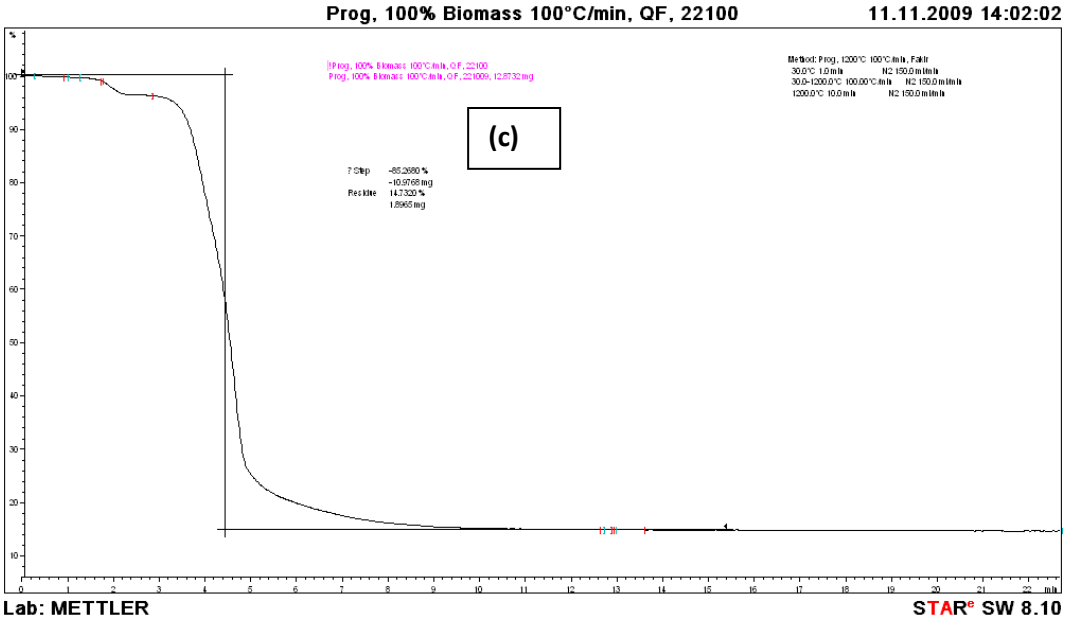

Figure B2: Pyrolysis Results from TGA Experiments at Three Heating Rates

(a) Pyrolysis profile for sawdust at 10°C/min
(b) Pyrolysis profile for sawdust at 25°C/min
(c) Pyrolysis profile for sawdust at 100°C/min

B3: Experimental Results for Coal-Biomass Blends

Figure B3 below shows the results of the thermal decomposition profile obtained via a top-loading TGA, for a coal-biomass blended sample at a heating rate of 10, 25 and 100°C/min, respectively for 25%, 50% and 75% increments of coal.

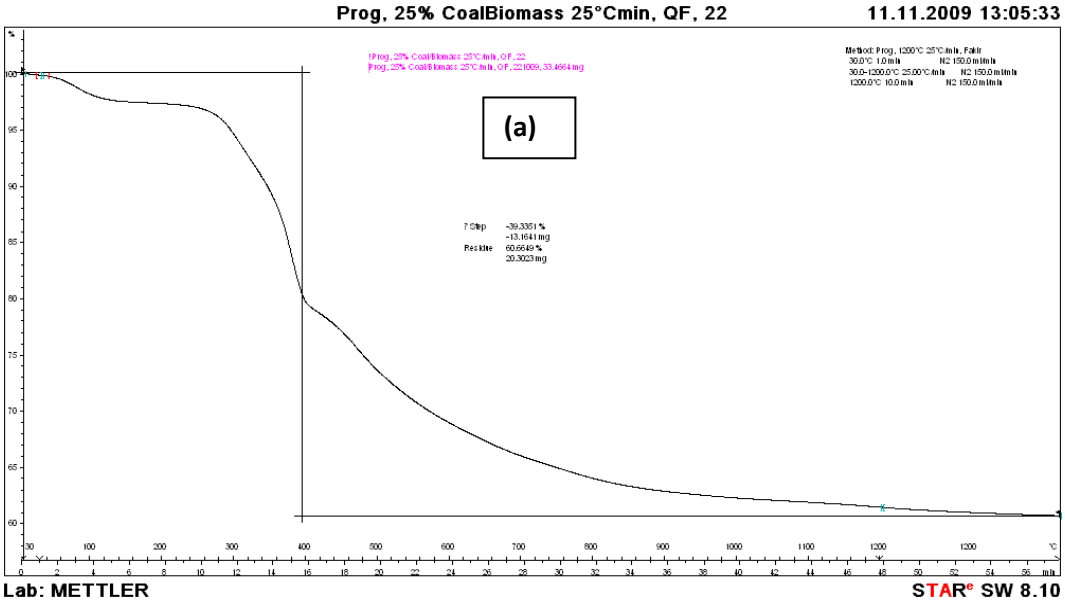
Prog, 25% CoalBiomass 25°Cmin, QF, 22
11.11.2009 13:05:33
(a)
Lab: METTLER
STARe SW 8.10

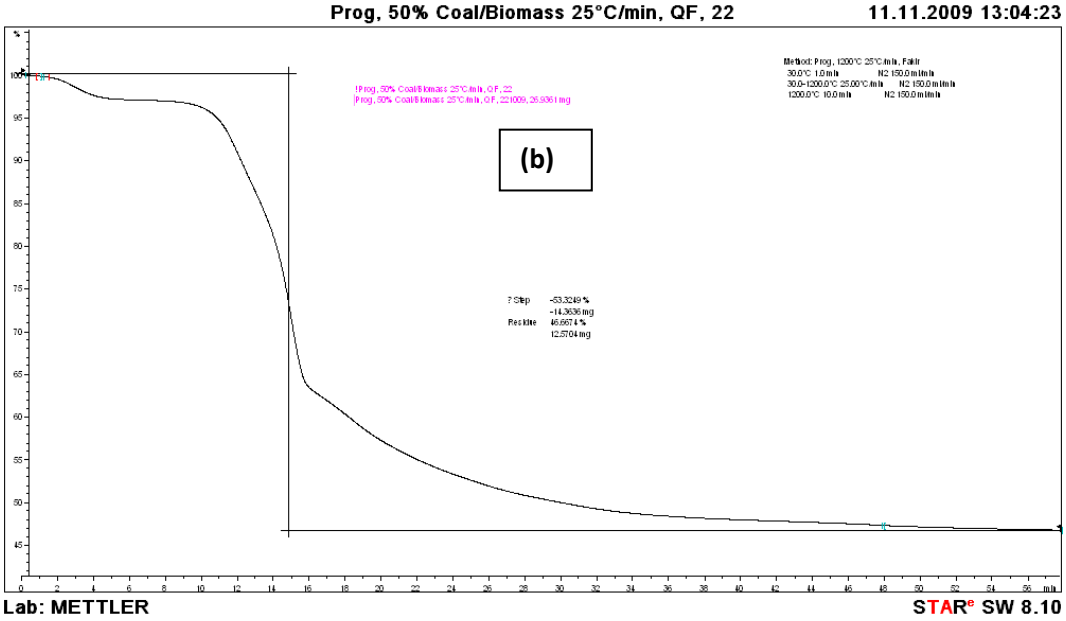
Prog, 50% Coal/Biomass 25°C/min, QF, 22
11.11.2009 13:04:23
(b)
Lab: METTLER
STARe SW 8.10

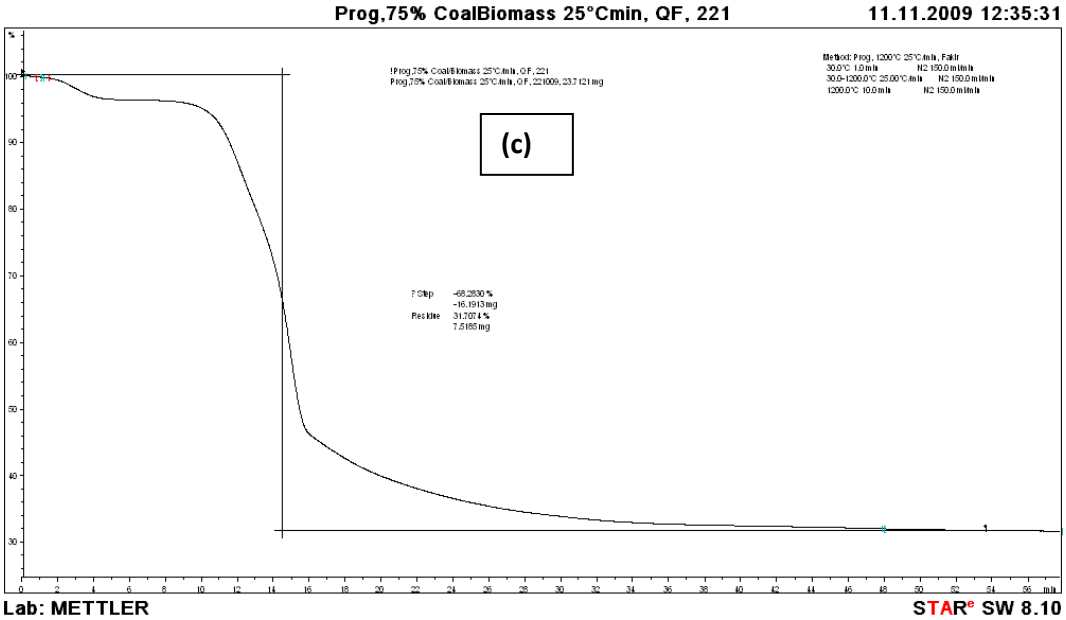

Figure B1: Pyrolysis Results from TGA Experiments at Three Heating Rates

(a) Pyrolysis profile for 25% coal & 75% biomass at 10°C/min
(b) Pyrolysis profile for 50% coal & 50% biomass at 25°C/min
(c) Pyrolysis profile for 75% coal & 25% biomass at 100°C/min

It is important to note that the results shown here are clearly for illustrative purposes. More precise and quantitative results can be found in easy, tabulated format, attached to the CD-ROM provided.

Appendix C: Summary of Experimental Methods & Pyrolysis Models

Table C1, extracted from Anthony & Howard (1976) gives a broad overview of the different experimental techniques used, and subsequent mathematical models obtained, to describe the pyrolysis process, for the period 1950-1980.

Table C1: Summary of Experimental Methods and Pyrolysis Models (Anthony and Howard, 1976)

Investigator[b]	Technique	Residence time (seconds)	Temperature (K)	Heating rate (K/s)	Pressure (atm)[c]	Ambient gas	Particle size (μm)
Coal flow techniques							
Stone *et al.* (1954)	Fluidized bed	10–2500	670–970	—	1.0	N_2	200–600
Peters *et al.* (1960, 1965)	Fluidized bed	1–15	870–1370	300	1.0	N_2	1000–3000
Pitt (1962)	Fluidized bed	10–6000	670–970	—	1.0	—	200–600
Jones *et al.* (1964)	Fluidized bed	~2400	700–1370	1000+	1.0	N_2, H_2O	≤1000
Friedman (1975)	Fluidized bed	1800–3600	570–920	—	1.0	H_2O	250–710
Zielke and Gorin (1955)	Fluidized bed	—	1090–1200	—	1–30	H_2, H_2O, etc.	150–212
Birch *et al.* (1960, 1969)	Fluidized bed	500–9500	770–1220	—	21–42	H_2, etc.	150–710
Eddinger *et al.* (1966)	Entrained flow	0.008–0.04	900–1270	2500+	1.0	He	6150
Howard and Essenhigh (1967)	Entrained flow	0–0.8	470–1820	22,000	1.0	Air	80% ≤ 74
Badzioch *et al.* (1967, 1970)	Entrained flow	0.03–0.11	670–1270	25,000–50,000	1.0	N_2	20
Kimber and Gray (1967a, b)	Entrained flow	0.012–0.34	1050–2270	150,000–400,000	1.0	Ar	22–50
Belt *et al.* (1971, 1972)	Entrained flow	≤1	1090–1310	—	1–28.2	H_2, N_2	70% ≤ 74
Sass (1972)	Entrained flow	A few	810–920	10,000	1.0	—	25–80
Coates *et al.* (1974)	Entrained flow	0.012–0.34	920–1640	—	1.0	H_2, H_2O, etc.	≤74
Moseley and Paterson (1965b)	Entrained flow	0.17–2.5	1060–1270	1000+	50–520	H_2	100–150
Glenn *et al.* (1967)	Entrained flow	2.4–10.4	1190–1240	—	70–84	H_2, CO, etc.	≤44
Johnson (1975)	Entrained flow	5–14	760–1120	28	18–52	H_2, He	75–90
Shapatina *et al.* (1960)	Free fall	0.45–14,400	≤820	—	45–490	N_2	150–200
Moseley and Paterson (1967)	Free fall	A few	1110–1270	—	45–490	H_2	100–150
Feldmann *et al.* (1970)	Free fall	A few	920–1170	—	35–205	H_2	150–300

[a] Data taken mostly from Anthony and Howard (1976).
[b] References in this table are identified in detail in Anthony and Howard (1976) or Smoot (1980).
[c] To convert to MPA, divide by 10.

Appendix D: Testing of Modified DAEM

This appendix gives the results of testing the DAEM model, by utilizing the same examples proposed by Scott et al. (2006[a]).

In order to validate the efficacy of the modified DAEM model, data obtained by Scott et al. (2006, a) was input into the algorithm to obtain the kinetic data.

D1. Test for the Validity of the Modified DAE Model

In their work, Scott et al. (2006[a]) proposes the thermal decomposition of a hypothetical fuel particle experiencing a fixed rate of heating. They assume that this solid contains no ash or char, and decomposes with specified kinetics, thus in essence, simulating a thermogravimetric experiment. They then apply the algorithm of the DAEM to the generated curves in order to regenerate the original parameters, the values of *A* and *E*, used for the simulation. Two test curves at low heating rates of 20 K/min and 30 K/min were produced and used for the subsequent calculation. A third theoretical curve is then generated for a heating rate of 10 000 K/min and this is then compared with the parameters recovered by the inversion algorithm at 20 K/min and 30 K/min.

Their intention with the hypothetical scenario is to provide a robust test of how well the kinetics extracted by the algorithm extrapolates at different heating rates. According to Scott et al. (2006[a]), in a real combustion or gasification system, a heating rate of 10 000 K/min is not unreasonable, and thus when small particles of fuel are added to a fluidized bed, the time constant for their heating could be of the order of a few seconds, resulting in a very high rate of heating.

Several scenarios are tested in this way, with increasing complexities. Scott et al. (2006[a]) ranged the tests from a solid decomposing with a single first-order reaction, through to one decomposing with a Gaussian distribution of activation energies.

Scott et al. (2006[a, b]) then applies the algorithm to the results of thermogravimetric experiments performed on dried sewage sludge, in order to determine the kinetics of the devolatilization process.

For purposes of this research, a duplication of these tests was carried out, by applying the DAEM algorithm to a hypothetical fuel decomposing at two heating rates of 15 K/min and 45 K/min. For this test, a value of E= 200 kJ/mol and $A=10^{15}s^{-1}$ was chosen, as chosen by Scott et al. (2006[a]). The results obtained were then used to compare the algorithm inversion for data at a heating rate of 10000 K/min. Figure D1.1 below shows the results of the hypothetical test method utilized by Scott et al. (2006[a]).

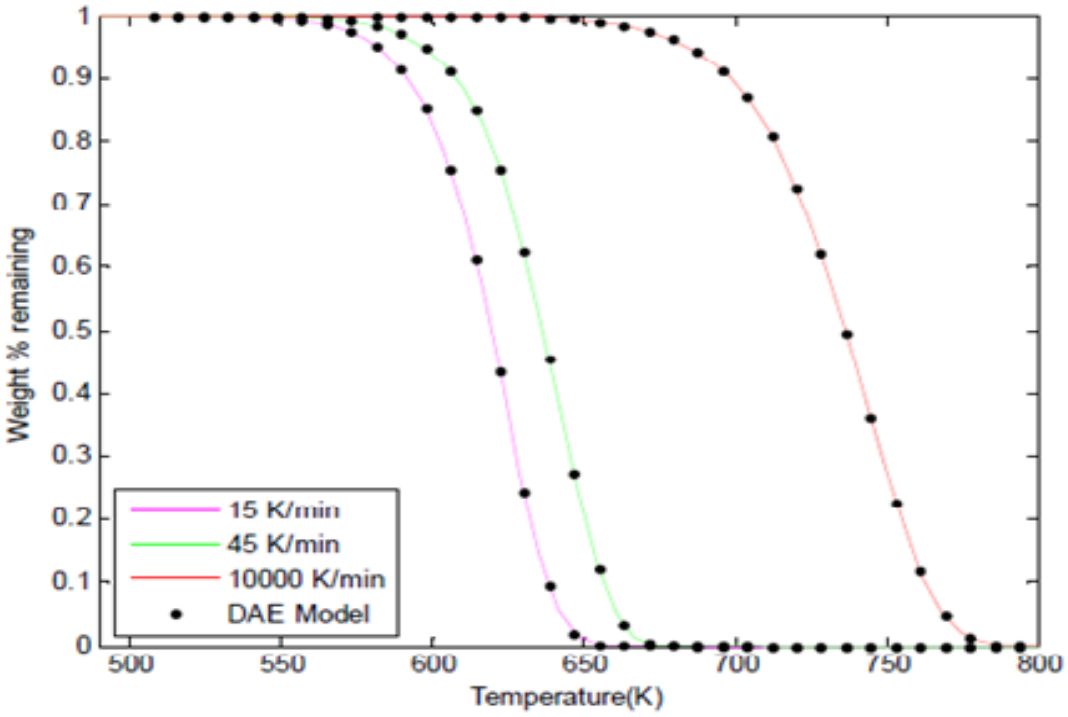

Figure D1.1: Hypothetical Fuel Which Decomposes by a Single First-order Reaction

From the figure above, it can be seen that the curves generated by the DAEM algorithm gives a precise fit for the hypothetical fuel proposed, with *E*= 200 kJ/mol and $A= 10^{15}\ s^{-1}$. By inverting the data obtained at the low heating rates and applying it to the generated curve at 10 000K/min, it can be seen that the DAEM is an effective model for predicting kinetic behaviour at extremely high heating rates.

According to Scott et al. (2006[a]), to test the robustness of the DAEM, three scenarios are hypothesized, and modelled using the modified DAEM. The three scenarios chosen to test the model are:

i. Test 1: Single, First-Order Reaction

For the case of a single first-order reaction, the DAEM should be able to produce a nearly exact answer. The results of the test are given in Figure D1.2.

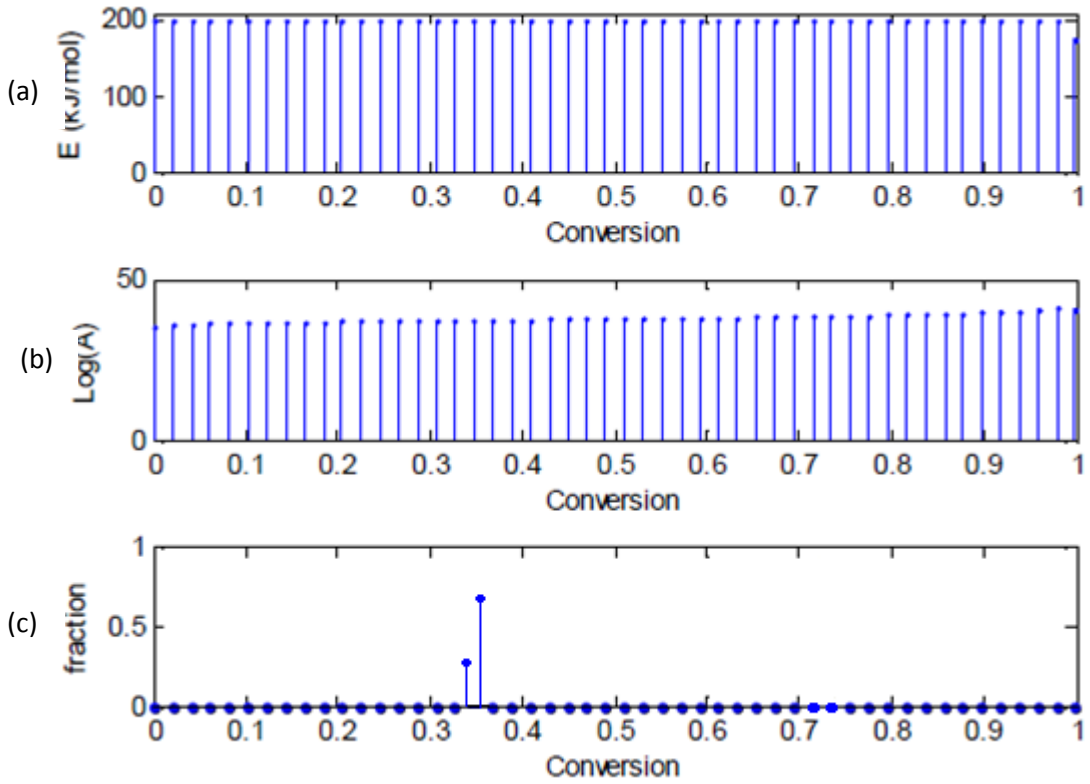

Figure D1.2: Hypothetical fuel which decomposes by a single first-order reaction with Parameters E = 200 kJ/mol and A = $10^{15}s^{-1}$

(a) And (b) give the Value of E and A (in Units of s^{-1}) for the 50 candidate reactions; (c) gives the mass fraction allocated to each of the 50 possible reactions, which is zero for all but the two straddling the point where the fraction of mass remaining = 0.368.

In the test, the inversion algorithm evaluated *E* and *A* at 50 equally spaced intervals of the conversion, corresponding to an unreacted fraction in the range 0.01-0.99. For this imaginary fuel, the values used were the same as those used by Scott et al. (2006[a]) of *E*= 200 kJ/mol and *A*= 10^{15} s^{-1}. The values of *E* and *A* calculated at each

value of the fraction of mass remaining are shown in Figure D1.2 (a) and Figure D1.2 (b).

Also shown in Figure D1.2(c), is the amount allocated to each reaction by the matrix inversion. Figure D1.2(c) shows that the amounts allocated to each reaction by the matrix inversion are zero for all intervals, except the two straddling the 0.368 abscissa. The values of *E* in Figure D1.2 (a) are exact i.e. 200 kJ/mol, apart from the values on the right, closest to complete conversion.

Scott et al. (2006[a]) suggests that this minor deviation arises from numerical errors during the inversion algorithm. The results can be seen in the table below.

Table D1.1: Error Analysis of DAEM vs. Actual Input Data

Parameter	Input Value	DAEM Determined Value	*Relative Error*
A	200 kJ/mol	199.95 kJ/mol	***0.025%***
E	10^{15} s^{-1}	Range of Values	***~40%***

A value of 200 kJ/mol was initially assigned for the activation energy; the algorithm predicts a value of 199.95 the relative error incurred is 0.025%. This relative difference can be attributed to numerical errors (Scott et al., 2006[a]). The algorithm therefore reproduces the exact value for the activation energy. This is not the case for the pre-exponential factor, the value assigned initially for the pre-exponential factor was $10^{15}s^{-1}$ and the model predicts a range of values, which presents a relative deviation of 40%. This marginable error can be attributed to the underlying assumption that the pre-exponential factor is calculated at the point where $\Psi_i(T, E) = f_i/f_{i,0} = 0.368$.

However, the values of *A* in Figure D1.2 (b) are only correct when the mass remaining is 0.368; the others are somewhat incorrect, because they were derived using a conversion of 1−0.368. According to Scott et al. (2006[a]), it is possible in this example to evaluate the value of *A* at each conversion correctly, because there is only one reaction.

However, in the more general case, with many reactions, it is not always possible to say what the conversion is for the dominating reaction. This error arises from the

simplification of calculating the approximate form for $\Psi_i = (f_i/f_{i,0})$. Scott et al. (2006[a]) shows that even though the value of E is determined correctly, the value of $A_{algorithm}/A_{actual}$, i.e., the ratio of the actual value of A to the value determined by the algorithm, can be given by the following equation:

$$\frac{\ln(\Psi = 0.368)}{\ln(\Psi_{actual})} = \frac{A_{algorithm}}{A_{actual}} \quad \text{(D1)}$$

Because the algorithm assumes that A is derived from the point where $\Psi_i = (f_i/f_{i,0}) = 0.368$, whereas in reality, the actual value of $\Psi_i = \Psi_{actual}$ could be anywhere from zero to unity. Equation (D1) shows that there can, at least in principle, be a considerable error in the value of the pre-exponential factor. However, according to Scott et al. (2006[a]), this is where this algorithm has two distinct advantages over the algorithm proposed by Miura and Maki (1998). Firstly, if there are, say 50 candidate reactions generated by the first part of the algorithm, and, as in this case, many of them have an incorrect pre-exponential factor, the amounts of these spurious reactions will be set to zero by the matrix inversion. This can clearly be seen in Figure D1.2 where a mass gets allocated only to the reactions with the correct value of A. Secondly, when several reactions are occurring, for a reaction to be dominating, its rate of reaction must be high, and thus an individual reaction is more likely to be important at a conversion near $\Psi_{actual} = 0.386$, where the error in the estimated value of A is low.

Plots of mass against temperature are shown in Figure D1.1 above. The plot for a heating rate of 10 000K/min, derived from the algorithm parameters is identical to the theoretical curve for a single first-order reaction. It can thus be deduced that for the case of a hypothetical fuel decomposing by a single first-order reaction, the DAEM produces the correct kinetic parameters.

This confirms that the Matlab® scripted coding is capable of reproducing the results of Scott et al. (2006[a]), and gives confidence in the use of the model for further pyrolysis scenario testing and manipulations.

ii. Test 2: Seven First-Order Reactions

In this test, the hypothetical fuel was assumed to decompose by seven reactions; the values of E were 150, 175, 190, 200, 225, 250, 275 kJ/mol respectively, each with $A = 10^{15}$ s^{-1}. An equal mass fraction was allocated to each reaction. The reactions with E = 190 and 200 were chosen by Scott et al. (2006[a]) because they overlap significantly and so should be more difficult for the algorithm to identify separately. The complete set of possible reactions generated by the first stage of the algorithm is shown in Figure D1.3 below.

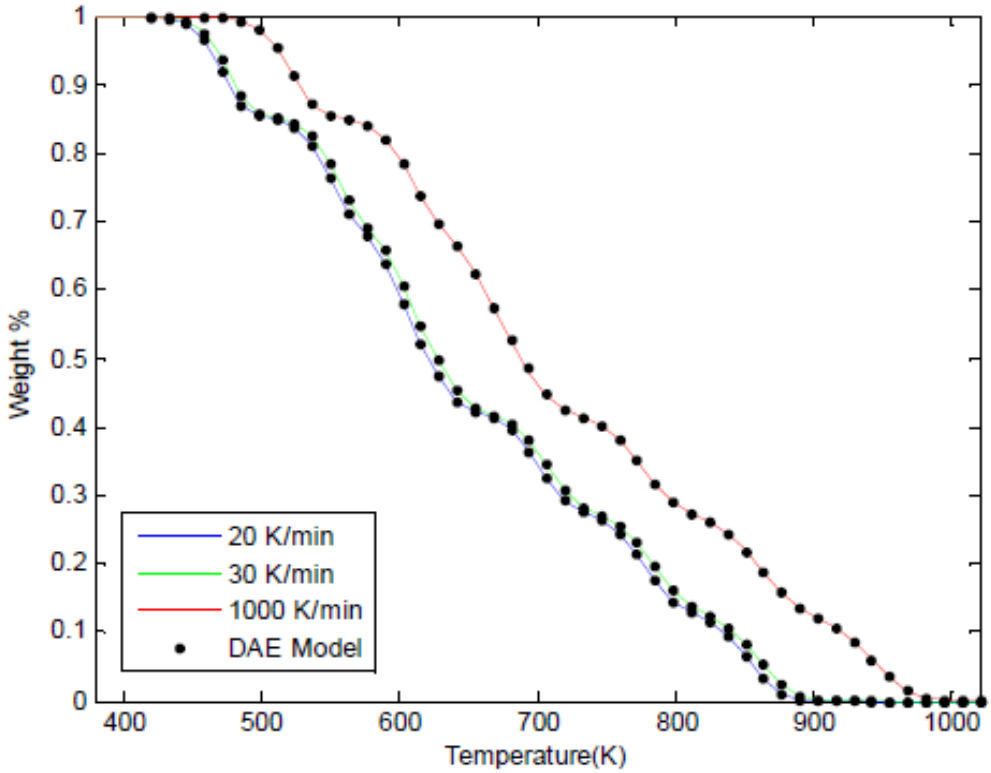

Figure D1.3: Hypothetical Plot for Seven First-Order Reactions Using DAEM

Again, from the figure, it can be seen that the DAEM provides an accurate fit at both the low heating rates, as well as the high heating rate of 1000 K/min. The curve appears more 'bumpy' then a traditional pyrolysis curve, with each 'bump' indicating the dominating reaction occurring at each temperature interval.

Figure D1.4(a) and (b) below the complete set of possible reactions generated by the first stage of the algorithm, as a function of the fraction of mass remaining at which the reaction was evaluated.

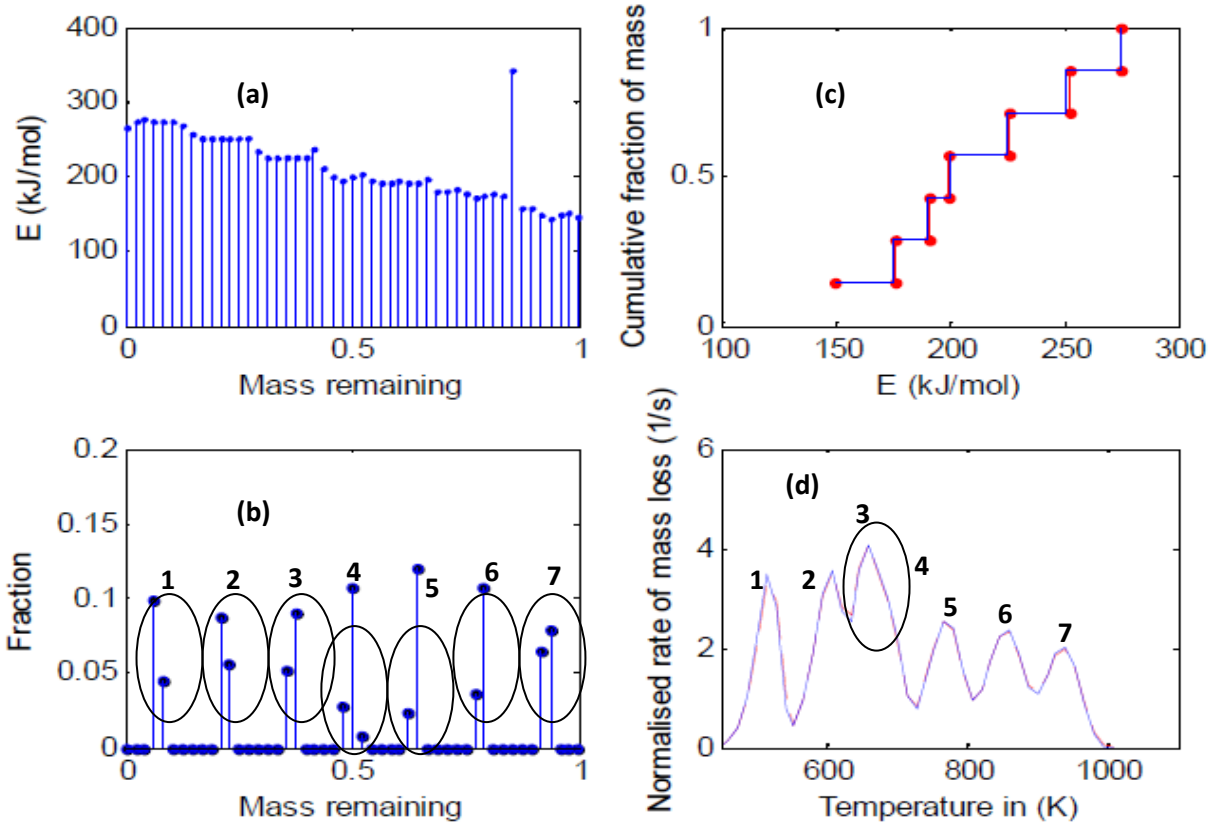

Figure D1.4: Hypothetical Fuel with Seven Components, Each Decomposing by a First-Order Reaction

The values of E were 150, 175, 190, 200, 225, 250 and 275 kJ/mol respectively, and A = 10^{15} s^{-1}; the mass fraction of each component was 1/7. The diagram gives the results from the DAEM: (a) the Values of E for each of the 50 values of conversion (resulting in a set of 50 reactions) used in the algorithm; (b) the mass fraction allocated to each of the 50 reactions and the dominating reactions occurring with the specified valued of E; (c) the cumulative mass fraction having activation energy less a given abscissa; (d) the rate of mass loss when the fuel is heated at a rate of 10 000K/s. In (c) and (d), the dashed lines show the results from the algorithm and the solid lines are for the original seven first-order reactions It is also important to note the overlap of reactions 3 and 4 in (d), as the clear distinct peak cannot be seen due to the similar E values assigned.

According to Scott et al. (2006[a]), for a single reaction the recovered activation energy was correct at all conversions, in this case when the reactions overlap (i.e. occur simultaneously), the recovered activation energy is incorrect. However the

inversion of Equation (17) in Chapter 4, Section 4.2.5, which generates the amounts of each reaction, will tend to set the amounts of these 'spurious' reactions to zero, thus indicating that the only requirement for the algorithm to correctly identify the activation energy of a reaction is that at some temperature that reaction must dominate completely the rate of mass loss. The distribution of activation energies recovered by the algorithm is compared with the assumed distribution in Figure D1.4 (c).

Despite the overlap of the reactions as can be seen in Figure D1.4 (d), where the value specified for E was 190 and 200 kJ/mol, respectively, the algorithm is still able to recover the original distribution of activation energies.

Scott et al. (2006[a]) purports that a good measure of the performance of the algorithm is how well the determined kinetics extrapolate to higher heating rates. The predicted rate of mass loss at a heating rate of 10 000 K/min is shown in Figure D1.4 (d). The solid blue line was generated using the original set of reactions, whilst the red line was generated using the parameters recovered by the algorithm at 20 and 30 K/min. The agreement between the pseudo-experiment and the extrapolated kinetics is near-perfect. The overlap between the reactions with E= 190 and 200 kJ/mol can be seen in Figure D1.4 (d), as the third peak from the left is, actually, a composite of the peaks produced by these two reactions. This is noticeable by the slight 'kink' on the decreasing side of this peak. These reactions were chosen to be relatively sharp, with A= 10^{15} s^{-1}. This large pre-exponential factor results in less overlap between reactions. However, when Scott et al. (2006[a]) reduced the value of A to 10^{8} (and reduced the activation energies by a factor of 0.75) the performance of the algorithm was the same.

iii. Test 3: A Gaussian Distribution of Activation Energies

In this test, Scott et al. (2006[a]) generates the theoretical curves of mass against time using a continuous, Gaussian distribution of activation energies, with a mean value of E = 225 kJ/mol and a standard deviation of 25 kJ/mol, while keeping A constant at 10^{15} s^{-1}.

Scott et al. (2006[a]) uses the algorithm to generate a set of 100 reactions by evaluating the activation energy at 100 discrete values of conversion, between 1% and 99%. Figure D1.5 shows the recovered distribution of activation energies compared with the original Gaussian distribution.

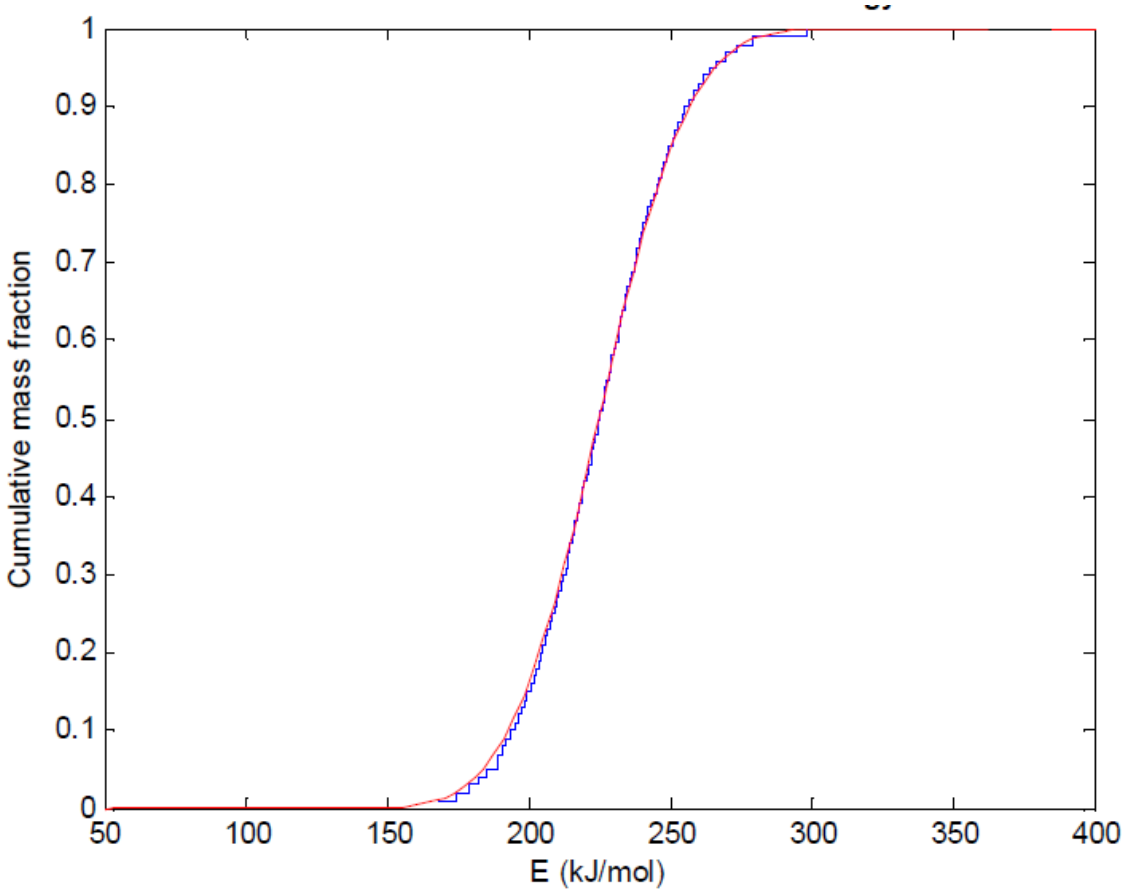

Figure D1.5: Cumulative Distribution of Activation Energies Determined by the DAEM (blue line) for a Hypothetical Fuel with a Gaussian Cumulative Distribution of Activation Energies (red line)

As can be seen in Figure D1.5, the recovered distribution contains bigger steps than the original distribution, which in part, according to Scott et al. (2006[a]), results from the algorithm having been forced to approximate a continuous distribution with a

discrete number, in this case 100, of reactions. Scott et al. (2006[a]) further points out that the final set of reactions recovered by the algorithm contained less than 100 reactions, because many of the reactions were equated to zero by the matrix inversion of Equation (17) in Chapter 4, Section 4.2.5. The first part of the DAEM generates the set of 100 reactions; however, some of these 100 reactions are very close in behaviour. Thus, it is possible to lump all the mass, which, according to Scott et al. (2006[a]), should be allocated to several neighbouring reactions, into one reaction. It is acceptable to note that using a relatively small number of discrete reactions, approximately 50 in this case, are more than enough to give a good approximation to a continuous distribution of activation energies.

The fact that the recovered distribution of activation energies provides a good approximation to the behaviour of a continuous distribution can be seen in Figure D1.6.

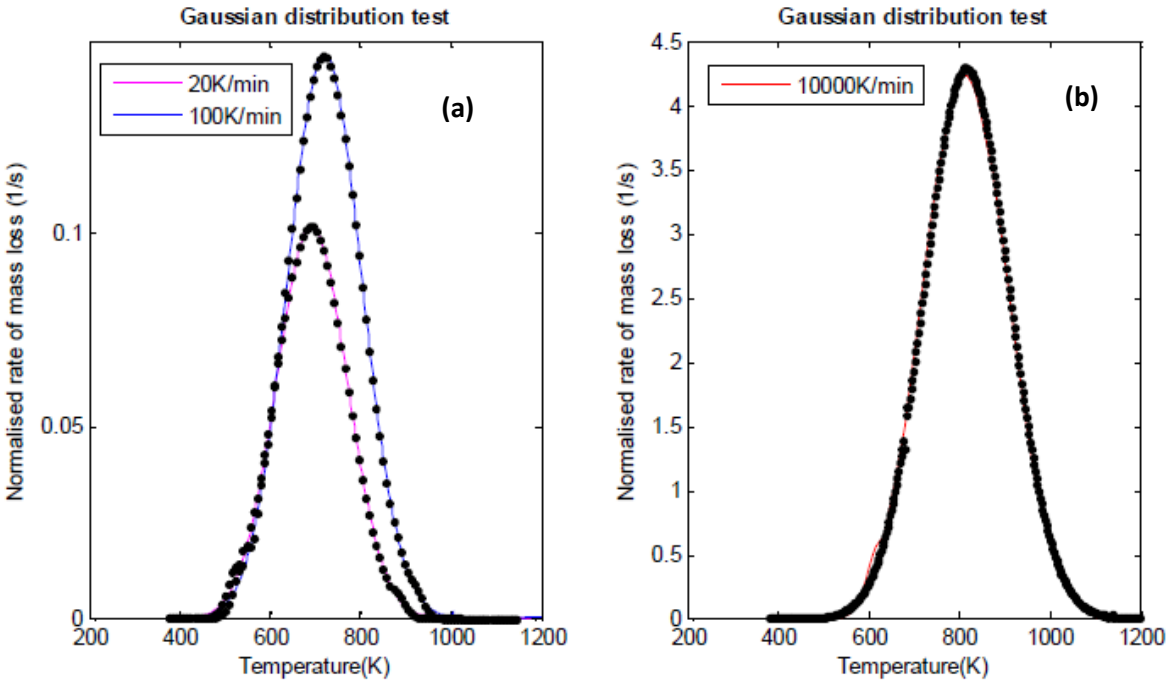

Figure D1.6: Rates of Mass Loss (solid lines) for a Hypothetical Fuel decomposing with a Continuous Distribution of Activation Energies (dots)

The black dots show the predicted results using the parameters from the ~50 reactions recovered by the DAEM algorithm. The heating rates were (a) 20 and 100 K/min (used by the algorithm to determine the kinetic parameters) and (b) 10000 K/min.

In Figure D1.6, the rate of mass loss is plotted as a function of temperature, for both the original Gaussian distribution and the distribution determined by the algorithm.

The algorithm determined these kinetic parameters from the pseudo-experiments at heating rates of 20, 100 and 10 000 K/min only; the rate of mass loss for the high heating rate of 10 000 K/min was calculated assuming that these parameters will be valid at such a high heating rate. The results of the tests conducted by Scott et al. (2006[a]) conclude that the modified form of the DAEM algorithm is accurate at predicting the *A* and *E* values for real or imaginary thermogravimetric experiments for both simple and complex fuels.

D2. Use of the DAEM for Ultra-Low Heating Rates

Section D1.1 has shown that the algorithm is duly capable of reproducing the results of Scott et al. (2006[a]). An interesting observation is the use of the DAEM to now predict the same results at extremely low, nearly isothermal heating rates, and observe the behavior of the resultant curve obtained.

The DAEM was run using the standard heating rate used in the Proximate Analysis of 10 K/min, as a standard with which to compare the resulting curves. Heating rates of 1 K/min and 10^{-6} K/min were chosen, and the DAEM was run using these two heating rates. The results can be seen in Figure D1.7 (a) below.

For purposes of the observation of the effects of ultra-low heating rates on the DAEM pyrolysis results, the example of the seven first-order reactions, as discussed in Section D1.1 was used.

Figure D1.7 (b) shows the results of the pyrolysis for the scenario hypothesized at a heating rate of 10^{-9} K/min.

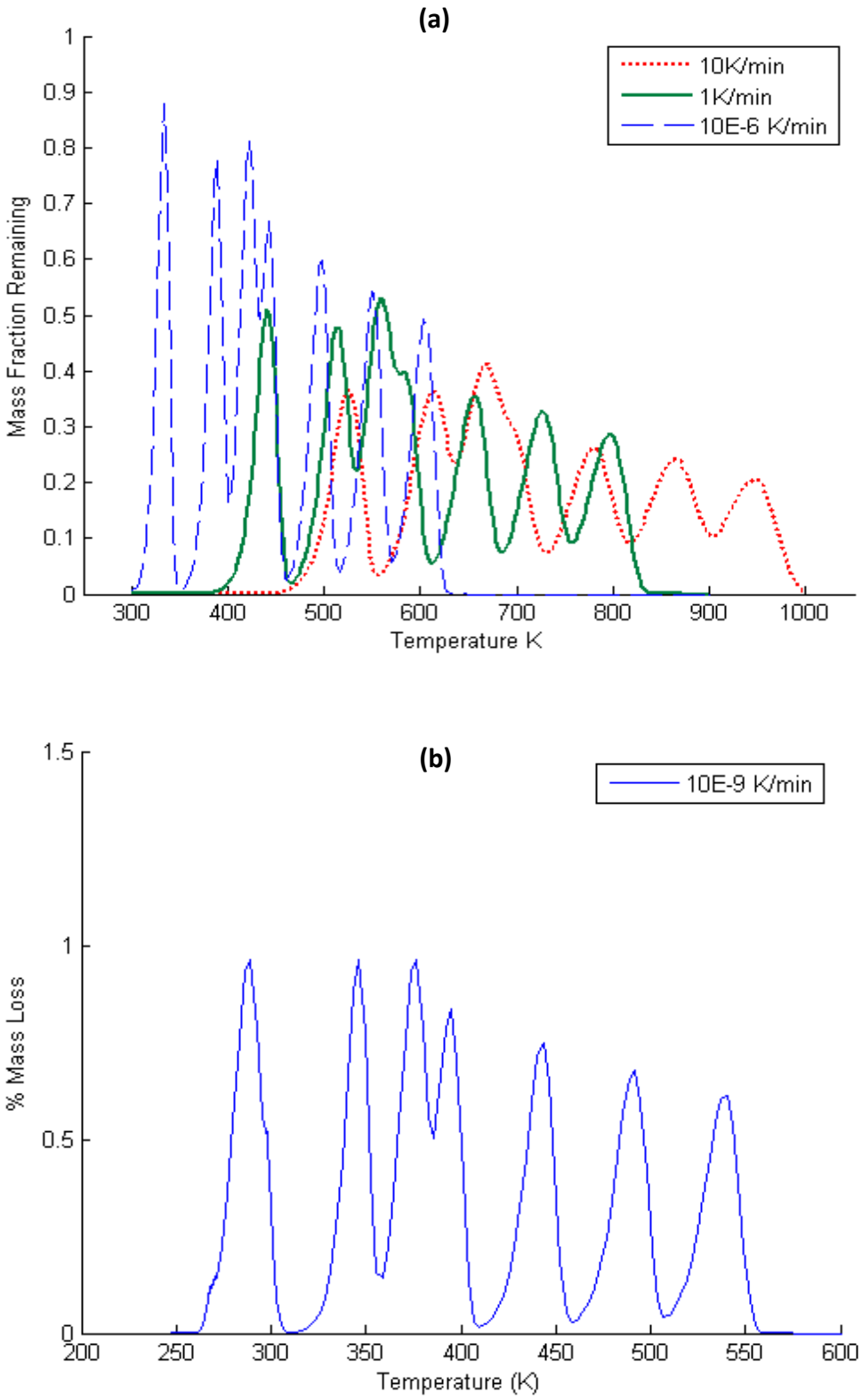

Figure D1.7: Use of DAEM at Low and Ultra-Low, Isothermal Heating Rates

As can be seen from the resulting curves, the curve resolution improves, as the heating rate decreases. In (a), it can be seen that as the heating rate decreases, the

peaks on the curve gradually begin to separate out into their individual representative reactions, with the dominating reaction occurring at a lower temperature as the curve begins to shift closer to the origin .

This can clearly be seen on (b), at the heating rate of 10^{-9} K/min, where the 3rd and 4th reactions, as proposed by Scott et al. (2006[a]) lie together at the heating rate of 10 K/min, observable only by the slight 'kink' on the descending arm of the 3rd reaction. This effect was deliberately chosen by Scott et al. (2006[a]), to demonstrate the capability of the DAEM to effectively distinguish between dominating reactions at a particular temperature interval, even though reactions might have similar *Activation Energy* values (in this case, reaction 3 and reaction 4 have *E* values of 190 and 200, respectively). At ultra-low heating rates, the two reactions can be identified as two separate, individual reactions. This effect is not easily observable at traditional heating rate values, and the use of ultra-low heating rates can be seen as a valuable tool in the identification of peak/reaction identifications. This further demonstrates the ability of the DAEM to simulate ultra-low, near-isothermal heating rates, which would normally be impractical to replicate in a laboratory-scale apparatus.